

Review

Electrochemical Amino Acid Sensing: A Review on Challenges and Achievements

Kaveh Moulaei^{1,2} and Giovanni Neri^{1,*} 

¹ Department of Engineering, University of Messina, C.Da Di Dio, I-98166 Messina, Italy; kaveh.moulaei@unime.it

² Center of Excellence in Electrochemistry, School of Chemistry, College of Science, University of Tehran, Tehran 16846-13114, Iran

* Correspondence: gneri@unime.it

Abstract: The rapid growth of research in electrochemistry in the last decade has resulted in a significant advancement in exploiting electrochemical strategies for assessing biological substances. Among these, amino acids are of utmost interest due to their key role in human health. Indeed, an unbalanced amino acid level is the origin of several metabolic and genetic diseases, which has led to a great need for effective and reliable evaluation methods. This review is an effort to summarize and present both challenges and achievements in electrochemical amino acid sensing from the last decade (from 2010 onwards) to show where limitations and advantages stem from. In this review, we place special emphasis on five well-known electroactive amino acids, namely cysteine, tyrosine, tryptophan, methionine and histidine. The recent research and achievements in this area and significant performance metrics of the proposed electrochemical sensors, including the limit of detection, sensitivity, stability, linear dynamic range(s) and applicability in real sample analysis, are summarized and presented in separate sections. More than 400 recent scientific studies were included in this review to portray a rich set of ideas and exemplify the capabilities of the electrochemical strategies to detect these essential biomolecules at trace and even ultra-trace levels. Finally, we discuss, in the last section, the remaining issues and the opportunities to push the boundaries of our knowledge in amino acid electrochemistry even further.

Keywords: amino acids; electrochemical sensors; cysteine; methionine; tryptophan; tyrosine; histidine



Citation: Moulaei, K.; Neri, G. Electrochemical Amino Acid Sensing: A Review on Challenges and Achievements. *Biosensors* **2021**, *11*, 502. <https://doi.org/10.3390/bios11120502>

Received: 19 October 2021
Accepted: 25 November 2021
Published: 7 December 2021

Publisher's Note: MDPI stays neutral with regard to jurisdictional claims in published maps and institutional affiliations.



Copyright: © 2021 by the authors. Licensee MDPI, Basel, Switzerland. This article is an open access article distributed under the terms and conditions of the Creative Commons Attribution (CC BY) license (<https://creativecommons.org/licenses/by/4.0/>).

1. Introduction

Small molecules and macromolecules are commonly regarded as building blocks of known life. Carbohydrates, proteins, nucleic acids and lipids are four main subgroups of macromolecules, whereas amino acids, hormones, vitamins, neurotransmitters and metabolites, as well as numerous drugs, are common examples of small molecules. In our body, there are thousands of proteins made up of 20 different amino acids which contain an amino group and a carboxyl group at each terminal [1]. Nine amino acids, i.e., methionine, tryptophan, histidine, phenylalanine, valine, threonine, lysine, leucine and isoleucine are called essential amino acids, as they cannot be synthesized endogenously in the human body. On the other hand, our body can synthesis the rest, known as non-essential amino acids, either from glucose, e.g., glycine, glutamate, glutamine, alanine, aspartate, arginine, asparagine, proline and serine, or from the metabolism of other amino acids, e.g., tyrosine from phenylalanine and cysteine from methionine [2]. These amino acids are building blocks and essential elements for synthesizing a large number of low-molecular-weight substances such as glutathione, thyroid hormones, creatine, melatonin, serotonin, melanin and heme, whose importance for body function is well-established [3]. The typical level of amino acids in plasma is in the micromolar range. For instance, the concentration of aspartic acid in plasma is as low as 2–11 μM , while glutamine can be found in plasma at levels as high as 352–689 μM [4]. Some inherited metabolic disorders like phenylketonuria,

tyrosinaemia and hyperglycinaemia can alter the level of amino acids in the body. Elevated levels of total plasma amino acid can be assigned to fructose intolerance, kidney failure and ketoacidosis. On the contrary, lowered level of total amino acids plasma can be a sign of nephrotic syndrome, Huntington's disease, rheumatoid arthritis and fever. Figure 1 presents a general schematic view of some of the most vital functions of amino acids in our body.

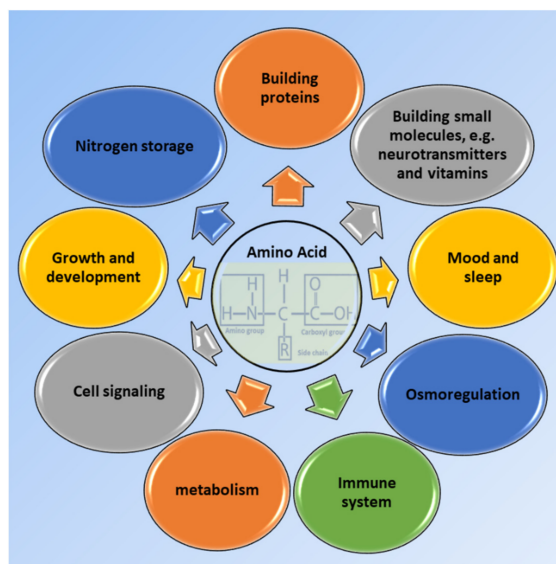


Figure 1. Some crucial roles of amino acids affecting our body functions.

Nowadays, the evaluation of the amino acids level in biological media, e.g., in blood, sweat, urine and saliva, is inspiring new approaches in the prevention and treatment of metabolic disorders such as diabetes, obesity and cardiovascular disorders, as well as infectious disease (including viral diseases), neurological dysfunction and infertility [4–6]. Table 1 summarizes some of the many crucial functions of five electroactive amino acids in both living organisms and industrial world.

Table 1. Highlighted functions of electroactive amino acids. (Note that the first column represents structures at neutral pH).

Amino Acid	Body Function Importance	Industrial Importance
Cysteine 	<ul style="list-style-type: none"> ✓ Being amphoteric, generally, amino acids can act as a biological buffer. ✓ Sulphydryl side chain of cysteine is known as a strong metal binder and, then, is frequently used in metal proteins to fix their metals in place. ✓ Being able to form disulphide bridge, cysteine residues stabilise the three-dimensional structure of proteins. ✓ Cysteine is used in the body to produce a strong antioxidant named glutathione. ✓ When needed, the body uses cysteine as a source of energy through converting cysteine to glucose. ✓ Cysteine is important in communication between immune cells [7] ✓ Cysteine is abundantly found in structural proteins, e.g., keratin and collagen ✓ WHO announced the amount of 4 mg/kg of body weight per day as estimated cysteine requirement for a healthy adult [8] 	<ul style="list-style-type: none"> ✓ In the food industry, cysteine is used as antioxidant to preserve fruit juice and as an additive to flour to enhance the kneading of the dough and as a processing aid for baking. ✓ Cysteine may be used in preparations to alleviate skin lipid production and acne, as well as in anti-dandruff shampoos. ✓ It is used in selective protein purification due to its appreciable reactivity at neutral pH and low abundance in intracellular proteins [9]. ✓ In pharmaceutical industry, cysteine is extensively used as antidote to counteract toxicity of other components, e.g., acetaminophen. ✓ In the cosmetics industry, cysteine is replacing thioglycolic acid owing to its ability to break the disulphide bond in keratin in haircare products. ✓ Cystine, formed from two cysteines, is widely used to produce nail-care products since it improves fingernail growth and hardness [10].

Table 1. Cont.

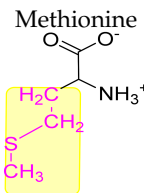
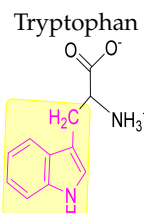
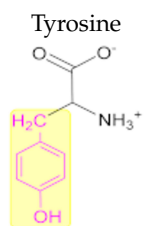
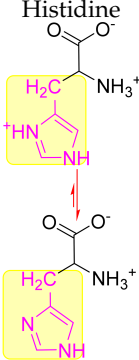
Amino Acid	Body Function Importance	Industrial Importance
<p>Methionine</p> 	<ul style="list-style-type: none"> ✓ Used as a methyl group donor to synthesis different organic compounds, e.g., alkaloids ✓ Preventing fatty liver through choline formation and transmethylation ✓ Alleviation of the toxic acetaldehyde level after alcohol digestion in human ✓ Preserving the cell membrane structure [7] ✓ In organisms, methionine is used as a precursor to produce amino acid cysteine. ✓ Methionine takes part in glutathione metabolism. ✓ As was mentioned for cysteine, methionine plays an important role in nourishing hair, nail and skin, as well as acetaminophen detoxification. ✓ The recommended allowance of sulphur-containing amino acids for a healthy adult is estimated to be 13 mg/kg per day [11], and its estimated requirement, recommended by WHO, is 10 mg/kg per day [8]. 	<ul style="list-style-type: none"> ✓ In the food industry, methionine is an additive to improve the nutritional quality of human food or animal feeds, e.g., methionine added to soybean as pig feed. ✓ Nowadays, a large amount of chemically produced methionine in the world is used in animal feed for livestock production. ✓ In the food industry, methionine is as antioxidant used in the preservation of milk powder, as well as a nutritive element for infant milk and in sports supplements production. ✓ Methionine is used in the pharmaceutical industry in hepatic therapeutics drugs and to prevent hepatic impairments [12].
<p>Tryptophan</p> 	<ul style="list-style-type: none"> ✓ Tryptophan is used as a substrate to produce plant hormones, e.g., indole acetic acid and vitamins B3 and B6. ✓ Tryptophan affects circadian rhythms through its role in the serotonin and melatonin production pathway. ✓ Tryptophan also plays role in the synthesis pathway of niacin, NAD/NADP and tryptamine [13]. ✓ The recommended allowance for a healthy adult is estimated to be in the range of 3.5–6 mg/kg of body weight per day [14]. 	<ul style="list-style-type: none"> ✓ Feed industry, e.g., as a feed additive, especially for weight gain in livestock production ✓ Food industries, e.g., as an essential nutrient in fortified infant foods, corn tortillas and dietary supplements ✓ Pharmaceutical industries, e.g., in sedative and antidepressant medicines for schizophrenia treatment [15]. “Tryptan” is a tryptophan-based drug prescribed for patients as an alternative to conventional antidepressants.
<p>Tyrosine</p> 	<ul style="list-style-type: none"> ✓ In the body, tyrosine serves as a substrate to produce hormones, e.g., epinephrine, norepinephrine and thyroid hormones (T3 and T4), skin pigment melanin and neurotransmitters like dopamine. ✓ Tyrosine contributes to the synthesis of body's natural pain-relieving agents, e.g., enkephalins. ✓ The WHO-recommended amount of (tyrosine + phenylalanine) for a healthy adult is 14 mg/kg per day. (Note that tyrosine pairs with phenylalanine to form an amino acid pair.) [8] 	<ul style="list-style-type: none"> ✓ In food industries, tyrosine is used as a flavouring agent. ✓ It is widely used in common dietary supplements, intended to act as appetite suppressant, to improve memory and to control depression and anxiety [16]. ✓ Tyrosine is used in the synthesis of <i>p</i>-hydroxycinnamic acid and <i>p</i>-hydroxystyrene, two key components in the production of advanced polymers, biocosmetics, adhesives and coatings, and nutrition products [16] ✓ Pharmaceutical industries, e.g., as a precursor for the production of high-value compounds like Levodopa as an anti-Parkinson's disease medication [17] ✓ It is an important precursor in the synthesis of flavonoids and alkaloids as a widely used compound in food, pharmaceutical and cosmetics industries [18].

Table 1. Cont.

Amino Acid	Body Function Importance	Industrial Importance
Histidine 	<ul style="list-style-type: none"> ✓ It is used to produce histamine in the body. ✓ It is found in the active site of enzymes and facilitates the formation and breaking of bonds. ✓ Histidine is the only amino acid that, due to pKa 6.0 of its side-chain, can switch between protonated and unprotonated forms in neutral pH and thereby can shuttle protons in many cellular enzymatic reactions [19]. ✓ Histidine participates in a broad spectrum of physiological processes such as inflammation, neurotransmission, allergic responses, the synthesis of hemoglobin and gastric acid secretion [20]. ✓ In nervous system, histidine take an important role in maintenance of myelin sheaths that protect neurons. ✓ WHO announced 8–12 mg/kg per day as an estimated histidine requirement for a healthy adult [8]. 	<ul style="list-style-type: none"> ✓ In the food industry, histamine is used, e.g., as an antioxidant for the preservation of milk powder. ✓ Histidine is the first limiting amino acid for cow milk protein production, and hence it is necessary to be added to the feed when cows are fed cereal-based and grass silage supplements [21] ✓ In the pharmaceutical industry, it is widely used as a component in nutritious products for infants and adults [22].

Due to the great nutritional, biotechnological and clinical significance of amino acids, a substantial part of research is being directed to develop effective and reliable analytical protocols for evaluating amino acids. Therefore, a wide variety of analytical strategies such as near infrared [23] and Raman spectroscopy [24], UV-Vis spectroscopy [25], surface-enhanced Raman spectroscopy [26], electrochemiluminescence [27], tandem mass spectroscopy [28] and electroanalytical methods [29] have been developed for the detection of amino acids. However, the lack of a strong chromophore hampers the direct detection of amino acids by using UV-Vis or fluorescence spectroscopy, and, hence, target amino acids should be converted into the chromophore-containing derivatives before using these methods [30]. Clearly, detection strategies that do not require derivatisation step(s) are strongly preferred, in terms of both cost and simplicity, over time-consuming, complicated and costly methods involving derivatisation protocols. Regarding this, electrochemical methods can offer a great advantage over other analytical protocols for obviating the necessity of derivatisation steps. However, the electrochemical analysis of amino acids, like all other analytical methods, has its limitations and drawbacks, which will be also addressed in this review.

Nowadays, clinical diagnoses are no longer carried out solely in clinical laboratories. Instead, they are routinely performed in several settings such as hospital point-of-care settings or by caregivers out of hospital and even by patients themselves at home [31,32]. Electrochemical methods are ideally well-adjusted for these emerging nonhospital analyses. Electrochemical sensing strategies potentially offer the simple, fast, cost-effective, sensitive and, to some extent, selective detection of bioanalytes relevant to clinical diagnostic tests and represent promising alternatives for common clinical methodologies [33]. To date, a wide spectrum of methods has been developed for signal transduction and target detection, which allows electrochemical techniques to be used as effective sensing protocols. Therefore, electrochemical sensing platforms are leaving the field of laboratory research and successfully stepping forward to the point-of-care detection of biomolecules such as lactate and glucose that mostly rely on bioaffinity recognition and electrochemical transduction approaches.

Even glimpsing at the well-known literature databases will reveal that the electrochemistry of amino acids is a dynamic ongoing subject that encompasses many scientific fields from biochemistry and genetics to chemistry and even engineering areas. Figure 2 presents the results of a literature survey using the Scopus database. It is seen from the

number of published papers (since 2010) concerning the electrochemistry of amino acids that research in this field is still appealing and being actively perused. Scientists in different fields such as chemistry, material science and engineering are actively investigating the electrochemistry of amino acids to fulfill their desired aims. It is frequently highlighted that there are five well-known electroactive amino acids [34–37], including cysteine, tryptophan, tyrosine, methionine and histidine, that have been the core of many research activities in the last decade. Of these, as can be seen in Figure 2C, cysteine has been the subject of about half of all published papers. In the following sections, we will discuss the importance of this amino acid as a benchmark in amino acid electrochemistry.

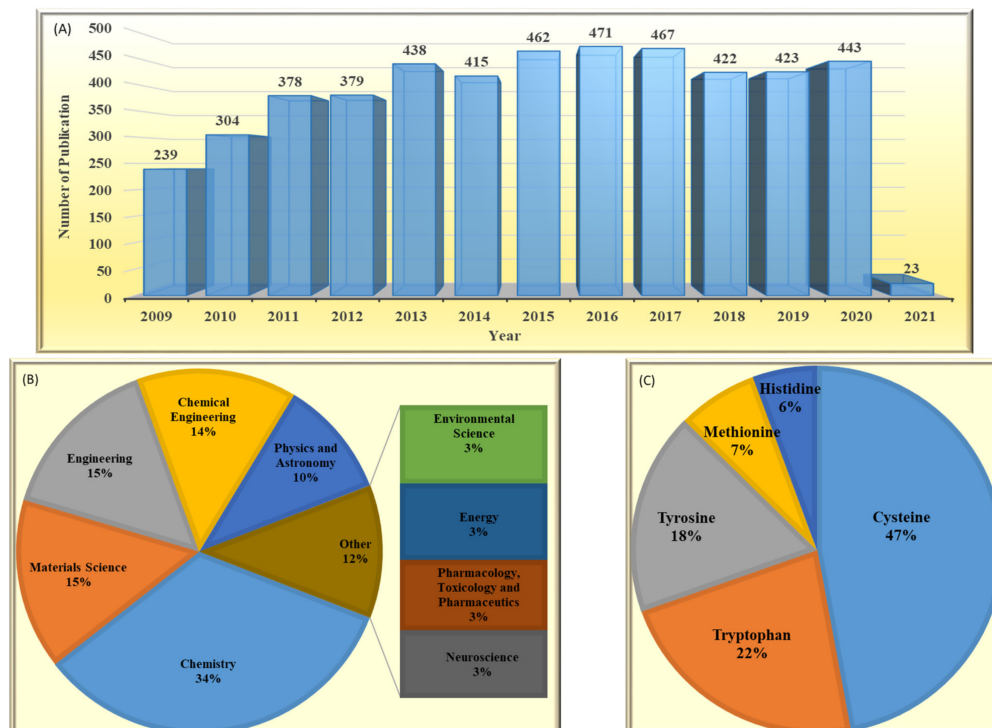


Figure 2. A comparative demonstration of (A) published papers per year searching ‘amino acid’ and ‘electrode’. (B) Categorized published papers in the first 10 scientific areas according to number of papers. (C) Published papers for 5 well-known electroactive amino acids searching the ‘name of the amino acid’ and ‘electrode’ and ‘detection’. All results refer to a search in the Scopus database (9 January 2021) by limiting the search to the title, abstract and keywords (Title, Abs and Key).

This review aims at acquainting the readers with different aspects of amino acid sensors based on electrochemical strategies. For this, we will start with a discussion on amino acid electroactivity to provide a general perspective for readers on the electrochemistry of amino acids. After that, in the following sections, we will go further into details and evaluate the proposed electroanalytical strategies, to date, for five well-known electroactive amino acids, namely cysteine, tyrosine, tryptophan, methionine and histidine. Throughout these sections, significant performance metrics including the limit of detection, linear dynamic range(s) and, sensitivity and durability of the proposed electrochemical sensors will be presented. Finally, in the last section, conclusions and outlooks, the main ongoing challenges and difficulties in the electrochemistry of amino acids that should be addressed to pave the way for future achievements are discussed, and possible guidelines are presented.

2. Amino Acid Electroactivity

The attractiveness of electroanalytical techniques lies greatly in their directness. In other words, despite most of the spectroscopic methods for the evaluation of amino acids

that require derivatisation, the proposed electroanalytical methods are mostly label-free. Moreover, it is worthwhile to mention that, since the electrochemical oxidation of both free and bounded amino acids, e.g., in enzymes and proteins, exhibit similar voltammetric profiles [37], electrochemical methods can be used in proteomics for proteins that contain at least one electroactive amino acid or another electroactive centre. As an example, Oliveira-Brett's group [38] reported that different amyloid beta peptides related to Alzheimer's disease were successfully evaluated thanks to the presence of five electroactive amino acids, in the structure of these peptides, i.e., one tyrosine, three histidines and one methionine. They reported that, depending on the length and content of these amyloid beta peptides, one or two oxidation peaks are observed. They ascribed the first peak to the electrooxidation of tyrosine residue and the second peak to the presence of both methionine and histidines residues. However, there are some drawbacks, like all other analytical methods, to be addressed for the electroanalysis of amino acids.

Despite the prominent merits of electrochemical methods, the electrochemical signal of D-amino acids and their L-isomer are both often indistinguishable, and discriminating between them is hard to achieve with bare electrodes. One serious concern is that, for electroactive amino acids, signal overlapping and/or large overpotential are still challenging. For example, the oxidation peaks of tyrosine and tryptophan overlap at the most common bare electrodes, or the oxidation of histidine and methionine in aqueous solution occurs at relatively high potentials, usually >1 V vs. Ag/AgCl reference electrode. In fact, even now, there are some major challenges that need to be thought about before using electrochemical sensors, beyond their current use, in practical application in point-of-care diagnostics. Nonetheless, the unprecedented efforts are being devoted in this field, especially to develop new sensing materials, hold great promise that this aim will be fulfilled in the upcoming years.

Another interesting subject in electrochemistry of amino acids is the evaluation of the possible oxidation pathway(s) by which amino acids participate in electrochemical reactions at the electrode surface. It is frequently reported in the literature that the electrooxidation of amino acids is often an irreversible, complicated and multistep phenomenon. Even though the reaction mechanism of amino acids at the electrode surface is still a controversial issue, it is usually assumed that, at first, amino acids are adsorbed onto the electrode via their carboxyl group facilitating electron transfer between the electrode and electroactive part of amino acids. These electroactive parts of amino acids are located in the side chain of amino acids [38]. For instance, the electroactivity of cysteine, tyrosine and tryptophan is assigned to a thiol, phenol and indole function, respectively, which exist in the side chain of these amino acids (Figure 3). Methionine and histidine are other electroactive amino acids whose electroactivity is ascribed to the sulphur- and imidazole-containing side chain, respectively.

There is a big controversy among researchers over the electrooxidation mechanism of amino acids. This, in the authors' opinion, stems from the high susceptibility of electrode reaction pathways to the reaction conditions, e.g., type and concentration of supporting electrolyte, pH, type of electrode and even amino acid concentration itself. This high dependency of amino acid electrochemistry on experimental conditions is a consequence of their structural features, since amino group, carboxyl group and mostly even the functional groups presented in the side chain are very liable to variation in measurement conditions. For example, variations in pH and electrolyte might affect the reaction pathway through changes in the type/density of the surface charge, the degree of solvation and the adsorption/desorption properties of amino acids. Figure 4 is drawn based on the general electrooxidation pathways reported in the literature for cysteine [39,40], methionine [41], tryptophan [42,43], tyrosine and histidine [37,44]. Since the main goal of this review is to collect and present recent findings concerning quantitative electrochemistry of amino acids, we inevitably have to skip going further into details. However, we strongly encourage the interested readers to see these qualitative studies as the basis for better understanding the current issues and to innovate new approaches to address them.

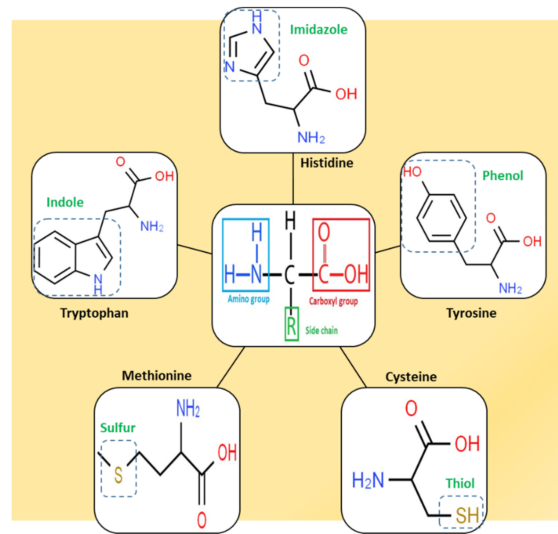


Figure 3. Chemical structure of the five well-known electroactive amino acids highlighting their electroactive side chain.

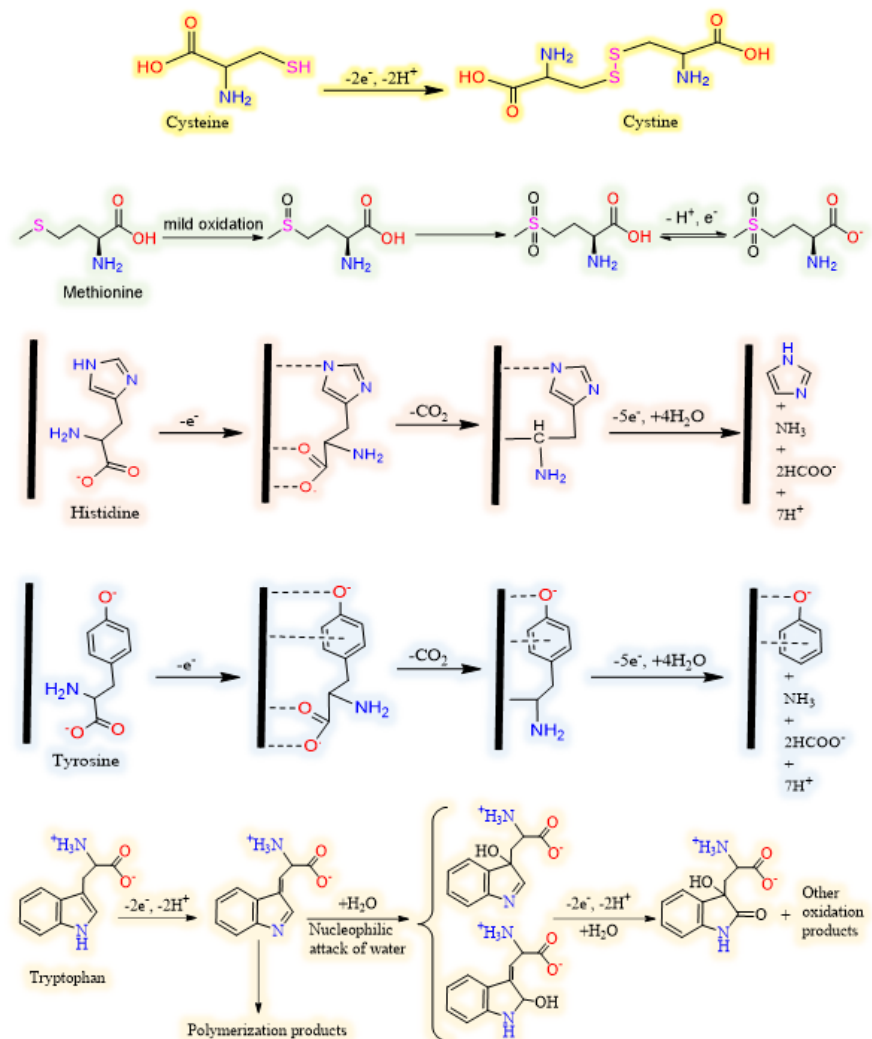


Figure 4. Schematic representations of typical electrooxidation pathway for cysteine, methionine, histidine, tyrosine and tryptophan (from up to down, respectively).

3. Electrochemical Analysis of Amino Acids

3.1. Sulphur Containing Amino Acids

3.1.1. Cysteine

Protein electrochemistry was born in the middle of 20th century, somehow, thanks to cysteine electroactivity when Heyrovsky invented polarography and observed a so-called 'pre-sodium wave' [45]. Later, it was concluded that the pre-sodium wave is caused by the cysteine residue of under-study proteins. Since then, cysteine, among five electroactive amino acids, has been a continuously appealing subject for researchers, such that ca. 50% of all developed electrochemical amino acid sensors has been reported for cysteine; see Figure 5C. It has been pointed out that human blood plasma contains three forms of cysteine, including free cysteine, cystine and protein-bound cystine. Cysteine is a thiol, while the latter two are in disulphide form [46]. The normal level of free cysteine in a healthy individual is reported to be in the range of 5–30 μM for blood plasma [47], while the urinary excretion of cysteine is in the range of 3–33 mg/24 h [48]. Therefore, to achieve the desired sensitivity to detect cysteine in these low concentration ranges, diverse modifiers have been proposed to be exploited in electrochemical cysteine sensors. Noble metals, e.g., gold [49–66], palladium [67], platinum [67], silver [68–70], noble metal composites, e.g., gold/copper [71], gold/silver [72], gold/nickel [73], gold/platinum [74] and silver/palladium [75], have been extensively used. Additionally, metal oxides, e.g., CeO_2 [76], $\text{Cu}_{(x)}\text{O}$ [77], Fe_2O_3 [78], MgO [79], MnO_2 [80], NiO [81], SnO_2 [82], TiO_2 [83], WO_3 [84], Y_2O_3 [85] and ZnO [86], as well as organic modifiers [87–100], have also been explored as potential alternatives for noble metals.

It is well-known that the side chain sulphur of cysteine has remarkable affinity for gold, silver and copper in order of $\text{Au} > \text{Cu} > \text{Ag}$ [101]. This has encouraged many researchers to explore the capability of these metals to design more effective cysteine sensors. Figure 5 illustrates the intense effect of these metals on enhancing the peak currents and, consequently, the sensitivity of the proposed modified electrodes compared to the bare ones.

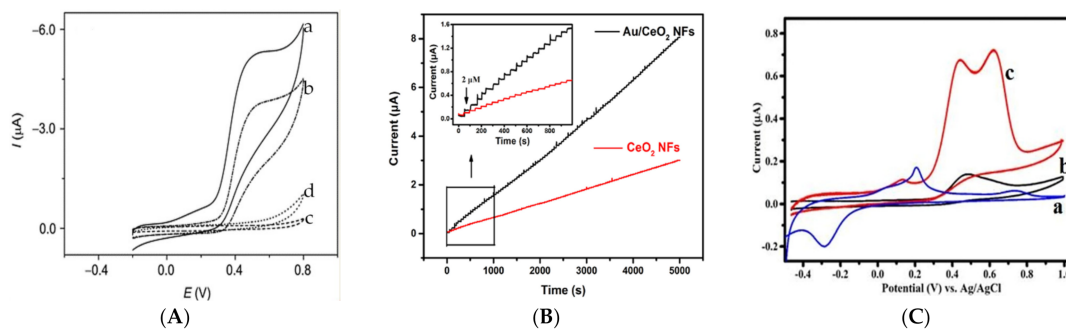


Figure 5. (A) Cyclic voltammograms of 0.5 mmol/L (a, c and d) and 0.2 mmol/L (b) cysteine at an Au/Nafion/GCE (a, b), Nafion/GCE (c) and bare GCE (d), Scan rate: 20 mV/s in PBS (pH 2.0) [65]. (B) Amperometric response curves of the CeO_2 NFs and Au/ CeO_2 NFs modified SPCEs in 0.01 M PBS (pH 7.4) in the concentration range of 2.0–200 μM (applied potential 0.7 V) [102]. (C) Cyclic voltammograms of (a) Ag/ITO, (b) Poly dopamine /ITO and (c) Ag-Poly dopamine /ITO in 0.1 M PBS (pH = 5.0) solution containing 25 μM cysteine at scan rate of 50 mV/s [68]. Copyright 2021 Royal Society of Chemistry.

Wang et al. [65] investigated the effect of Au NPs on cysteine electroanalysis, Figure 5A, and no detectable peak was observed for cysteine at bare GCE and Nafion/GCE (Figure 5A, d and c). However, after adding gold NPs to the electrode, an oxidation peak emerged whose peak current increased upon increasing cysteine concentration (Figure 5A, b and a). Interestingly, sensor performance was explored in acidic (pH = 2) and neutral (pH = 7) solutions, and they reported that, in acidic medium, narrower linear range (3.0–50 μM) and higher sensitivity (22.7 $\mu\text{A}/\text{mM L}^{-1}$) are obtained compared with neutral pH (2.0–80 μM and 4.08 $\mu\text{A}/\text{mM L}^{-1}$). Additionally, the interference effect of ascorbic acid and uric acid were found to be more effectively suppressed in neutral pH. Figure 5B clearly

shows that the addition of Au nanoparticles to the as-prepared cerium oxide nanofibers (CeO₂ NFs) results in a notable promotion in the sensitivity (2.7 times) of the proposed amperometric cysteine sensor. Using this composite, Au/CeO₂ NFs, Cao et al. [102] developed an ultra-sensitive cysteine whose LOD was as low as 10 nM. Despite the substantial effect of gold, finding a less-expensive material, e.g., silver, to undertake the role of gold is an active area for researchers due to the prohibitive cost of gold. Since cysteine showed no electroactivity at an indium tin oxide (ITO) electrode, Thota et al. [68] modified the bare ITO with poly dopamine and silver nanoparticles. They found a remarkable promotion in peak current for this modified electrode (Ag-polydopamine/ITO), wherein both Ag/ITO and polydopamine/ITO showed significantly lower peak currents (Figure 5C). This is a valuable example of the synergistic effect of polydopamine and silver nanoparticles on the cysteine electrochemical signal. Moreover, two oxidation peaks were observed at Ag-polydopamine/ITO during the forward potential sweep (Figure 5C) that are likely due to the presence of two different catalytic sites on the electrode modified for cysteine oxidation. This sensor exhibited a linear range of 0.05–300 µM, and the LOD was calculated to be 0.02 µM. In spite of being both noble and precious metals, just a few reports have found that used palladium [67] or platinum [103,104] nanoparticles for electrochemical cysteine determination.

In addition to noble metals, copper compounds, in either oxide [77,105], sulphide [106] or other complex forms [107–111] have also been interesting options for researchers in this field owing to the high affinity of copper for the sulphur moiety of cysteine. In an interesting study, Li et al. [105] synthesized an octahedral Cu₂O/polystyrene composite and, consequently, removed the styrene from the Cu₂O lattice easily by treating the Cu₂O/polystyrene composite with tetrahydrofuran to obtain hollow cubic Cu₂O particles. They showed that, generally, the presence of Cu₂O particles promotes the sensitivity of the sensor, compared to bare GCE, and more importantly, the electrochemical response of cysteine significantly improves (about 2.8 times) for hollow cubic Cu₂O particles with respect to the Cu₂O/polystyrene composite (Figure 6A). Linear measurement ranges were found to be 6.0–100 µM and 0.5–200 µM for Cu₂O/polystyrene and hollow cubic Cu₂O particles, respectively, whereas the LOD for the latter (0.14 µM) was about 16 times lower than the first one (2.3 µM). This revealed that both the nature and structure of modifier should be wisely tuned to reach the optimum performance for this sensor. Iron compounds, after copper ones, are by far the most studied non-noble-metal-based modifiers in cysteine electroanalysis [56,78,112–122]. Duan et al. [112] developed an outstanding sensor taking advantage of extreme stability, excellent electrocatalytic activity and the redox properties of Prussian blue (PB, Fe₄[Fe(CN)₆]₃). To build this sensor (Figure 6A), metal organic-framework-derived porous carbon (PC) was first synthesized, mixed ultrasonically with carbon nanotubes (CNT) and drop-cast on the GCE surface. PB was electrodeposited on CNTs-PC/GCE, and then, this electrode, PB-CNTs-PC/GCE, was transferred to a solution containing both pyrrole and cysteine to electropolymerize pyrrole in the presence of cysteine template. Here polypyrrole works as a molecularly imprinted polymer (MIP). In the last step, the MIP-PB-CNTs-PC/GCE electrode was immersed in PBS, and cysteine templates were removed from the polypyrrole structure through an overoxidation process to leave imprinted cavities behind. The extraordinary selectivity and sensitivity of this sensor are closely related to the presence of imprinted cavities and Prussian blue, respectively. This sensor was very selective so that it could differentiate even D-cysteine from L-cysteine and detect the L-isomer in a linear range of 10⁻¹³–10⁻⁷ mol L⁻¹ with LOD as low as 6.0 × 10⁻¹⁵ mol L⁻¹. Figure 6B clearly exhibits the remarkable effect of PB on the sensitivity of the sensor, wherein slope of calibration curve is much lower in the absence of PB. Though the preparation process of this sensor was rather complex (Figure 6A), the resultant sensor was extremely sensitive and selective. In another approach, Zhou et al. [113] proposed a magnetic GCE modified with a Fe₂O₃/polydopamine/Cu₂O composite to detect cysteine and reported an ultra-sensitive sensor with an outstanding LOD of 83.0 pM (83.0 × 10⁻¹⁵ mol L⁻¹). In contrast to the work of Duan et al. [112], in

this sensor, the iron oxide moiety is used, mainly because of its magnetic properties, and iron oxide is not directly involved in electrochemical signal production because Cu^{2+} ions undertake this task.

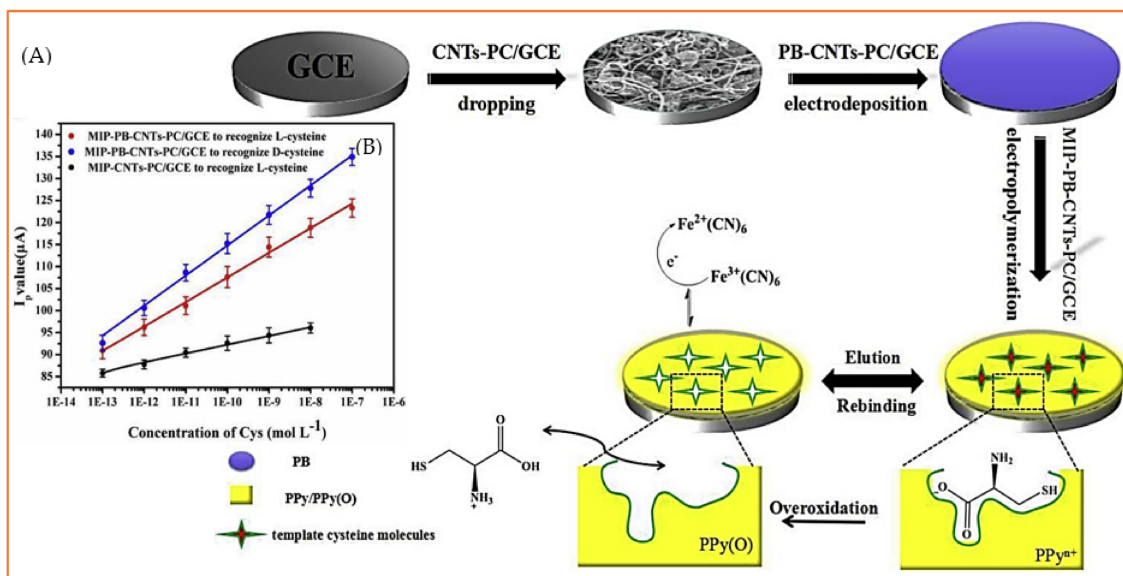


Figure 6. (A) The preparation process for a MIP-PB-PC-CNTs/GCE sensor. (B) The relationship of the peak values of MIP-PB-CNTs-PC/GCE and MIP-CNTs-PC/GCE with the concentration of L-cysteine and D-cysteine. Reprinted with permission from ref. [112]. Copyright 2019 Elsevier.

Although a big share of developed cysteine sensors exploit metal-based modifiers, some valuable reports are found in which merely organic materials serve as modifiers. These organic modifiers for electrochemical cysteine detection are mainly either simple carbon structures, e.g., carbon nanofiber [87,99], carbon black [90], nanocarbon [94] and ordered mesoporous carbon [95], or benzene-derivative compounds, e.g., *p*-coumaric acid [88], catechol [89,92,93,96], xanthene [123], *p*-aminophenol [98] and quinizarin [100]; see Figure 7.

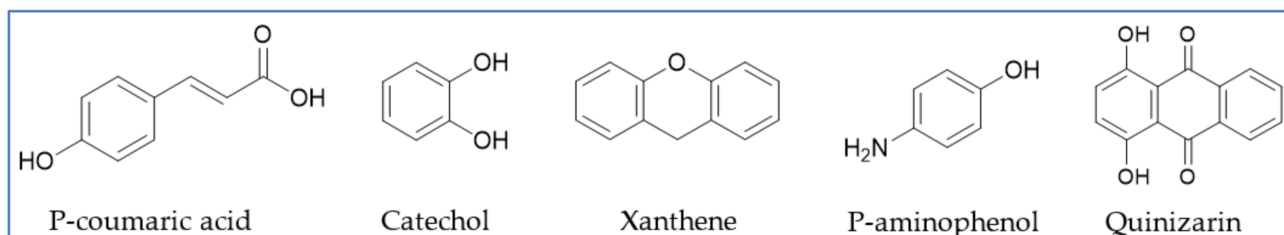


Figure 7. Benzene-derivative organic modifiers used in electrochemical cysteine sensors.

It has widely been accepted that the first category members, carbonaceous materials, enhance the performance of sensors mainly through improving the electrode surface features such as specific surface area and conductivity, while the latter ones, benzene-derivative compounds, promote the function of sensors through mediating the electron transfer between cysteine and electrode as electrocatalyst. It is noteworthy to mention that these mediators not only bring about a great enhancement in sensitivity by electron shuttling between cysteine and electrode but also may effectively improve the selectivity of the sensor. Interesting works have been reported by Compton's group wherein they selectively measured cysteine and homocysteine in the presence of ascorbic acid and glutathione [94] or homocysteine in a medium containing cysteine ascorbic acid and glutathione [92]. Table 2 summarizes the reported works, from 2010 to now, in the field of cysteine electrochemical detection, and the most important related figures of merit to give readers the recent orientations and achievements in this field.

Table 2. Proposed electrochemical cysteine sensors, since 2010, along with the most important respective figures of merit.

Sensing Part	Method	LDR ¹ (μM)	LOD ² (μM)	L.T. Stability ³	Real Sample	Ref.
screen-printed diamond electrode	CV	1–194	0.62	-	bovine plasma	[124]
Co–La oxides/rGO composite	AMP	1–888	0.1	-	serum and commercial syrup	[125]
Mn–La oxides/reduced graphene oxide composite	AMP	0.5–832.5	0.1	93.2% after one week	commercial serum and syrup samples	[126]
cobalt hydroxide nanosheets	AMP	0.2–1940	0.0765	-	human blood serum	[127]
silver metal-organic frameworks coated onto nitrogen-doped porous carbon	LSV	0.1–1300	0.05	>6 months	milk sample	[128]
CuO/Boron Nitride Nanocomposite	AMP	1–10	0.58	98% after 25 days	blood serum	[129]
Co ₃ O ₄ nanoparticles	AMP	0.2–75	0.07	-	urine sample	[130]
functionalized MWCNT	DPV	0.7nM–200 μM	0.16 nM	>one week	blood serum	[131]
graphite-polyurethane composite	AMP	30–130	4.24	-	food supplements	[132]
3D pothole-rich hierarchical carbon framework-encapsulated Ni nanoparticles	CV	0.8–85	0.15	90% after one week	Blood serum and urine	[133]
copper pentacyanonitrosylferrate and octa(aminopropyl)silsesquioxane	AMP	200–2000	125	-	-	[134]
Cu ²⁺ -phen-dione@rGO	AMP	10–32,344	2	>15 days	urine sample	[135]
ferrocene-functionalized mesoporous silica	CV	3–20	3	-	-	[136]
CeO ₂ -CuO nanocomposite	AMP	10–5000	0.16	93.7% after 5 days	pond water	[137]
Au–Cu@Cu _x O	AMP	1.25–1940	1.25	>5 weeks	human blood serum	[138]
Pd@Ti ₃ C ₂ T _x nanocomposite	AMP	0.5–10	0.14	>one week	urine sample	[139]
CeO ₂ -SnO ₂ nanocomposite	AMP	10–2000	0.016	>4 days	pond water	[140]
CuFe ₂ O ₄ /rGO–Au composite	CV	50–200	0.383	93% after 4 week	urine sample	[141]
Co(II)–Al(III) layered double hydroxide	DPV	10 ⁻⁴ –1	10 ⁻⁴	-	pharmaceutical samples	[142]
fluorinated cobalt phthalocyanine and ordered mesoporous carbon	DPV	20–20,000	1	90% after 2 weeks	cell lysate, human serum and urine	[143]
ethyl 2-(4 ferrocenyl [1-3]triazol-1-yl) acetate/graphene	SWV	4.0–2300.0	0.9	-	blood serum and urine	[144]
free-standing TiO ₂ nanotube	AMP	100–10,000	100	93% after 80 days	human serum sample	[145]
bacteriophage particles-carbon nanofiber	CV	20–1000	20	-	-	[87]
cobalt-poly (naphthylamine)/sodium dodecyl sulphate	AMP	1–100	0.8	>5 weeks	human urine	[146]

Table 2. Cont.

Sensing Part	Method	LDR ¹ (μM)	LOD ² (μM)	L.T. Stability ³	Real Sample	Ref.
Au nanoparticles/ anthraquinone-2-carboxylic acid	DPV	15–500	1.873	92.5% after 2 weeks	blood serum	[49]
electrodeposited copper/SPE	AMP	1–1800	0.21	-	human and rabbit blood serum	[147]
imine substituted cobalt(II) phthalocyanine	CV	0.01–0.10	0.003	-	human urine and cysteine tablet samples	[148]
molecularly imprinted Prussian blue-porous carbon-CNTs/polypyrrole	DPV	$1.0 \times 10^{-z^7} - 0.1$	6.01 pM	94.42% after 15 days	blood serum	[112]
poly(<i>p</i> -coumaric acid)/MWNT	DPV	7.5–1000	1.1	-	human urine	[88]
Cu ²⁺ modified Fe ₃ O ₄ @polydopamine	SWV	0.010–500	83.0 pM	-	blood serum	[113]
polyaniline/zinc bismuthate	AMP	50–2000	0.19	-	-	[149]
⁴ RGO/Nafion film decorated Pd nanoparticles	AMP	0.5–10	0.15	92.27% after 5 days	human urine	[67]
silver-copper sulphide	AMP	1–100	0.24	Should be kept in dark condition	dietary supplement	[106]
Fe ₃ O ₄ @NiO magnetic nanoparticles	DPV	0.1–120	0.014	89% after one month	human breast milk, cow milk and honey	[150]
Co-Gd ₂ O ₃ nanocomposite	AMP	1–100	0.23	92.3% after one month	milk, cysteine capsule	[151]
bismuth tellurate nanospheres	CV	0.1–2000	0.46	>2 weeks	-	[152]
hollow cubic Cu ₂ O particles/Nafion	CV	5–200	0.4	96% after 10 days	amino acid injections	[105]
MgO nanoparticle/acetylferrocene	DPV	0.1–7000	0.03	95% after 25 days	urine, pharmaceutical serum	[79]
Au/CeO ₂ nanofibers composite	AMP	2–200	0.01	90% after one week	blood serum	[102]
CeO ₂ nanofibers	AMP	2–200	0.02	-	blood serum	[76]
Prussian blue	AMP	100–600	67.4	-	-	[114]
MnO ₂ -TiO ₂ nanocomposite/2-(3,4 dihydroxyphenethyl) isoindoline-1,3-dione	SWV	0.025–200	0.013	94% after one month	blood serum, urine, cysteine capsule	[153]
CuO–Cu ₂ O heterojunction	⁵ PEC	0.2–10	0.05	>6 weeks	urine sample	[77]
ZnO nanoparticle/N-doped RGO	AMP	0.1–705.0	0.1	-	cysteine capsule	[86]
nickel oxide NPs/N-doped RGO	AMP	0.3–1620.8	0.1	93.1% after 7 days	syrup sample	[81]
thiolated catechol	AMP	0.12–34.6	0.0605	-	urine sample	[89]
Li-doped bismuth oxide nanorods	CV	0.1–2000	0.17	-	blood serum	[154]
Au-nanoparticles/ poly-Trypan Blue	DPV	5–270	0.006	-	blood serum and urine	[50]

Table 2. Cont.

Sensing Part	Method	LDR ¹ (μ M)	LOD ² (μ M)	L.T. Stability ³	Real Sample	Ref.
carbon black functionalized with syringic acid	CV	20–1000	0.639	-	chicken flesh and blood serum	[90]
Impurity-containing carbon black	AMP	50–700	0.0459	-	blood serum	[51]
bismuth nickelate nanorods	CV	0.5–2000	0.087	-	-	[155]
gold nanoparticles incorporated polypyrimidine derivative	DPV	2–500	0.02	94.9% after one month	blood serum and urine	[52]
CdSe quantum dot-modified/MWCNT ⁶ hollow fiber	DPV	0.287–33,670	0.116	-	bodybuilding supplements	[156]
magnetic CoFe ₂ O ₄ /SiO ₂ spinel-type	DPV	0.02–425	0.2	70% after one week	milk sample	[115]
MIP ⁷ /CuNPs/nonporous gold	DPV	0.5–10,000 nM	70 nM	95.4% after one week	bovine serum and sauce of instant noodle samples	[71]
Y ₂ O ₃ nanoparticles/nitrogen-doped RGO	AMP	1.3–720	0.8	-	syrup sample	[85]
polythiophene layer sensitized anatase TiO ₂	PEC	100–800	12.6	93.9% after 2 weeks	-	[83]
Pt-Fe ₃ O ₄ /RGO	AMP	100–1000	10	94.2% after 2 weeks	-	[116]
polypyrrole/graphene quantum dots@Prussian Blue	AMP	0.2–1000	0.15	-	cysteine tablets	[117]
polydopamine-capped silver nanoparticles	LSV ⁸	0.05–300	0.023	>2 months	blood serum	[68]
Au nanoparticles/poly(E)-4-(p-tolyldiazenyl)benzene-1,2,3-triol	DPV	2–540	0.04	-	human urine	[53]
thulium hexacyanoferrate	DPV	0.5–8.92	0.016	91% after one week	human urine, river water	[157]
zinc bismuthate nanorods	CV	0.1–2000	0.074	>2 weeks	-	[158]
Ru(III) Schiff base complex, multi-walled carbon nanotubes and Nafion	AMP	50–500 mg/L	0.11 mg/L	-	pharmaceutical products	[159]
Co(II)-phthalocyanine	SWV	2.6–200	4	-	embryo cell culture	[160]
Fe(II)-exchanged zeolite	SWV	0.005–300	0.00015	>8 months	human serum, urine and N-acetyl cysteine tablets	[161]
molybdenum nitride nanosheets/N-doped MWCNT	CV	5–12,600	3.64	92.9% after 2 weeks	blood serum	[162]
carbon ionic liquid electrode with terpyridine copper(II) complex	CV	0.1–40	0.01	93.4% after 15 days	blood serum	[107]
zirconium (IV) phosphate/Ag hexacyanoferrate (III)	AMP	10–80	10.2	-	-	[163]

Table 2. Cont.

Sensing Part	Method	LDR ¹ (μ M)	LOD ² (μ M)	L.T. Stability ³	Real Sample	Ref.
bare glassy carbon electrode	CV	1–10	0.03	-	-	[164]
V-substituted polyoxometalates/Au@2Ag core-shell nanoparticles	AMP	0.025–7.625	0.0276	90% after 2 weeks	milk sample	[72]
Fe ₂ O ₃ nanoparticles supported on N-doped graphene	AMP	0.2–400	0.1	90.6% after one week	syrup sample	[78]
Au NPs-Ni-Al layered double hydroxide composite	DPV	10–1000	6.0	79.3% after 4 days	-	[73]
GO/CCNTs/AuNPs@MnO ₂ ⁹	DPV	0.01–7.0	0.0034	-	human urine	[55]
bismuth nanostructure incorporated into ionic liquid	SWV	1–2000	0.5	-	blood serum	[165]
silver nanoparticles modified hierarchically structured ZnO	PEC	0.67–34.77 pM ₁₀	0.21 pM	94.1% after one month	human urine	[69]
cyclotricatechylene	CV	0–20	0.9	-	cell tissue media	[166]
(DMBQ) ¹¹ /ZnO nanoparticles	SWV	0.09–340.0	0.05	>one month	urine, water and pharmaceutical serum	[167]
iron tetrasulphonated phthalocyanine decorated MWCNT	AMP	10–200	1	95.16% after one month	blood serum	[118]
copper inorganic-organic hybrid coordination compound	AMP	10–80	2.1	-	-	[108]
14-(4-hydroxyphenyl)-14-H-dibenzo[a,j]-xanthene/MWCNT	DPV	4–1000	1	-	human serum, acetyl cysteine tablets	[123]
gold nanoparticle (AuNP)-iron (iii) phthalocyanine	DPV	50–1000	0.27	-	pharmaceutical sachets, dietary supplement	[56]
Sulphonated Graphene-poly(3,4-Ethylenedioxythiophene)/Au NPs	AMP	0.1–382	0.02	95.25% after 10 days	human urine	[57]
bismuth film	SWV	1–10	0.028	-	dietary supplement	[168]
carbon ionic liquid	LSV	1–450	0.298	-	artificial urine and nutrient broth	[91]
polyaniline/CuGeO ₃ nanowire	CV	1–2000	0.44	-	-	[109]
nanocarbon (carbon black)	SWV	0–100	5	-	-	[94]
SnO ₂ -MWCNTs	AMP	0.1–554.5	0.03	92% after one month	-	[82]
MWCNTs/gold NPs stabilized with calcium cross-linked pectin	AMP	0.1–1000	0.019	-	blood serum	[58]
methacrylic acid based MIP	DPV	0.02–0.18	0.0096	-	blood plasma, tapwater samples	[169]
protoporphyrin/WO ₃ /RGO	PEC	0.1–100	0.025	93.74% after 4 weeks	-	[84]
MWCNTs/ gold nanorods	AMP	5.0–200	0.0085	>3 months	blood serum	[59]

Table 2. Cont.

Sensing Part	Method	LDR ¹ (μ M)	LOD ² (μ M)	L.T. Stability ³	Real Sample	Ref.
graphene nanosheets/manganese oxide nanoparticles	AMP	1–24	0.075	-	-	[170]
MnO ₂ nanoparticles	AMP	10–640	0.8	-	blood serum	[171]
dispersion of MWCNTs in metallopolymer	AMP	0.025–0.151	0.006	>one month	-	[119]
Ce-doped Mg–Al layered double hydroxide	AMP	10–5400	4.2	92.7% after 2 weeks	syrup sample	[172]
gold nanoparticles	CV	1–14 pM	0.6 pM	-	-	[61]
Co(II)-exchanged zeolite Y	CV	1 nM–1 mM	0.24 nM	>9 months	blood serum, urine, N-acetylcysteine tablet and powdered poultry feed samples	[173]
nanoporous gold	AMP	1–400	0.05	-	human urine	[62]
Au-NPs/poly-eriochrome black T	AMP	0.05–100	0.008	95% after 10 days	-	[63]
graphene oxide/Au nanocluster	CV	0.05–20	0.02	87.3% after 12 weeks	human urine	[64]
titanium (IV) phosphate composite	CV	200–9000	334	-	-	[174]
benzoylferrocene-modified MWCNTs	SWV	0.7–350	0.1	-	human hair, N-acetylcysteine tablet	[97]
vertically aligned MWCNTs modified with Pt nanoparticles	AMP	1–500	0.5	-	human urine	[103]
caterpillar-like manganese dioxide–carbon nanocomposite	AMP	0.5–680	0.022	-	>one month	[175]
Au NPs dispersed in Nafion	AMP	4.0–80.0	1.0	-	-	[65]
cobalt hexacyanoferrate NPs with a core-shell structure	AMP	3–37	0.04	-	blood serum and urine samples	[39]
yttrium hexacyanoferrate nanoparticle /MWCNT/Nafion	AMP	0.2–11.4	0.16	-	-	[176]
CdS quantum dot-methyl viologen complex	PEC	0.2–2.8	0.1	-	-	[177]
silver pentacyanonitrosylferrate	CV	0.1–20	0.035	-	>three months	[121]
gold-aminomercaptothiadiazole core-shell NPs	AMP	0.01–0.14	3 pM	96.5% after 10 days	blood serum and urine samples	[178]
conducting polymer/Au NPs	AMP	0.5–200	0.05	-	L-cysteine capsule	[66]
<i>p</i> -aminophenol/MWCNTs	DPV	0.5–100	0.3	-	urine, river water, blood plasma and serum samples	[98]
electrospun carbon nanofibers	AMP	0.15–64	0.1	-	-	[99]
1,1'-Ferrocenedicarboxylic acid	DPV	20–500	9.8	-	water samples	[122]

Table 2. Cont.

Sensing Part	Method	LDR ¹ (μM)	LOD ² (μM)	L.T. Stability ³	Real Sample	Ref.
AuPt alloy/MWCNTs-ionic liquid	AMP	0.5–40	-	95% after 15 days	-	[74]
quinizarine	DPV	1–1000	0.22	-	blood serum, acetylcysteine tablet	[100]
copper hexacyanoferrate	AMP	1–13	0.13	-	human urine	[110]
Pt nanoparticles/poly(o-aminophenol) film	AMP	0.4–630	0.08	93% after one month	syrup sample	[104]
gallium nitride nanowires	CV	0.5–75	0.5	86% after 5 days	-	[179]
silver nanoparticles coated polyquercetin	CPM ¹²	0.1–90 nM	0.03 nM	-	-	[70]
CuGeO ₃ nanowire	CV	1–1000	0.9	>2 weeks	tapwater	[111]

¹ Linear dynamic range in $\mu\text{mol/L}$ (unless otherwise specified); ² Limit of detection in $\mu\text{mol/L}$ (unless otherwise specified); ³ Long-term stability; ⁴ Reduced graphene oxide; ⁵ Photoelectrochemical; ⁶ Multi-walled carbon nanotube; ⁷ Molecularly imprinted polymer; ⁸ Linear sweep voltammetry; ⁹ Graphene oxide/carboxylated multiwalled carbon nanotube/manganese dioxide/gold nanoparticles composite; ¹⁰ Pico mol/L (= 10^{-12} mol/L); ¹¹ 8,9-dihydroxy-7-methyl-12H-benzothiazolo [2,3-b]quinazolin-12-one; ¹² Chronopotentiometry.

3.1.2. Methionine

Methionine, unlike cysteine, is an essential amino acid in human and other animals as it is not synthesized in the body, and the needed methionine should enter the body through methionine-containing foods or supplements. The literature survey showed that, in spite of the importance of methionine in body function, far fewer reports are found on the electrochemical detection of methionine in comparison to cysteine. This may originate from the lower electroactivity of the sulphur group of methionine that usually results in, if any, an ill-defined oxidation peak with high over-potential in aqueous solution (see Figure 8). Methionine occurs in our biological fluids at almost the same levels as cysteine. For example, for a healthy individual, the concentration of methionine in the blood serum is, on average, 25.5 μM (the range can be 13.7–43.5 μM) and in the urine sample is, on average, 5.9 μM (the range can be 0.4–35.1 μM) [180]. Therefore, to be applicable in biological-sample analysis, methionine sensors should practically have almost the same sensitivity as cysteine sensors, though the sulphur moiety of methionine is not as electroactive as the cysteine one. Nevertheless, some valuable studies have been carried out to face this challenge.

Noble metals and their alloys, as expected, are the main modifiers used in electrochemical methionine sensors [181–184]. These noble metals are exploited either in monometallic form [181,184] or as a bimetallic compound, e.g., Ru/Pt [182] and Ag/Au [183]. Bimetallic modifiers are expected to surpass their monometallic counterparts through improving the effective surface area, electron transfer rate, biocompatibility, electrocatalytic activity and invulnerability against interfering species and/or intermediate by-products of electrochemical reactions. In a study, Tavakkoli et al. [182] deposited a bimetallic monolayer of ruthenium/platinum (Ru/Pt) on gold electrodes. For this, first, the underpotential deposition of copper on gold electrode was carried out and followed by the replacement of this copper layer with Ru and Pt at open-circuit potential. This method results in an ultrathin Ru/Pt coating on the gold electrode that effectively facilitates the electrooxidation of methionine, as is seen in Figure 8A. A wide linear measurement range, 0.006–102 μM and a low LOD of 2.0 nM, were reported for this electrochemical sensor. Apart from precious noble metals, other more earth-abundant and cost-effective metal compounds such as MoS₂ [185], ZnO [186], MnO₃ [187], NiO [188], TiO₂ [189], Cu(II) phthalocyanine [190] and cobalt hydroxide nanoparticles [191] have shown acceptable performance as well.

Turning our attention to organic modifiers, some interesting reports are found in which a member of the carbon allotrope family, e.g., graphene derivatives, carbon nanotubes or diamond, is the key player [192–195]. Regardless of being eco-friendly, cost-effective and biocompatible, carbon-based modifiers owe a big part of their importance to the facility of surface and bulk modification in these materials. For example, the nature and abundance of oxygen functional groups on graphene oxide can be easily altered by applying different reduction potential, as Zhang et al. reported [193].

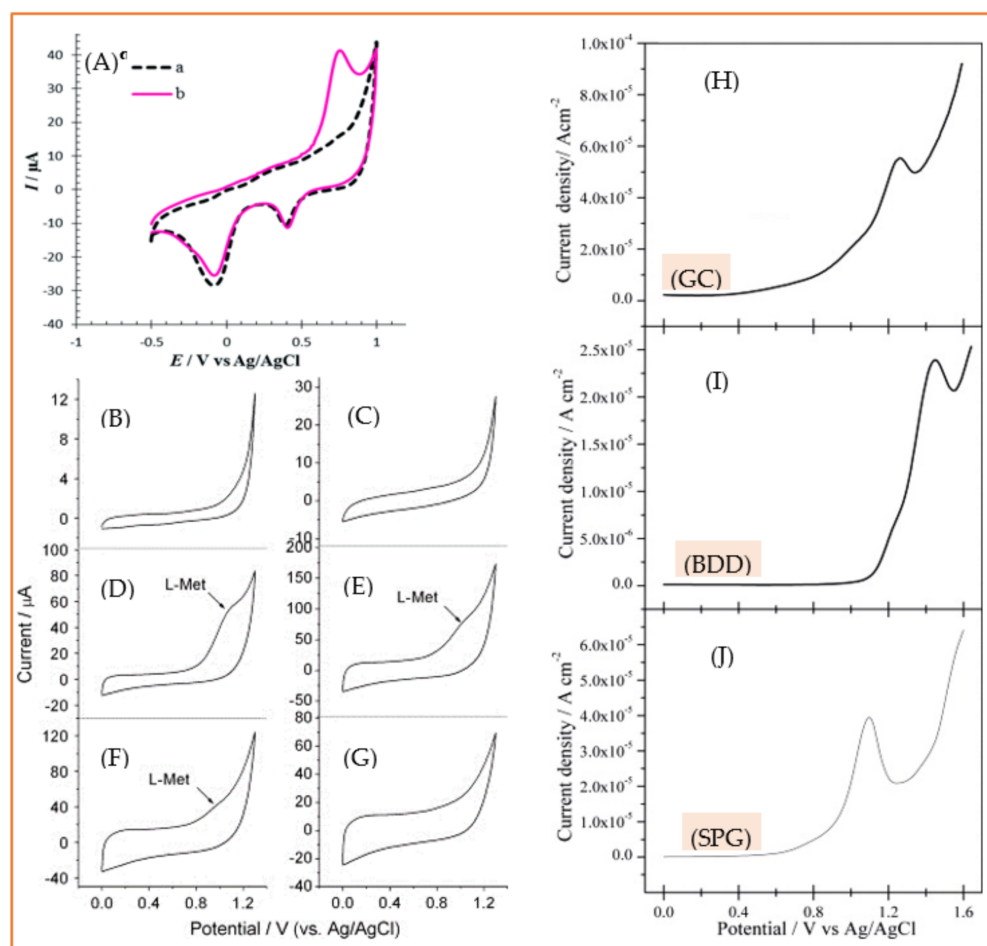


Figure 8. (A) Cyclic voltammograms of Ru/Pt-modified electrode (A) without and (B) with 100 μM methionine in 0.1 M phosphate buffer solution (pH = 7), with a scan rate 10 mV s^{-1} . Reprinted with permission from ref. [184]. Copyright 2017 Royal Society of Chemistry. CVs of 5 mM methionine in pH 5.5 PBS at bare GC (B) and GO/GC electrodes pretreated at different potentials. (C): -0.65 V ; (D): -0.75 V ; (E): -0.8 V ; (F): -0.9 V ; (G): -1.2 V , Reprinted with permission from ref. [195]. Copyright 2011 Elsevier. Comparison of the DPV of different carbon-based electrodes: GC (H), BDD (I) and SPG (J) electrodes for the direct oxidation of 1 mM methionine in 0.1 M phosphate buffer solution (pH 7). Reprinted with permission from ref. [196]. Copyright 2014 Elsevier.

As shown in Figure 8B, no oxidation peak for methionine is observed in the cyclic voltammograms of bare glassy carbon electrodes (GCE). After adding graphene oxide (GO) to the GCE, different pretreatment potentials were applied to convert GO to reduced graphene oxide (rGO). The reduction of GO to rGO results in an increase in conductivity by removing the oxygen functional groups from GO. This has two contradictory effects on the electrochemical performance of the sensor. On one hand, converting GO to rGO is beneficial since rGO is much more conductive compared to GO. On the other hand, the presence of these functional groups is critical, as they play the key role in the electrooxidation of methionine. Considering this, the best performance for this sensor is observed when an

intermediate reduction potential is applied in the conversion of GO to rGO (Figure 8C). This example clearly shows that how much an electrochemical sensor can be susceptible to the surface features insofar as even 0.1 V variation in applied potential can result in a completely different response.

Regardless of all modification strategies, Gómez-Mingo et al. [194] compared the performance of three well-known bare electrodes, namely glassy carbon (GC), boron doped diamond (BDD) and screen-printed graphite (SPG) electrodes, as electrochemical sensors using differential pulse voltammetry (Figure 8H–J). No chemical or electrochemical treatment was carried out to activate the bare electrodes where the SPG electrode showed the best performance, taking into account both lower oxidation peak potential and higher peak current. Although the linear dynamic range (50–5000 μM) and LOD (95 μM) were not appropriate enough to be used for measuring methionine in biological fluids, this simple electrochemical sensor can be successfully used to evaluate methionine in pharmaceutical samples. Table 3 presents various developed strategies for electrochemical methionine detection over the last decade.

Table 3. Proposed electrochemical methionine sensors, since 2010, along with the most important respective figures of merit.

Sensing Part	Method	LDR ¹³	LOD ¹⁴	L.T. Stability ¹⁵	Real Sample	Ref.
3D-printed electrodes	SWV	5–230	1.39	-	human serum	[196]
silver oxide	AMP	60–500	0.42	-	blood serum	[181]
single layer MoS ₂	PEC	0.1–1000 nM	0.03 nM	>28 days	blood serum	[185]
Mn ₂ O ₃	DPV	1–610	0.001		seafood sample	[187]
ruthenium/platinum bimetallic monolayer coated on a nanoporous gold film	DPV	0.006–102	0.002	97.3% after 3 weeks	human urine	[182]
Ag–Au core-shell bimetal nanoparticles	AMP	50–1000	30	96% after a week	-	[183]
ZnS/ZnAl ₂ S ₄ nanocomposite	SWV	0.05–800	0.01	-	blood serum and urine	[197]
RGO/ α -cyclodextrin	AMP	170–1200	40	>7 days	-	[192]
graphene oxide	DPV	450–4950	100	-	-	[193]
imprinted polybenzidine/MWCNTs functionalized –COOH	DPV	11.7–206.3 ng/L	3 ng/L	-	pharmaceutical and blood serum samples	[41]
Pt doped TiO ₂ NPs/CNT	AMP	0.5–100	0.1	88% after 2 weeks	blood serum	[189]
benzoylferrocene modified MWCNTs	SWV	0.1–200	0.058	-	urine sample	[198]
electropolymerized functionalized triazole polymer	AMP	0.1–100	4.1×10^{-4}	97.65% after 2 weeks	urine sample	[199]
electropolymerized film of non-peripheral amine substituted Cu(II) phthalocyanine	DPV	50–500	0.027	>one month	blood serum	[190]
bare screen-printed graphite electrodes	DPV	50–5000	95	-	pharmaceutical products	[194]
cobalt hydroxide nanoparticles	AMP	245–1210	160	-	-	[191]
MWCNTs	AMP	360–6900	270	-	pharmaceutical product	[195]
fullerene-C ₆₀ modified gold electrode	CV	Up to 100	8.2	-	root beer syrup and methionine pill	[200]

¹³ Linear dynamic range in $\mu\text{mol/L}$ (unless otherwise specified); ¹⁴ Limit of detection in $\mu\text{mol/L}$ (unless otherwise specified); ¹⁵ Long-term stability.

3.2. Aromatic Amino Acids

3.2.1. Tryptophan

The recommended daily dose of tryptophan (Trp) for a healthy adult is estimated to be in the range of 250–425 mg. This means that, since Trp is an essential dietary requirement for human and cannot be synthesized in the body, a dietary intake of approximately 3.5–6.0 mg/kg of body weight should be daily provided through foods, supplements or medicines [14]. Of this dietary Trp, less the 1% enters through the protein synthesis pathway, while the rest is degraded and used to produce some physiologically significant

substances such as melatonin, serotonin, tryptamine, niacin and kynurenine. Clinical relevant urinary Trp in a healthy adult is in the range of 20–70 μM . It is worth mentioning that, due to the fluctuation in substance concentration in urine samples with time of day and intake of water, it is more acceptable to report total 24-h amount rather than the measured concentrations at any time. However, a 24-h urine collection is not convenient. This normal range of urinary Trp can even increase to 0.1–10 mM in people suffering from some inborn metabolic diseases [201]. Likewise, abnormalities in the blood level of Trp, which is in the range of 45.5–83.1 μM for a healthy individual, can also be a sign of the body malfunctioning [202]. Considering the biological significance and widespread usage in food and feed industries, and of course its relatively high electroactivity, tryptophan has acquired the second place, after cysteine, with respect to the number of published paper in this field; see Figure 2C.

In contrast to cysteine and methionine, noble metals are not at top of the list of the most-used modifiers for electrochemical Trp sensors; this place is taken by organic modifiers. Designing these organic-based electrochemical sensors can be as easy as adding MWCNTs to a carbon paste electrode [203] or blending carbon dots with chitosan [204], or it might require a more sophisticated process, e.g., the functionalization of graphene with poly(sodium 4-styrenesulphonate) [205], carbon black with oxygenated groups [206] or graphene quantum dots with amino groups [207]. In a very simple approach, Zanini et al. [42] modified an electrochemically activated GCE by dipping it in a solution containing 0.5 wt% chitosan for 20 min. Though the preparation process was quite easy, this electrochemical sensor could effectively measure Trp in acidic media (PBS, pH = 4) wherein the peak current for the oxidation of Trp at a chitosan-modified electrode was more than 40 times higher than that of bare GCE; see Figure 9A. This significant enhancement in sensitivity was ascribed to the proton relay effect of chitosan (Figure 9B), through hydrogen bonding between chitosan and Trp. Roushani et al. [204] went further and incorporated carbon nanodots into the chitosan film, attempting to fabricate a sensor with higher electrical conductivity and larger specific surface area. MWCNT [208], graphene oxide [209] and graphene quantum dots [210] were also mixed with chitosan and used to develop Trp sensors.

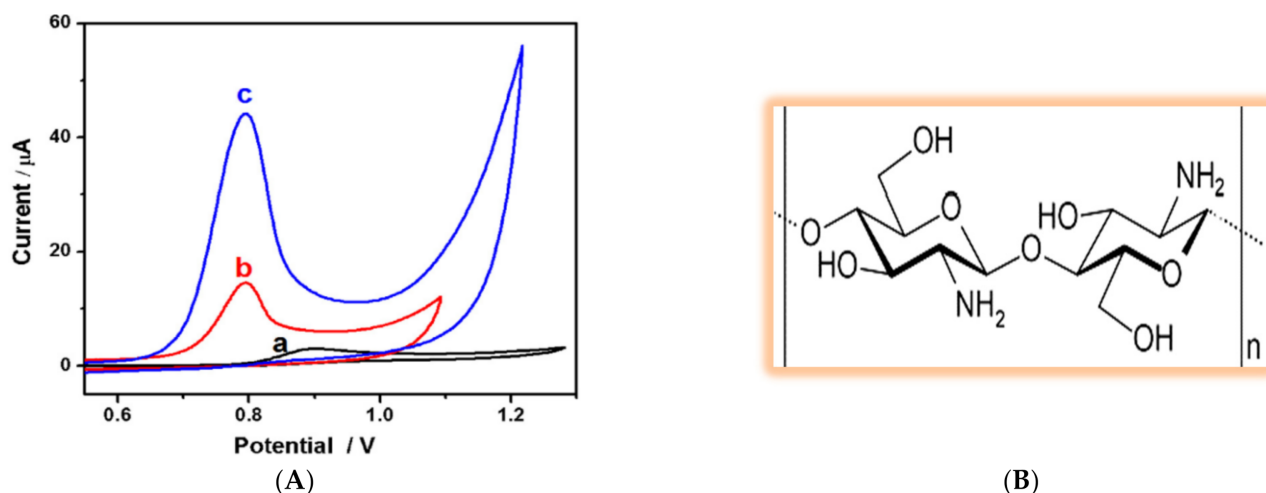


Figure 9. (A) Cyclic voltammograms of 100 μM tryptophan (in 0.1 M PBS pH 4.0) at (a) bare GCE, (b) electrochemically activated bare GCE and (c) chitosan-modified GCE. Reprinted with permission from ref. [42]. Copyright 2015 Elsevier. (B) The chemical structure of chitosan.

In addition to promoting sensitivity, modifiers have also been used to suppress the interference effect of some potential interferences. Benzenesulphonic acid derivatives, for example, have been shown to successfully alleviate the interference effect of uric acid, UA and ascorbic acid (AA), especially when they are used in near-neutral or slightly acidic medium. When used, poly(sulphosalicylic acid) [211] and poly(sodium 4-styrenesulphonate) [205] caused, respectively, about 3- and 100-fold enhancement in the peak currents of Trp oxida-

tion with respect to the bare electrode (Figure 10A,B), while, concurrently, the interference issue of UA and AA was acceptably resolved. The enhanced sensitivity is related to, on one hand, the hydrophobic interaction between the hydrophobic moiety of Trp (indole ring) and the benzene part of these modifiers and, on the other hand, electrostatic interaction between the negatively charged benzenesulphonic part and the positively charged Trp in relatively acidic medium. Additionally, the anti-interference effect against AA and UA stems from the electrostatic repulsion of negatively charged AA and UA and benzenesulphonic moiety in a slightly acidic condition. Apart from UA and AA, the presence of other amino acids can be challenging for electrochemical Trp sensors. Kumar et al. [212] successfully used a flower-like cerium vanadate (CeVO_4) microstructure as a modifier to resolve this issue. Using this modifier in neutral medium, 0.05 M PBS pH = 7, led to an enhancement in peak current (sensitivity) (Figure 10C), whereas other electroactive amino acids, e.g., cysteine, methionine and histidine, did not show an interference effect (Figure 10D). However, the most severe interfering amino acid for electrochemical Trp detection is tyrosine, which has not been investigated by authors.

Alongside the aforementioned issues, i.e., sensitivity and interference effect, electrode fouling is another challenge in electrochemical Trp sensing. This problem mainly arises from the by-products and/or products that are produced and that cover the electrode surface during electrochemical measurements. Electrode fouling or electrode passivation leads to decay in signal current over time and, consequently, the loss of the original sensitivity. Occupying the active reaction sites at the electrode surface by adsorbate species and the potential drop across the adsorbed fouling layer at the electrode surface is assumed to cause this decay in sensitivity [213]. Polymeric products, as shown in the proposed electrochemical oxidation pathway of Trp (see Figure 4) are the main suspect for electrode fouling in electrochemical Trp sensors. Figure 11A clearly shows this undesired phenomenon when a bare GCE is placed in PBS solution containing 1mM Trp, and five consecutive cyclic voltammograms are recorded. As is seen, in the first potential scan, a strong oxidation peak is observed for Trp, while the second oxidation peak declines significantly and for the next potential cycles almost no oxidation peak is detectable. Ionic liquids, i.e., molten salts whose melting point is lower than 100 °C [214], have shown great potential to face this challenge. Figure 11B shows that, in the presence of ionic liquid, just a slight decay in the oxidation peak of Trp occurs even after applying five successive potential cycles. Safavi and Momeni [215] ascribed this resistance of the electrode against fouling to the ionic liquid content of the electrode and its polarity. The ability of ionic liquid to dissolve the reaction products and drag them inside, as is seen for mercury electrodes, is assumed to play the key role. This anti-fouling capability was also reported when ionic liquids are mixed with MWCNTs [216].

Besides the aforesaid reports whose aim was mainly promoting the sensitivity of Trp sensors and, concurrently, addressing other critical issues, i.e., selectivity and electrode fouling, other reports are found in the literature that aimed at reducing the analysis time [201,217] and/or the cost [49,102] of the sensors. The reports on electrochemical Trp measurement, since 2010, were collected and tabulated and are presented in Table 4.

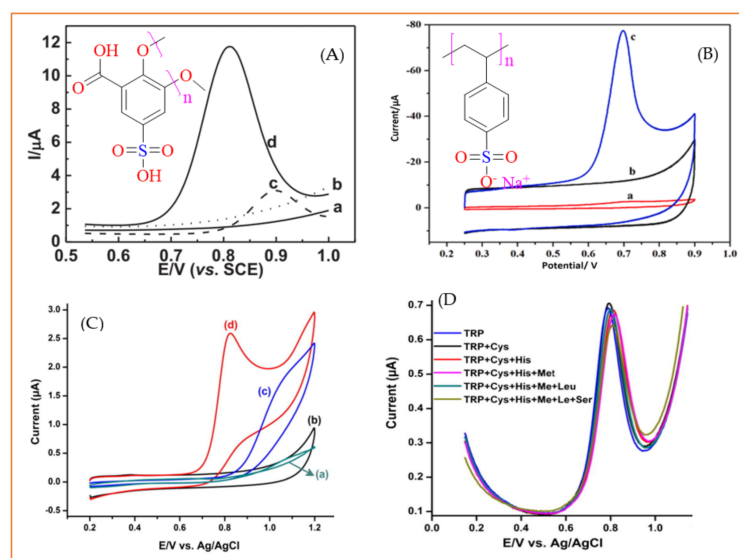


Figure 10. (A) Differential pulse voltammograms of the bare GCE (a,c) poly(sulphosalicylic acid)/GCE (b and d) in a PBS solution (0.1 M, pH = 3.5) in the absence (a,b) and presence (c,d) of 100 μM Trp. Reprinted with permission from ref. [214]. Copyright 2013 Elsevier. (B) Cyclic voltammograms of (a) bare GCE in PBS (pH = 6) containing 20 μM Trp, PSS–graphene/GCE in (b) blank solution (c) PBS containing 20 μM Trp. Reprinted with permission from ref. [208]. Copyright 2019 Elsevier. (C) Cyclic voltammograms obtained in PBS (pH 7) at bare GCE (a,c) and modified CeVO_4 /GCE (b,d) in the presence (c,d) and the absence (a, b) of 100 μM tryptophan. (D) Differential pulse voltammograms of tryptophan in the presence of some representative amino acids including serine (Ser), leucine (Leu), cysteine (Cys), methionine (Met) and histidine (His) Reprinted with permission from ref. [215]. Copyright 2017 Elsevier. Inset (A) and (B) are the chemical structures of poly(sulphosalicylic acid and poly(sodium 4-styrenesulphonate)), respectively.

Table 4. Proposed electrochemical tryptophan sensors, since 2010, along with the most important corresponding figures of merit.

Sensing Part	Method	LDR (μM)	LOD (μM)	L.T. Stability	Real Sample	Ref.
octahydropyrimido[1,2-a] azepine	DPV	1.5–750	0.05	>one month	blood and urine samples	[218]
nickel nanoparticle/Nitrogen-carbon nanohybrid	SDLSV ₁₆	0.01–80	0.006	92.77% after 2 weeks	human serum and pharmaceutical samples	[219]
3-neomenthylindene	DPV	2.5–300	1.71	95.4% after 5 days	urine and blood plasma	[220]
CeO_2 /rGO composite	SDLSV	0.01–10	0.006	88.7% after 2 weeks	amino acid injection, human serum and urine	[221]
CeO_2 /rGO composite	DPV	0.2–25	0.08	>one month	milk and bovine serum samples	[222]
silver zeolite nanocomposite	DPV	0.01–1.2	0.0063	-	wheat flour, goat and cow milk	[223]
pencil graphite electrode	ASDPV ₁₇	0.154–200	0.046	-	urine sample	[224]
rGO decorated with 18-crown-6 and gold nanoparticles	SWV	0.1–2.5	0.05	77% after 50 days	human serum	[225]
poly (3,4-proplenedioxy thiophene)@nitrogen-doped carbon hollow spheres composites	DPV	0.1–100	0.0092	-	-	[226]

Table 4. Cont.

Sensing Part	Method	LDR (μM)	LOD (μM)	L.T. Stability	Real Sample	Ref.
rGO/gold nanoparticles	DPV	0.5–500	0.39	-	saliva, serum and plasma	[227]
polythiophene/silver dendrites composite	SWV	0.2–400	0.02	-	soybeans extract	[228]
MWCNT and molecularly imprinted polymer	SDLSV	0.002–100	0.001	91% after 2 weeks	human serum	[229]
polyvinylpyrrolidone functionalized graphene	SDLSV	0.06–100	0.01	88% after 20 days	urine, serum and injection samples	[230]
CuSn(OH) ₆ microsphere decorated on rGO	DPV	0.05–175.8	0.002	95% after 15 days	urine sample	[231]
Pd-Ag nanoparticles	DPV	0.1–1000	0.1 (at pH 4)	-	-	[232]
polydopamine/rGO/MnO ₂ composite	AMP	1.23–303.26	0.24	94% after one month	tomato fruit and juice	[233]
molecularly imprinted copolymer/MWCNT	DPV	0.008–26	0.006	92.7% after 30 days	amino acid oral liquid and human serum samples	[234]
nitrogen-doped ordered mesoporous carbon	CV	0.5–200	0.035	95.4% after one month	amino acid cocktails	[235]
rGO, gold nanoparticles, poly-L-cysteine, and poly-L-phenylalanine methyl ester	AMP	100–800	44	87.7% after 5 weeks	-	[236]
perovskite-type SrTiO ₃ nanocubes/rGO	AMP	0.03–917.3	0.0071	96.2% after 2 weeks	urine and blood serum	[237]
hydroxyapatite/graphene oxide	LSV	7–1000	5.5	-	sunflower and pumpkin seeds	[238]
poly(3,4-ethylenedioxythiophene)	CV	10–400	7.2	-	urine and serum samples	[239]
3D nitrogen-doped reduced graphene oxide and self-assembled polysaccharides	DPV	10–5000	0.0035	96.9% after 22 days	human urine and serum	[240]
silver molybdate/rGO	AMP	0.002–146.9	0.0057	-	milk and oat samples	[241]
molecularly imprinted chitosan film	SDLSV	0.01–100	0.008	91% after 20 days	human serum, amino acid injections	[242]
graphene functionalized with 3,4,9,10-perylene tetracarboxylic acid and chitosan	DPV	1–10 mM	1.2	96.7% after 2 weeks	human urine and serum	[243]
Ta ₂ O ₅ -rGO	SDLSV	1–800	0.84	-	human serum	[244]
MWCNT@polydopamine composite loaded with copper(II)	DPV	1–100	0.15	93.4% after 30 days	-	[245]
exfoliated graphene and poly(3,4-ethylenedioxythiophene):poly(styrene sulphonate)	DPV	0.1–1000	0.015	98.9% after 2 weeks	-	[246]
cuprous oxide and electrochemically rGO	SWV	0.02–20	0.01	94.28% after 2 weeks	human serum and commercial amino acid injections	[247]
poly(sodium 4-styrenesulphonate) functionalized graphene	LSV	0.04–10	0.02	89.2% after 7 days	human serum sample	[205]

Table 4. Cont.

Sensing Part	Method	LDR (μM)	LOD (μM)	L.T. Stability	Real Sample	Ref.
manganese cobaltite entrapped rGO	AMP	0.004–112.9	0.001	-	milk sample	[248]
Fe ₃ O ₄ /C composite	SDLSV	1–800	0.26	90.4% after one week	human blood serum	[249]
gold nanoparticles electrodeposited onto graphite-polyurethane	DPV	0.6–2.0	0.053	-	synthetic urine and commercial poly-amino acids supplement	[250]
anionic/cationic-pillar [5]arenes multilayer film	DPV	1–300	0.3	-	blood serum	[105]
alumina/graphene/Cu hybrid	DPV	1–1000	0.009	>10 days	urine sample	[251]
flowerlike Fe ₃ O ₄ @NiO magnetic nanoparticles	DPV	0.1–120	0.014	89% after one month	human breast milk, cow milk and honey	[150]
NiO/carbon nanotube/PEDOT ¹⁸ composite	DPV	1–41	0.21	100.5% after 37 days	blood serum	[252]
amino-modified β -cyclodextrin (NH ₂ - β -CD), gold-platinum core-shell microspheres	DPV	10–5000	4.3	91.7% after 15 days	milk samples	[253]
surface-confined chromium-salen complex	EIS ¹⁹	4–60 nM	0.78 nM	-	blood serum	[254]
functionalized carbon black/poly-L-histidine nanocomposite	AMP	0.025–125.0	0.008	92% after 2 weeks	milk and human urine	[206]
Schiff-based Cu(II) complex	CV	7–48	0.185	>3 weeks	milk sample	[255]
activated MWCNTs Ionic Liquid	CV	5–1000	2.3	-	commercial amino acid injection and blood serum	[256]
silver nanodendrites implemented in poly(lactide-thiocalix [4]arene copolymer	DPV	0.1–100	0.03	90% after 6 weeks	tryptophan sedative medication	[257]
cerium-doped ZnO and functionalized MWCNTs	DPV	0.01–0.1	0.001	97% after one week	blood serum and milk samples	[258]
tetrabutylammonium bromide on the β -cyclodextrin incorporated MWCNTs	DPV	1.5–30.5	0.07	90% after 20 days	blood serum	[259]
magnetic coreshell manganese ferrite nanoparticles/ionic liquid	SWV	5–400	1.1	-	urine sample	[260]
Pd–Cu@Cu ₂ O/N-rGO	DPV	0.01–40.0	1.9 nM	-	urine and milk samples	[261]
bismuth sulphide/sulphur doped graphene nanocomposite	DPV	0.01–120	0.004	-	-	[262]
poly(L-arginine)/rGO and gold nanoparticles	DPV	0.01–100	0.1	95% after 2 weeks	urine sample	[263]
MWCNTs-CTAB ²⁰ nanocomposite	DPV	4.9–64.1	1.6	-	blood serum	[264]
mesoporous silica nanoparticles	DPV	0.05–600	0.011	-	artificial urine	[265]
Fe ₃ O ₄ magnetic nanoparticles/graphene quantum dots	DPV	0.08–150	0.08	-	-	[266]

Table 4. Cont.

Sensing Part	Method	LDR (μM)	LOD (μM)	L.T. Stability	Real Sample	Ref.
nanoporous carbon	AMP	1–103	0.03	93.7% after 3 weeks	amino acid injection, fetal calf serum samples	[102]
rGO decorated with polypyrrole nanofibers and zinc oxide-copper oxide	DPV	0.053–480	0.01	97.86% after 2 weeks	blood serum	[267]
Ni-doped Lewatit FO36 nano ion exchange resin	DPV	4–560	0.38	89.7% after 2 months	water, urine, serum and pharmaceutical samples	[268]
tricobalt tetroxide nanoparticles decorated carbon nanofibers	AMP	0.005–40	0.002	96% after 20 days	pharmaceutical samples	[269]
rGO decorated with $\text{SnO}_2\text{-Co}_3\text{O}_4$ nanoparticles.	DPV	0.02–6.0	0.0032	95.7% after 14 days	blood serum, urine and pharmaceutical samples	[270]
amino-functionalized graphene quantum dots/ β -cyclodextrin	DPV	1–30	0.65	94% after 2 months	-	[207]
unzipped MWCNT incorporated overoxidized poly(<i>p</i> -aminophenol)	DPV	5–1265	0.47	94.7% after one month	blood serum and urine samples	[271]
AgNPs/graphene oxide-poly(L-arginine)	DPV	1–150	0.122	-	urine sample	[272]
graphene oxide/NiO nanocomposite and <i>n</i> -hexyl-3-methylimidazolium hexafluoro phosphate	SWV	5–700	1	-	urine and pharmaceutical samples	[273]
mixed oxide $\text{SiO}_2/\text{Nb}_2\text{O}_5/\text{ZnO}$ metallization with iron(III) and inserted into the porphyrin ring	SWV	10–70	3.28	-	pharmaceutical samples	[274]
polythiophene nanostructures	LSV	6–180	0.61	-	blood serum and urine	[275]
graphite-like carbon nitride nanosheets	LSV	0.1–110	0.024	91.8% after 30 days	amino acid injection and rat blood serum	[276]
flower-like cerium vanadate	DPV	0.1–94	0.024	98.4% after one week	milk and urine samples	[212]
rGO) decorated with SnO_2	DPV	1–100	0.04	>2 weeks	milk and amino acid injection samples	[277]
poly(β -cyclodextrin)/carbon quantum dots composite	DPV	5–270	0.16	94.7% after 2 weeks	urine sample	[278]
MWCNT/ ionic liquid nanocomposite	DPV	0.5–70	0.32	-	dough sample	[279]
ZnFe_2O_4 nanoparticles	DPV	0.1–200	0.04	-	blood serum and urine samples	[280]
MWCNTs	DPV	0.6–100	0.065	-	blood serum	[203]
MWVNTs/1-(allyloxy)-4-nitrobenzene	DPV	0.06–40	0.007	-	blood serum, milk and pharmaceutical samples	[281]
polyoxometalate functionalized rGO	SWV	0.001–1 nM	0.002 nM	97.75% after 45 days	blood serum	[282]
CTAB/phosphotungstic acid/rGO	DPV	0.1–300	0.02	99.73% after one month	amino acids injection sample	[283]

Table 4. Cont.

Sensing Part	Method	LDR (μM)	LOD (μM)	L.T. Stability	Real Sample	Ref.
β -cyclodextrin-platinum nanoparticles/graphene nanohybrids	DPV	50–5000	17	93.7% after one week	Trp enantiomers mixture	[284]
N-doped carbon dots/ β -cyclodextrin	DPV	5–70	1.7	-	Trp enantiomers in riboflavin sample	[285]
poly(L-methionine) and graphene composite film	DPV	0.2–150	0.017	89.7% after one month	milk and blood serum samples	[286]
β -cyclodextrin modified magnetic graphene oxide	DPV	0.5–750	0.3	97.4% after 15 days	commercial amino acid preparations	[287]
tellurium nanorods	AMP	0.02–11.48	0.01	90% after 20 days	commercial amino acid injection	[288]
nickel and copper oxides-decorated graphene	SWV	0.3–40	0.1	95% after one month	blood serum and pharmaceutical samples	[289]
4-amino-3-hydroxy-1-naphthalenesulphonic acid/rGO based polymer	SWV	0.5–200	0.31	93.33% after one month	pharmaceutical formulations, human urine and plasma samples	[290]
SiO ₂	DPV	0.05–400	0.034	>2 months	artificial urine sample	[291]
NiO nanoparticle coupled ionic liquid	SWV	0.08–350	0.04	-	urine and water samples	[292]
metal-organic framework/silver nanoparticles composite	DPV	1–150	0.14	-	urine sample	[293]
Pt/CNTs nanocomposite/ionic liquid	SWV	0.1–400	0.04	>40 days	meat and pharmaceutical samples	[294]
nitrogen-incorporated tetrahedral amorphous carbon thin film	AMP	0.1–100	0.089	-	-	[295]
silver film loaded on carbon paper	LSV	0.1–330	0.04	93% after 2 weeks	milk sample	[296]
carbon-supported NiCoO ₂ nanoparticles	DPV	50–943.4	5.7	90.31% after 20 days	blood serum, urine and pharmaceutical samples	[297]
Cu NPs/overoxidized poly(3-amino-5-mercapto-1,2,4-triazole) film	DPV	4–144	0.16	-	blood serum and urine samples	[298]
Fe ₂ O ₃ /SnO ₂ composite	DPV	0.6–70	0.1	-	blood serum and pharmaceutical samples	[299]
nitrogen-doped graphene nanosheets/CuCo ₂ O ₄ nanoparticles	DPV	0.01–3.0	0.0041	-	urine, serum and pharmaceutical samples	[300]
carbon nanodots/chitosan	DPV	Up to 90	0.09	98.4% after 3 days	blood serum	[204]
chitosan film	DPV	0.1–130	0.04	>one week	pharmaceutical samples	[42]
graphene/silicon oxide	DPV	0.5–200	0.495	96.5% after 2 months	-	[301]

Table 4. Cont.

Sensing Part	Method	LDR (μM)	LOD (μM)	L.T. Stability	Real Sample	Ref.
MWCNTs decorated with Nickel NPs	SWV	0.02–1.0	0.0066	95.1% after 3 weeks	milk and pharmaceutical samples	[302]
SWCNTs	LSV	0.5–50	0.05	-	blood serum	[303]
Ag-MoS ₂ /chitosan	DPV	0.5–120	0.05	-	urine sample	[304]
MIP from co-electropolymerization of o-phenylenediamine and hydroquinone	DPV	0.01–1.0	0.005	-	Trp enantiomers mixture	[305]
MWCNT functionalized with 5-amino-2-mercapto-1,3,4-thiadiazole	AMP	25–300 nM	0.54 nM	-	blood serum	[306]
<i>p</i> -sulphonated calix[4]arene complex	CV	0.1–10	0.03	90% after one week	blood serum and amino acid injection samples	[307]
gold nanoparticles decorated graphene oxide nanocomposite	AMP	5–25	0.29	-	-	[308]
acetylene black/graphene	DLSV ²¹	1–100	0.06	92% after 2 weeks	compound amino acid injections and humanserum samples	[309]
<i>p</i> -phenylenediamine covalently linked with cysteamine capped cadmium sulphide quantum dots	SWV	100–500	14.74	-	beverage sample	[310]
ruthenium xanthate complex	DPV	0.25–50	0.083	>3 days	pharmaceutical samples	[311]
boron-doped diamond (BDD) electrodes and wires	DPV	Up to 250	0.5	-	blood serum	[216]
MWCNTs	AMP	0.6–100	0.033	94.6% after one week	milk and blood serum samples	[216]
MWCNT modified sol-gel	DPV	0.2–15	0.139	-	milk sample	[312]
Au NPs/poly(alizarin red S) film	AMP	0.02–20	0.0067	-	-	[313]
carbon fiber ultramicroelectrodes	CV	50–200	16.7	-	pharmaceutical samples	[217]
MWCNT/Mg-Al-CO ₃ layered double hydroxide	LSV	3–1000	0.0068	93.7% after one week	milk and blood serum samples	[314]
poly-sulphosalicylic acid	DPV	0.05–10	0.0068	95.24% after 4 weeks	blood serum and amino acid injection samples	[211]
electrochemically reduced graphene oxide	DPV	0.2–40	0.1	91.6% after 2 weeks	-	[315]
gold nanoparticles/macroporous carbon composites	DPV	10–1000	0.024	91% after 3 weeks	blood serum	[316]
Co ₃ O ₄ nanoparticles-decorated graphene	AMP	0.05–10	0.01	94% after 4 weeks	liquid Dulbecco's modified Eagle medium and amino acid injection samples	[317]
SiO ₂ nanoparticles	LSV	0.1–50	0.036	95.4% after one week	blood serum and pharmaceutical samples	[318]

Table 4. Cont.

Sensing Part	Method	LDR (μM)	LOD (μM)	L.T. Stability	Real Sample	Ref.
TiO ₂ -graphene/4-aminobenzenesulphonic acid composite	DPV	1–400	0.3	96.08% after 20 days	human blood serum	[319]
β -cyclodextrin functionalized Fe ₃ O ₄ magnetic nanoparticles	DPV	0.8–300	0.5	-	amino acid injection sample	[320]
Si-doped nano-TiO ₂	CV	1–400	0.5	90.3% after one month	amino acid injection sample	[321]
oxidation product of TRP	DPV	0.5–50	0.05	>30 days	blood serum	[322]
cobalt(II) coordination polymer	DLSV	0.2–80	0.1	>30 days	amino acid injection sample	[323]
binuclear manganese(II) complex	DLSV	0.1–80	0.08	>30 days	amino acid injection sample	[324]
nano-mixture of graphite/diamond	LSV	0.1–80	0.03	-	human synthetic serum	[325]
copper hexacyanoferrate film on cysteamine-gold nanoparticle graphite-wax composite	CV	0.085–120	0.0185	>25 days	milk sample	[326]
chemical vapor deposited MWCNTs	CV	0.001–100	0.22 nM	>2 months	pharmaceutical samples	[327]
poly(9-aminoacridine) functionalized MWCNT	DPV	1–500	0.81	>2 months	pharmaceutical samples	[328]
nano-structured Ni (II)/(2-amino-1-cyclopentene-1-dithiocarboxylic acid) film	AMP	0.085–43.0	0.023	-	blood serum	[329]
nafion and TiO ₂ -graphene nanocomposite,	DPV	5–140	0.7	92% after 2 weeks	-	[330]
<i>p</i> -aminophenol/MWCNTs	DPV	10–300	5.7	-	urine, river water, blood plasma and serum samples	[98]
boron-doped diamond nanowires	DPV	0.5–50	0.5	-	-	[331]
dibenzo-18-crown-6 and Ni ²⁺ ion	DPV	1.96–1010	0.0979	-	apple, guava, red grape juice, milk and pharmaceutical samples	[332]
gold nanoparticles	SWV	5–900	4	-	amino acid injection sample	[215]
carbon ionic liquid	CV	8–1000	4.8	96.87% after 4 weeks	synthetic amino acid mixtures	[333]
poly(methyl red) film	LSV	0.1–100	0.04	-	amino acid injection sample	[334]
gold nanoparticles (AuNPs) onto carbon nanotube (CNT) films	AMP	0.03–2.5	0.01	-	pharmaceutical samples	[335]

¹⁶ Second-order derivative linear sweep voltammetry; ¹⁷ Adsorptive stripping differential pulse voltammetry; ¹⁸ Poly(3,4-ethylenedioxythiophene); ¹⁹ Electrochemical impedance spectroscopy; ²⁰ Cetyltrimethylammonium bromide; ²¹ Derivative linear sweep voltammetry.

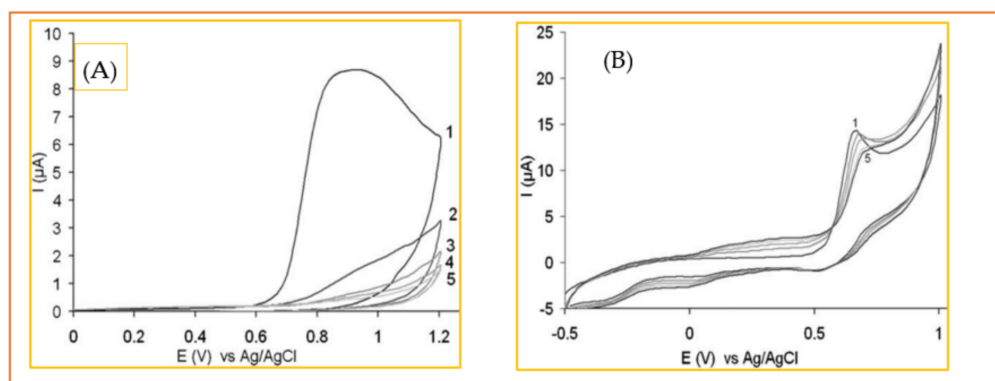


Figure 11. Cyclic voltammograms of 1 mM solution of tryptophan in 0.1 M PBS (pH 7) for five consecutive scans at (A) bare GCE and a (B) gold nanoparticle/ionic liquid electrode. Reprinted with permission from ref. [218]. Copyright 2010 Wiley.

3.2.2. Tyrosine

Tyrosine (Tyr) is known as a non-essential amino acid since, naturally, the body can produce it from another amino acid called phenylalanine. Additionally, Tyr is found in meats, wheat, nuts, eggs and dairy products, especially in cheese, where it was first discovered. Tyr is the main ingredient in protein supplements that are commonly used to treat an inherited disorder called phenylketonuria. Note that the phrase “non-essential amino acid” should not lead to a false conclusion that the function of Tyr is not important for the body. On the contrary, Tyr is one of the most important amino acids in terms of body function and application in different industries; see Table 1. Since the level of Tyr, like other amino acids, is affected by different factors, e.g., gender, age, dietary habits, physical activity, etc., different values have been reported so far for the normal level of Tyr in biological fluids. The normal level of Tyr in human blood has been reported to be $48.6 \pm 3.0 \mu\text{M}$ [336], $77 \pm 12 \mu\text{M}$ [337], $90.6 \pm 22.9 \mu\text{M}$ [338] and $30\text{--}120 \mu\text{M}$ [339], while for a healthy individual, free tyrosine excretion in urine could be in the range of $88\text{--}270 \mu\text{mol}$ per day [340]. However, adverse clinical manifestations of elevated Tyr level do not typically appear until the Tyr concentration of blood exceeds $500 \mu\text{M}$ [341].

Undoubtedly, carbon-based materials are of among the most important modifiers used to construct electrochemical Tyr sensors in terms of both enhancing the sensitivity and/or selectivity of the sensor. Various typologies of carbon nanomaterials have been used so far for Tyr detection, including reduced graphene oxide [342], MWCNTs [343], SWCNTs [344], graphene quantum dots [345] and boron-doped diamond [346]. Baig and Kawde [342] proposed a very cheap, simple and reusable electrochemical sensor for Tyr simply through the electrodeposition of graphene oxide on a graphite pencil electrode (GPE). Though the preparation method was quite straightforward, the resultant sensor showed an extraordinary enhancement in oxidation peak current (ca. 104 times compared to unmodified GPE), as shown in Figure 12A. The LOD of this sensor was calculated to be $0.07 \mu\text{M}$, and it was successfully used to measure Tyr in urine samples. In another simple yet effective strategy, D’Souza et al. [343] blended MWCNTs with carbon paste electrode (CPE) to fabricate a sensor that was able to measure Tyr in a linear range of $0.8\text{--}100 \mu\text{M}$ with LOD of $0.014 \mu\text{M}$ in neutral pH. Authors reported that carboxylic-acid-functionalized MWCNTs offer a significant improvement in sensitivity compared to pure MWCNT (see Figure 12B) due to the electrocatalytic activity of the carboxylic functional groups. Single-walled carbon nanohorns (SWCNHs), as a member of CNT family, was exploited by Zhu and colleagues [303] to develop a sensor for both Tyr and Trp. Adding this modifier to a bare GCE led to a sharp promotion in the Tyr oxidation peak current, as shown in Figure 12C. This enhanced sensitivity is supposed to be a consequence of the significantly high surface area and edge plan-like defects of SWCNHs that provide numerous favorable active sites for electron transfer to occur. In spite of the above-mentioned carbon nanostructures,

graphene quantum dots (GQD) have not yet been used alone in Tyr sensing, and they have always been combined with other modifiers such as β -cyclodextrin [345] and RuCl_3 [347].

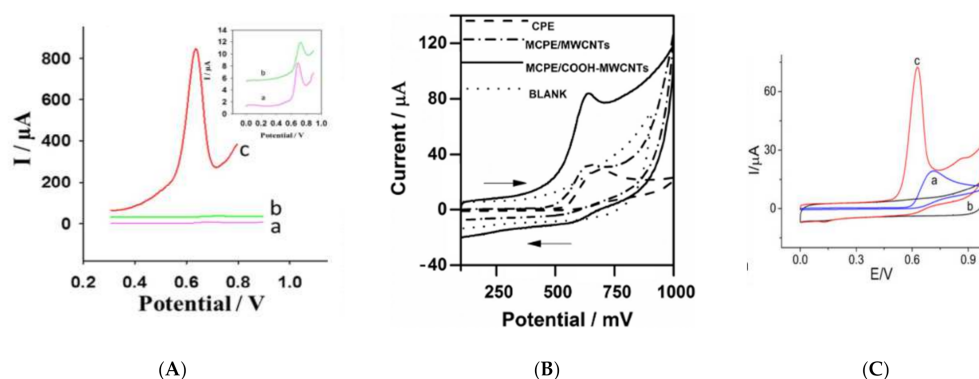


Figure 12. (A) SW voltammograms of 50 μM Tyr in 0.1 M PBS (pH 6.7) on (a) bare GPE, (b) electrochemically pretreated GPE and (c) rGO-modified GPE. Reprinted with permission from ref. [342]. Copyright 2015 Royal Society of Chemistry (B) Cyclic voltammograms of 500 μM Tyr in PBS (0.1 M, pH 7.0) at a CPE, modified CPE-MWCNTs and modified CPE/COOH-MWCNTs at a scan rate of 50 mV s^{-1} . Reprinted with permission from ref. [346]. Copyright 2016 Springer. (C) Cyclic voltammograms of a SWCNH-modified GCE in the absence (b) and presence (c) of 1 mM Tyr and (a) a bare GCE in the presence of 1 mM Tyr. The scan rate is 50 mV/s , and the supporting electrolyte is 0.1 M PBS (pH 7.0). Reprinted with permission from ref. [306]. Copyright 2014 Springer.

Figure 13 represents an example of a general pathway that is extensively used to prepare electrochemical sensors. This method commonly involves the following steps. Firstly, one, two or more desired modifiers are synthesized separately by different chemical methods. Afterwards, these modifiers are mixed together in a film-forming agent such as chitosan (CS) or Nafion using ultrasonication. The resulting homogenous dispersion is then dropped on the working electrode surface and left to dry in air or in a nitrogen stream or under infrared radiation. Zhu and colleagues [348] used this relatively simple method by mixing functionalized MWCNT and copper sulphide (CuS) nanosheets in chitosan (CS) and dropping $4 \mu\text{L}$ of this dispersion on a glassy carbon electrode (GCE) surface. This electrochemical sensor (CuS/MWCNT/GCE) showed a quite effective function with an obtained linear measurement range of $0.08\text{--}1.0 \mu\text{M}$ and limit of detection of 4.9 nM . A selectivity test revealed that even a 50-fold higher concentration of methionine, histidine and other 12 non-electroactive amino acids showed no interference effect. However, this sensor could tolerate an interference effect of just 2-fold of Trp concentration, and cysteine was not tested. Gu et al. [349] synthesized functionalized MWCNT by acid treatment, as was done by [348], and used copper oxide nanoparticles instead of CuS to fabricate a Tyr electrochemical sensor ($\text{CuO}_x/\text{MWCNT}/\text{GCE}$). This sensor was used to measure Tyr in the linear range of $0.2\text{--}200 \mu\text{M}$. Additionally, this sensor was claimed to be insensitive to tryptophan even when its concentration is 50-fold higher than Tyr. D'Sousa et al. [350] has also reported an amperometric sensor based on a MWCNT/poly-2, 6-dichlorophenolindophenol film modified electrode that is able to measure Tyr in the presence of a 10-fold excess of Trp.

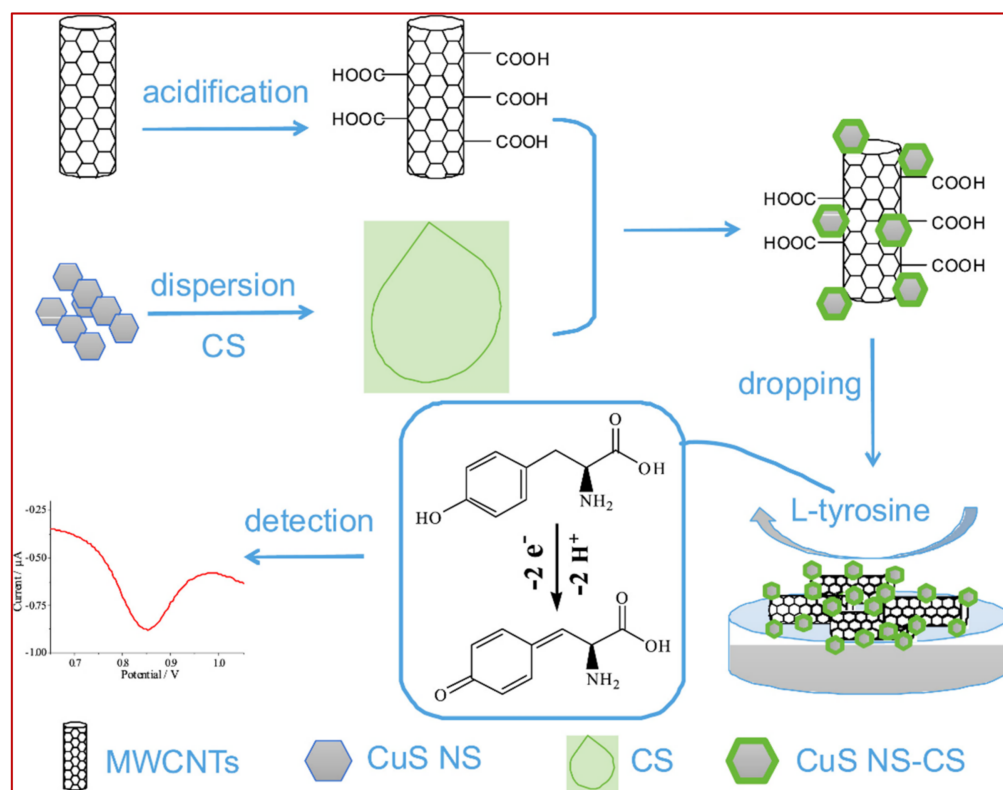


Figure 13. A schematic pathway of constructing the electrochemical Tyr sensor by dropping functionalized-MWCNT and CuS nanosheets in chitosan (CS) dispersions on a GCE surface. Adapted from. Reprinted with permission from ref. [351]. Copyright 2019 Elsevier.

Of electroactive amino acids, methionine and histidine are usually reported to show negligible interfering effect on Tyr measurement, wherein cysteine [351–353] and, especially, Trp [316,354] are the main concerns. To resolve the peak overlapping issue, both new numerical methods and sensing materials have been proposed so far. Ghoreishi and Malekian [280] proposed a numerical solution named multivariate curve resolution-alternating least squares (MCR-ALS) to resolve the overlapped peaks of Tyr and Trp and quantify these two amino acids simultaneously. The proposed strategy was successfully applied to measure Tyr and Trp in the linear range of 0.4–175.0 μM and 0.1–200.0 μM with LOD as low as 0.1 μM and 0.04 μM , respectively. Karimi and Heydari [265] synthesized mesoporous silica nanoparticles and incorporated them into a carbon paste electrode (MSNs/CPE) to be used for the simultaneous determination of Tyr and Trp. However, this proposed electrochemical sensor suffered from severe overlapping of Tyr and Trp oxidation peaks. To alleviate this deficiency, a clustering-of-variables concept based on partial least squares (PLS) regression models was proposed, and the developed sensor was used to measure Trp and Tyr in an artificial urine sample. Tashkhourian and coworkers [291] approached this issue by developing a so-called H-point standard addition method to resolve overlapping oxidation peaks of Tyr and Trp.

In addition to mathematical solutions, a few successful attempts have also been reported to address this issue by altering the sensing materials and conditions. In a very simple and quite effective strategy, Zhao et al. [355] showed that overlapped oxidation peaks of Tyr and Trp can be completely separated into two distinct peaks at an unmodified boron-doped diamond (BDD) electrode simply by changing the pH of solutions; see Figure 14A. They reported that, in acidic medium (pH = 2.95), oxidation peaks of Tyr and Trp emerge as an overlapped peak, while no oxidation peak was observed in a neutral pH of 6.86. However, in alkaline media with pH = 9.18 and especially pH = 11.2, oxidation peaks of both Tyr and Trp were clearly observed at 1.50 V and 0.86 V (vs. SCE), respectively. In contrast to [355], Deng et al. [309] designed an electrochemical

sensor by mixing an acetylene black paste electrode with graphene for the simultaneous determination of Tyr and Trp, and the best performance was observed in an extremely acidic medium (1 M sulphuric acid). When the concentration of H_2SO_4 was less than 0.4 M, the oxidation peaks of Tyr and Trp were fully merged and resulted in a broad overlapped peak. Yocus et al. [282] modified a GCE using a similar methodology as shown in Figure 13, i.e., they synthesized two modifiers separately, dispersed them in a solution and then dropped 15 μL of that solution onto a GCE. Taking advantage of rGO and polyoxometalate, as modifiers, not only separated the oxidation peaks of Tyr and Trp but also resulted in an ultrahigh-sensitivity sensor, which was able to detect Tyr and Trp in the linear range of 0.01–1.0 nM with a LOD as low as 2.0 pM (2.0×10^{-12} M). This extraordinarily high sensitivity was attributed to the higher electroactive surface area of the modified electrode and the synergistic effect of rGO and polyoxometalate, wherein rGO shows high electrical conductivity, and polyoxometalate offers excellent redox properties and electron relaying effect. Zhou et al. [95] tried to resolve the overlapping oxidation peaks of Tyr and Cys using ordered mesoporous carbon (OMC) as a sensing material. As shown in Figure 14B, at bare GCE, a single oxidation peak (at 0.67 V) is observed for both Cys and Tyr; it is split into two well-resolved peaks at 0.49 V and 0.69 V on the OMC-modified electrode. This differentiating effect is related to the very high electroactive surface area of OMC that carries numerous oxygen-containing functional groups. These functional groups are able to change the reaction pathway and favor an electrochemical reaction over other possible pathways. Trypan blue, an azo dye, was electropolymerized on the GCE surface and then decorated through the electrodeposition of gold nanoparticle to be used as an electrochemical sensor to measure Tyr and Cys simultaneously. Taeli and colleagues [53] reported that proposed sensor can resolve the overlapped oxidation peaks of these amino acids and detect them in the range of 5.0–270 μM (for Cys) and 0.5–880.0 (for Tyr). The presence of abundant phenolic and amine functional groups on Trypan blue was likely responsible for this oxidation peak separation. In spite of very few reports, as mentioned above, it seems that this issue, i.e., the simultaneous determination of electroactive amino acids, is still challenging and needs more attention since, in many real samples, both biological fluids and industrial products, these amino acids occur together.

Table 5 summarizes the most important figures of merit for reported Tyr electrochemical sensors (since 2010) to give a panoramic view to readers concerning the latest achievements and orientations in this field.

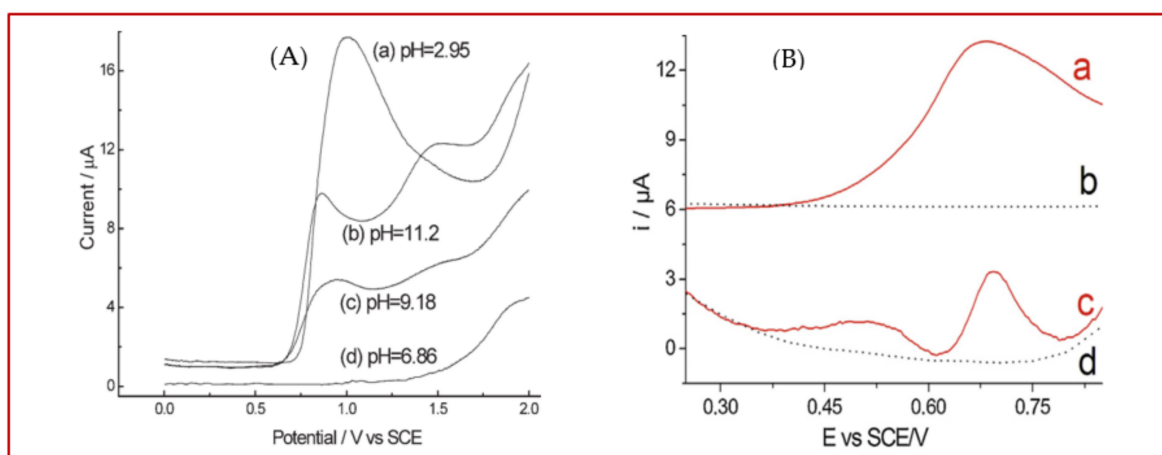


Figure 14. (A) Differential pulse voltammograms (DPVs) of Tyr and Trp using a BDD electrode in PBS with different pHs. Reprinted with permission from ref. [356]. Copyright 2006 Wiley. (B) DPVs of a mixture containing 2.4 mM Cys and 0.4 mM Tyr in PBS (0.1 M, pH = 7.4) at GCE (a) and OMC-GCE (c) where dotted lines present DPVs of GCE (b) and OMC-GCE (d) in a blank solution (PBS 0.1 M, pH = 7.4). Reprinted with permission from ref. [95]. Copyright 2013 Elsevier.

Table 5. Proposed electrochemical tyrosine sensors, since 2010, along with the most important corresponding figures of merit.

Sensing Part	Method	LDR	LOD	L.T. Stability	Real Sample	Ref.
2D-MoS ₂	LSV	1–500	0.5	70% after 4 months	-	[356]
macroporous carbon embedded β -cyclodextrin	DPV	1–500	0.2	-	tapwater	[357]
double-chain Cu metal organic framework	DPV	10–90	5.8	-	-	[358]
black phosphorus nanosheets/ β -cyclodextrin	SWV	10–100	4.81	-	-	[359]
CdO/SnO ₂ nanoparticle	AMP	0.1nM-10 μ M	0.098 nM	-	human, rabbit and mouse blood serum samples	[360]
rGO-hemin-Ag	DPV	0.1–1000	0.03	92.1% after 15 days	urine sample	[361]
plain graphite	DPV	0.01–100	0.002	-	pharmaceutical capsule	[362]
Au nanoparticles @metal organic framework/polythionine loaded with molecularly imprinted polymer	DPV	0.01–4	0.79 nM	96.8% after 2 weeks	blood serum	[363]
ErVO ₄ /MnWO ₄ heterostructure	DPV	0.08–400	0.0077	-	blood serum	[364]
2D-MoS ₂ nanosheets	CV	0–100	0.5	-	commercial food integrator	[365]
cupric oxide decorated β -cyclodextrin	AMP	0.01–100	0.0082	97% after 15 days	food sample, urine and serum samples	[366]
acetylene black paste electrode modified by oxygen-functionalized MWCNTs	SDLSV	0.04–600	0.02	92.5% after 2 weeks	milk, yogurt, beer and cheese samples	[367]
ultrathin g-C ₃ N ₄ /Ag layers	DPV	1–150	0.14	85.8% after 4 weeks	pharmaceutical samples	[354]
copper sulphide nanosheets modified with chitosan and acidified MWCNTs	DPV	0.08–1.0	4.9 nM	93.54% after 10 days	pig serum samples	[348]
NiO nanoparticles	DPV	0.15–450	0.1	-	urine and pharmaceutical samples	[368]
electrodeposited Cysteic acid	DPV	3.5–96	1.1	>one month	blood serum	[369]
iron oxide nanoparticles	DPV	0.4–270	0.05	>3 weeks	blood serum	[370]
molecularly imprinted polymer/rGO	DPV	0.1–400	0.046	90.6% after 20 days	blood serum and urine samples	[371]
MWCNT/TiO ₂	DPV	0.001–100	0.001	-	human serum albumin and bovine serum albumin samples	[336]
graphene quantum dot- β -cyclodextrin	DPV	0.1–1.5	0.03	>6 days	-	[345]

Table 5. Cont.

Sensing Part	Method	LDR	LOD	L.T. Stability	Real Sample	Ref.
mesoporous silica nanoparticles	DPV	0.3–600	0.049	-	artificial urine sample	[265]
lead-doped carbon ceramic	AMP	5–1458	0.77	-	pharmaceutical samples	[372]
filtered MWCNTs	DPV	25–750	8	-	plasma and whole blood samples	[373]
molecularly imprinted polypyrrole film	SWV	0.005–0.025	0.0025	94.4% after 10 days	plasma sample	[374]
poly-(diallyldimethylammonium chloride)/gold nanoparticles	CCR ²²	0.3–10	0.01	-	-	[375]
graphene oxide/MnO ₂ microspheres/chitosan	DPSV ²³	0.02–20	0.0083	98.2% after one month	milk and dried blood spots samples	[376]
graphene nanowalls deposited on a tantalum	DPV	8–100	0.8	>94 days	blood serum and pharmaceutical samples	[377]
Au-nanoparticles/poly-Trypan blue	DPV	0.5–880	0.008	97.1% after 4 weeks	blood serum and urine samples	[50]
graphene-zinc oxide (ZnO/GR) nanocomposite film	DPV	1–800	0.5	-	urine sample	[378]
graphene oxide/ZnO nanocomposite	SWV	0.1–400	0.07	-	pharmaceutical serum and water samples	[379]
silver nanoparticle patterned functional liquid crystalline gel	DPV	0.2–500	0.01	95% after one month	blood serum	[380]
acetylene black and chitosan	DPV	2.5–430	0.92	90.4% after 28 days	urine sample	[381]
ZnFe ₂ O ₄ nanoparticles	DPV	0.4–175	0.1	-	blood serum and urine samples	[280]
SiO ₂ @Fe ₃ O ₄ /GR nanocomposite decorated graphene/carbon ionic liquid	DPV	1–800	0.5	-	urine sample	[382]
graphene quantum dots (GQDs) and β-cyclodextrins	CV	6–1500	0.0067	98.31% after 10 days	blood serum	[383]
polyoxometalate (H ₃ PW ₁₂ O ₄₀) functionalized rGO	SWV	0.01–1 nM	0.002 nM	99.03% after 45 days	blood serum	[282]
SiO ₂	DPV	0.5–600	0.15	>2 months	artificial urine sample	[291]
MWCNT/poly (Bromocresol purple)	AMP	2–100	0.191	95.8% after 7 days	milk and blood serum samples	[384]
graphene quantum dot/RuCl ₃ nanocomposite	AMP	1–937	0.23	94% after 6 weeks	-	[347]
carboxylic acid functionalized MWCNT	AMP	0.8–100	0.014	93.1% after one week	milk and blood serum samples	[343]
phthalic anhydride functionalized chitosan/carbon nanotube film	AMP	1–800	0.3	85% after 2 weeks	blood erum	[353]

Table 5. Cont.

Sensing Part	Method	LDR	LOD	L.T. Stability	Real Sample	Ref.
gold nanoparticles involved in 2-aminoethanethiol functionalized graphene oxide	DPV	1–20 nM	0.15 nM	98.13% after 60 days	milk sample	[385]
poly(thionine)	DPV	1–250	0.57	95% after one week	blood serum	[386]
copper oxide/cuprous oxide nanoparticles/MWCNT nanocomposite	AMP	0.2–200	0.0096	90% after 3 weeks	urine sample	[349]
MWCNT/poly-2,6-dichlorophenolindophenol film	AMP	0.3–110	0.075	93.8% after 2 weeks	blood serum and soya sauce	[350]
rGO	SWV	0.8–60	0.07	-	urine sample	[342]
SWCNTs	LSV	2–30	0.4	-	blood serum	[303]
Nafion and cerium dioxide nanoparticles	DPV	2–160	0.09	94% after 2 weeks	blood serum	[387]
Fe-doped hydroxyapatite nanoparticles	AMP	0.1–10	0.245	80% after 2 weeks	-	[388]
palladium decorated MWCNT	LSV	0.1–10 nM	0.146 nM	-	-	[389]
ordered mesoporous carbon	DPV	15–900	10	95.4% after 2 weeks	-	[95]
old nanoparticles/macroporous carbon (GNPs–MPC) composites	DPV	5–1000	0.074	87% after 3 weeks	blood serum	[316]
thiolated β -cyclodextrins	DPV	36–240	12	-	pharmaceutical samples	[351]
hemin immobilized onto the poly (amidoamine)/MWCNT	AMP	0.1–28.8	0.01	-	-	[352]
europium hexacyanoferrate film	AMP	10–600	8	-	-	[390]

²² real-time channel current response; ²³ differential pulse stripping voltammetry.

3.3. Basic Amino Acid

Histidine

As another essential amino acid for human and other mammals, histidine (His) must also be supplied from dietary sources. Owing to the presence of an imidazole functional group (see Figure 3), histidine shows some matchless properties compared to other amino acids that are of vital importance for body function. This imidazole moiety of His, pK_a 6.0, is partially protonated at physiological pH and is commonly involved in many enzyme-catalyzed reactions through the proton shuttling effect [391]. His exists throughout all human tissues and has been detected in most biofluids, such as urine, blood and sweat. For normal individuals, the concentration of His in blood plasma is reported to be in the range of 70–125 μ M, while the His level in urine is in the range of 52–162 (μ mol/mmol creatinine) according to [392] or 130–2100 μ mol/L, as reported in [393]. Comparatively, the electrochemical analysis of histidine in urine is preferred over blood samples, since urine sampling is easier, safer, non-invasive, and generally, urine samples contain less potential interference. Moreover, monitoring the urinary level of histidine is of clinical importance for some serious disorders, such as histidinemia [394].

Among all electroactive amino acids we mentioned so far, histidine shows the lowest electroactivity insofar as some researchers consider it as a non-electroactive amino acid [395]. Because of this weak electroactivity in aqueous solution, very few papers are found on the electrochemical detection of histidine (see Table 6). This lower electroactivity

can be seen either as a challenge or as a great opportunity to devise new strategies for the electrochemical detection of histidine, as there is plenty of room for improvement. Hua et al. proposed a novel sensor for histidine based on the solid-state electrochemistry of copper chloride [396]. Their strategy involves following the oxidation signal of CuCl in a solution containing chloride ions after the gradual addition of histidine. They found out that the presence of Cl^- is critical for the proper function of this sensor. As Figure 15A shows, in the absence of chloride ions in the test solution, oxidation peak current of CuCl remained almost unchanged after addition of Histidine to the solution (Figure 15A, curves a and b). However, if Cl^- is added to the test solution, the oxidation current of CuCl decreased significantly, i.e., turn-off sensor upon the addition of histidine (Figure 15A, curves c and d). This sharp decrease in the solid-state CuCl signal is mainly due to the stronger Cu–His interaction, thanks to the imidazole group of His, compared to CuCl. This electrochemical sensor could be used in urine samples and detects His at concentrations as low as 0.025 pM. Noteworthy, the same group proposed another sensor for His that worked based on the same principals, CuCl solid-state electrochemistry, wherein the oxidation peak current of CuCl increased upon the addition of His (turn-on sensor) [397,398]. This sensor was also very selective for His, and, apart from lysine and cysteine, other tested species did not show an interference effect.

Focusing on Cu electrochemistry, Parsad et al. [399] reported that Cu (II) ions in a complex imprinted polymer (CIP) could trigger the electroactivity of His where no electroactivity was observed in the absence of Cu (II) ions. Authors supposed that this enhancement in His electroactivity in the presence of Cu (II) is related to the bond formation between Cu (II) and the amino and imidazole groups of His, as shown in Figure 15B. This complex formation between Cu (II) (present inside the CIP) can enhance the electroactivity of His through the inhibition of tautomerization ($-\text{NH}-\text{C}=\text{N}- \leftrightarrow -\text{N}=\text{C}-\text{NH}-$) in the imidazole ring of His.

Stepping away from copper as the key element, some researchers have tried other alternatives to construct electrochemical His sensors. Zhang and coworkers [400] aimed at improving both the sensitivity and selectivity of His sensors by using functionalized MWCNT and a molecular imprinted film on an ITO electrode. The developed sensor exhibited a limit of detection as low as 2.0 μM and ability to detect His in human blood serum. Staden [401] has proposed a potentiometric sensor that could detect His in a very wide linear range of 10^{-5} to 10^{-11} mol/L. In this electrochemical sensor, a fullerene-based compound played the key role as the sensing part. Interestingly, fullerene-based modifiers used in this study also showed enantioselectivity features. D-His isomer showed a stronger electrochemical signal over L-His, since the complex formed by D-histidine with the fullerene-C70 compound is more stable than that of L-histidine. This sensor was successfully used to measure D-His in pharmaceutical samples. The same author reported another potentiometric His sensor using maltodextrins as the sensing element [402]. The applicability of this potentiometric sensor was compared to capillary electrophoresis, wherein both methods showed almost the same performance for His determination. Among metal oxides, NiO [403,404] and Co_3O_4 [405] have been evaluated as His sensors so far; the function of these electrochemical sensors is mainly related to the electrocatalytic activity of these metal oxides in alkaline media (e.g., 0.1 M NaOH).

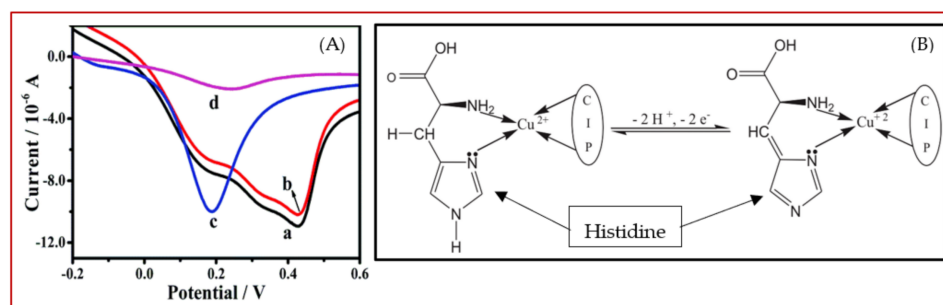


Figure 15. (A) Comparison of the linear sweep voltammograms for Cu-modified electrodes in the (a) absence and (c) presence of Cl^- ions, after the addition of His (b) and (d). Reprinted with permission from ref. [400]. Copyright 2019 Royal Society of Chemistry. (B) The proposed structure of the complex formed between Cu (II) and histidine. Reprinted with permission from ref. [403]. Copyright 2011 Elsevier.

Not surprising, due to the very weak electroactivity of His, almost all developed electrochemical His sensors so far rely on an intermediate element, e.g., CuCl, NiO, Co_3O_4 , fullerene etc., to resolve the very low electroactivity issue of His. Therefore, very few reports are found that mentioned the direct oxidation of His at a bare electrode [406]. The developed electrochemical sensors for His, from 2010 to date, were collected and compared with respect to their important figures of merit in Table 6.

Table 6. Proposed electrochemical histidine sensors, since 2010, along with the most important corresponding figures of merit.

Sensing Part	Method	LDR	LOD	L.T. Stability	Real Sample	Ref.
graphene quantum dot-scaffolded melamine and copper nanocomposites	LSV	0.1 pM ²⁴ –70 μM	0.025 pM	-	urine	[396]
tetrahedral copper metal organic framework	LSV	0.1–200 μM	0.025 μM	>6 months	human blood	[397]
reduced copper metal-organic framework	SWV	0.010–100 μM	0.002 μM	>12 months	red wine and urine	[398]
polydopamine Decorated $\text{Co}_3\text{O}_4/\text{rGO}$	AMP	10–260	1.5	-	L-His supplement	[405]
dl-homocysteine functionalized fullerene- C_{60} -gold nanocomposite	SWV	0.01 pM–100 μM	1 fM ²⁵	82% after 25 days	bovine serum albumin	[407]
copper germanate nanowires	CV	5–2000	1.3	-	-	[408]
hourglass-like nickel hydroxide nanostructure	CV	0.1–500	0.08	-	blood serum	[403]
nickel hydroxide nanostructures	CV	0.1–100	0.013	-	blood serum	[404]
complex imprinted polymers	ASDPV ²⁶	9.99–323.6 ng/mL	1.98 ng/mL	90% after one month	pharmaceutical and blood serum	[399]
MIP/MWCNTs	DPV	2–1000	5.8 nM	-	human blood serum	[400]

²⁴ Pico mol/L ($= 10^{-12}$ mol/L); ²⁵ Femto mol/L ($= 10^{-15}$ mol/L); ²⁶ Anodic stripping differential pulse voltammetry.

4. Conclusions: Challenges and Opportunities

Thanks to many attractive analytical features, electrochemical sensors represent promising candidates for future clinical and even point-of-care diagnostic tests. Many of the electroanalytical approaches presented in this review allow an inexpensive, straightforward, rapid and highly sensitive analysis of five electroactive amino acids and even proteins containing at least one of these amino acids [409–412], without involving pre-concentration and derivatisation step(s). However, apart from these prominent features, there are some major challenges to overcome before electroanalytical approaches become approved, more than what they are today, for real-world applications. The most critical remaining issues as follows:

The first issue in the electroanalysis of amino acids is the inactivity of many amino acids on common bare carbon electrodes like glassy carbon electrodes, screen-printed carbon electrodes and boron-doped diamond and carbon paste electrodes. Indeed, tryptophan, tyrosine and cysteine usually show well-defined oxidation peaks, whereas methionine and histidine electrooxidation results in, if any, a relatively weak oxidation peak. Apart from the five abovementioned amino acids, other amino acids show almost no detectable voltammetric signal in aqueous solutions. Exploiting electrochemical methods like potentiometry [402] or electrochemical impedance spectroscopy (EIS) might be the solution, since these methods do not require electroactive analytes to work. On the other hand, some literature mentioned that the addition of some substances can trigger the electroactivity of amino acids, e.g., Cu (II) for the detection of histidine [399].

The second challenge in the electroanalysis of amino acids arises from the lack of selectivity in the electrochemical detection of amino acids. It is mostly reported that electrochemical methods cannot differentiate a D-isomer from a related L-isomer of a given amino acid. More challenging, even the oxidation peak potentials of electroactive amino acids themselves are very close, and, hence, recognizing amino acids in a mixture is hard to achieve. To solve this difficulty, researchers have proposed some effective strategies. Molecularly imprinted polymers (MIP) [346] and the cyclodextrins family [413] were successfully used to alleviate this issue by adding extra selectivity to electrochemical methods. This strategy is based on the shape-recognition ability of these materials. They can be successfully used to separate one amino acid from another and even to distinguish an L-isomer of an amino acid from its D-enantiomer. Besides, chemometrics methods, e.g., partial least squares (PLS) regression [265] and multivariate curve resolution-alternating least squares (MCR-ALS) [280], are being used in electrochemical analysis to alleviate the selectivity challenges.

The third critical issue in the electrochemical detection of amino acid that electroanalysts encounter is electrode fouling due to the adsorption of reagents, products and/or intermediate species during electrochemical analysis. This drawback prevents the prolonged use of an electrode and brings about difficulties in using electrochemical detection in the continuous monitoring of amino acids. This issue is mostly encountered when electrochemical amperometric detection is coupled with chromatography, capillary electrophoresis and flow-injection analyses [414]. To overcome this issue, different approaches have thus been developed. One of the most interesting solutions is applying innovative pulsed potential sequences with three [415], four [416], five [417] and even six steps to clean and/or regenerate the electrode surface. Additionally, ionic liquids are reported to greatly prevent electrode fouling and passivation when they are used to construct an electrode [215,216]. Additionally, flow-injection analysis (FIA) is another approach to alleviate electrode fouling since the electrochemical measurements are carried out in a continuous flowing carrier stream. During the measurement, the analyte of interest is alternately injected to the carrier stream. Here, once electrochemical measurement for an injection is done, the electrode is exposed to the pure carrier stream (without the analyte) in order to wash away the by-products produced during the electrochemical measurements and to provide a clean surface for the next injection. Moreover, coating the electrode with special polymers such as nafion, chitosan, poly(ethylene glycol), poly(vinyl chloride) and

polypyrrole might be used to prevent the fouling agent from reaching the electrode surface and thereby reduce the electrode passivation [418].

Looking backward, although acceptable progress has been made in the electrochemical sensing of amino acids, further advances are still needed, mainly based on developing new materials and methods. Looking forward, thanks to unprecedented efforts devoted by researchers all over the world, there is great optimism that the previously mentioned challenges can be overcome in the upcoming years.

Author Contributions: Conceptualization, K.M.; writing—original draft preparation, K.M.; supervision, G.N. All authors have read and agreed to the published version of the manuscript.

Funding: This research received no external funding.

Institutional Review Board Statement: Not applicable.

Informed Consent Statement: Not applicable.

Conflicts of Interest: The authors declare no conflict of interest.

References

- Jane, B.; Reece, L.A.U.; Cain, M.L.; Wasserman, S.A.; Minorsky, P.V.; Jackson, R.B. *Campbell Biology*, 9th ed.; Pearson: London, UK, 2011.
- Aliu, E.; Kanungo, S.; Arnold, G.L. Amino acid disorders. *Ann. Transl. Med.* **2018**, *6*, 471. [[CrossRef](#)] [[PubMed](#)]
- Wu, G. Functional amino acids in growth, reproduction, and health. *Adv. Nutr.* **2010**, *1*, 31–37. [[CrossRef](#)] [[PubMed](#)]
- Labib, M.; Sargent, E.H.; Kelley, S.O. Electrochemical Methods for the Analysis of Clinically Relevant Biomolecules. *Chem. Rev.* **2016**, *116*, 9001–9090. [[CrossRef](#)] [[PubMed](#)]
- Tan, I.K.; Gajra, B. Plasma and urine amino acid profiles in a healthy adult population of Singapore. *Ann. Acad. Med. Singap.* **2006**, *35*, 468–475.
- Wu, G. Functional amino acids in nutrition and health. *Amino Acids* **2013**, *45*, 407–411. [[CrossRef](#)] [[PubMed](#)]
- Burns, A.; Olszowy, P.; Ciborowski, P. 2—Biomolecules. In *Proteomic Profiling and Analytical Chemistry*, 2nd ed.; Ciborowski, P., Silberring, J., Eds.; Elsevier: Boston, MA, USA, 2016; pp. 7–24.
- Joint, F.A.; World Health Organization. Amino Acid Requirements in Human, Food, N, Agriculture Organization of the United, O. World Health, and U. United Nations. In *Protein and Amino Acid Requirements in Human Nutrition: Report of a Joint FAO/WHO/UNU Expert Consultation*; World Health Organization: Geneva, Switzerland, 2007.
- Cho, W.; Yoon, Y.; Liu, S.L.; Baek, K.; Sheng, R. Chapter Two—Fluorescence-Based In Situ Quantitative Imaging for Cellular Lipids. In *Methods in Enzymology*; Gelb, M.H., Ed.; Academic Press: Cambridge, MA, USA, 2017; pp. 19–33.
- Nur Izzah Ismail, Y.Z.H.-Y.H.; Jamal, P.; Othman, R.; Salleh, H.M. Production of Cysteine: Approaches, Challenges and Potential Solution. *Int. J. Biotechnol. Wellness Ind.* **2014**, *3*, 95–101.
- Kurpad, A.V.; Regan, M.M.; Varalakshmi, S.; Vasudevan, J.; Gnanou, J.; Raj, T.; Young, V.R. Daily methionine requirements of healthy Indian men, measured by a 24-h indicator amino acid oxidation and balance technique. *Am. J. Clin. Nutr.* **2003**, *77*, 1198–1205. [[CrossRef](#)]
- Willke, T. Methionine production—A critical review. *Appl. Microbiol. Biotechnol.* **2014**, *98*, 9893–9914. [[CrossRef](#)]
- Richard, D.M.; Dawes, M.A.; Mathias, C.W.; Acheson, A.; Hill-Kapturczak, N.; Dougherty, D.M. L-Tryptophan: Basic Metabolic Functions, Behavioral Research and Therapeutic Indications. *Int. J. Tryptophan Res.* **2009**, *2*, 45–60. [[CrossRef](#)] [[PubMed](#)]
- Kałużna-Czaplińska, J.; Gałtarek, P.; Chirumbolo, S.; Chartrand, M.S.; Bjørklund, G. How important is tryptophan in human health? *Crit. Rev. Food Sci. Nutr.* **2019**, *59*, 72–88. [[CrossRef](#)]
- Sadeghiyan-Rizi, T.; Fooladi, J.; Sadrai, S. Preliminary Study on Cost-Effective L-Tryptophan Production from Indole and L-Serine by *E. coli* Cells. *Avicenna J. Med. Biotechnol.* **2016**, *8*, 188–192. [[PubMed](#)]
- Lütke-Eversloh, T.; Santos, C.N.S.; Stephanopoulos, G. Perspectives of biotechnological production of L-tyrosine and its applications. *Appl. Microbiol. Biotechnol.* **2007**, *77*, 751–762. [[CrossRef](#)] [[PubMed](#)]
- Xu, S.; Zhang, Y.; Li, Y.; Xia, X.; Zhou, J.; Shi, G. Production of L-tyrosine using tyrosine phenol-lyase by whole cell biotransformation approach. *Enzyme Microb. Technol.* **2019**, *131*, 109430. [[CrossRef](#)] [[PubMed](#)]
- Jo, M.; Noh, M.H.; Lim, H.G.; Kang, C.W.; Im, D.K.; Oh, M.K.; Jung, G.Y. Precise tuning of the glyoxylate cycle in *Escherichia coli* for efficient tyrosine production from acetate. *Microb. Cell Fact.* **2019**, *18*, 57. [[CrossRef](#)] [[PubMed](#)]
- Kulis-Horn, R.K.; Persicke, M.; Kalinowski, J. Histidine biosynthesis, its regulation and biotechnological application in *Corynebacterium glutamicum*. *Microb. Biotechnol.* **2014**, *7*, 5–25. [[CrossRef](#)]
- Nagashima, Y.; Kako, K.; Kim, J.D.; Fukamizu, A. Enhanced histamine production through the induction of histidine decarboxylase expression by phorbol ester in Jurkat cells. *Mol. Med. Rep.* **2012**, *6*, 944–948. [[CrossRef](#)]
- Huhtanen, P.; Vanhatalo, A.; Varvikko, T. Effects of abomasal infusions of histidine, glucose, and leucine on milk production and plasma metabolites of dairy cows fed grass silage diets. *J. Dairy Sci.* **2002**, *85*, 204–216. [[CrossRef](#)]

22. Malykh, E.A.; Butov, I.A.; Ravcheeva, A.B.; Krylov, A.A.; Mashko, S.V.; Stoyanova, N.V. Specific features of L-histidine production by *Escherichia coli* concerned with feedback control of AICAR formation and inorganic phosphate/metal transport. *Microb. Cell Fact.* **2018**, *17*, 42. [[CrossRef](#)]
23. Wang, L.; Wang, Q.; Liu, H.; Liu, L.; Du, Y. Determining the contents of protein and amino acids in peanuts using near-infrared reflectance spectroscopy. *J. Sci. Food Agric.* **2013**, *93*, 118–124. [[CrossRef](#)]
24. Faizan, M.; Ahmad, S. Experimental vibrational spectroscopy (FTIR and FT-Raman) of D-tryptophan and its anharmonic theoretical studies using density functional theory. *J. Mol. Struct.* **2018**, *1171*, 315–322. [[CrossRef](#)]
25. Del Galdo, S.; Mancini, G.; Daidone, I.; Polzi, L.Z.; Amadei, A.; Barone, V. Tyrosine absorption spectroscopy: Backbone protonation effects on the side chain electronic properties. *J. Comput. Chem.* **2018**, *39*, 1747–1756. [[CrossRef](#)] [[PubMed](#)]
26. Lu, Y.; Lu, D.; You, R.; Liu, J.; Huang, L.; Su, J.; Feng, S. Diazotization-coupling reaction-based determination of tyrosine in urine using Ag nanocubes by surface-enhanced Raman spectroscopy. *Nanomaterials* **2018**, *8*, 400. [[CrossRef](#)] [[PubMed](#)]
27. Wu, J.; Ran, P.; Zhu, S.; Mo, F.; Wang, C.; Fu, Y. A highly sensitive electrochemiluminescence sensor for the detection of L-cysteine based on the rhombus-shaped rubrene microsheets and platinum nanoparticles. *Sens. Actuators B Chem.* **2019**, *278*, 97–102. [[CrossRef](#)]
28. Miyamoto, T.; Sekine, M.; Ogawa, T.; Hidaka, M.; Homma, H.; Masaki, H. Generation of enantiomeric amino acids during acid hydrolysis of peptides detected by the liquid chromatography/tandem mass spectroscopy. *Chem. Biodivers.* **2010**, *7*, 1644–1650. [[CrossRef](#)]
29. Mika, J.; Berek, J.; Zima, J.; Prokešová, E.; Dejmková, H. Comparison of Glassy Carbon and Copper Microparticles as a Renewable Working Electrode Material for Amperometric Determination of Amino Acids Using Flow Through Detector. *Electroanalysis* **2019**, *31*, 357–362. [[CrossRef](#)]
30. Deo, R.P.; Lawrence, N.S.; Wang, J. Electrochemical detection of amino acids at carbon nanotube and nickel-carbon nanotube modified electrodes. *Analyst* **2004**, *129*, 1076–1081. [[CrossRef](#)] [[PubMed](#)]
31. Liu, J.; Geng, Z.; Fan, Z.; Liu, J.; Chen, H. Point-of-care testing based on smartphone: The current state-of-the-art (2017–2018). *Biosens. Bioelectron.* **2019**, *132*, 17–37. [[CrossRef](#)]
32. Citartan, M.; Tang, T.H. Recent developments of aptasensors expedient for point-of-care (POC) diagnostics. *Talanta* **2019**, *199*, 556–566. [[CrossRef](#)]
33. García-Carmona, L.; González, M.C.; Escarpa, A. Nanomaterial-based electrochemical (bio)-sensing: One step ahead in diagnostic and monitoring of metabolic rare diseases. *Trends Anal. Chem.* **2019**, *118*, 29–42. [[CrossRef](#)]
34. Paleček, E.; Tkáč, J.; Bartošík, M.; Bertók, T.; Ostatná, V.; Paleček, J. Electrochemistry of nonconjugated proteins and glycoproteins. Toward sensors for biomedicine and glycomics. *Chem. Rev.* **2015**, *115*, 2045–2108.
35. Xu, J.J.; Peng, Y.; Bao, N.; Xia, X.H.; Chen, H.Y. Simple method for the separation and detection of native amino acids and the identification of electroactive and non-electroactive analytes. *J. Chromatogr. A* **2005**, *1095*, 193–196. [[CrossRef](#)] [[PubMed](#)]
36. Enache, T.A.; Oliveira-Brett, A.M. Peptide methionine sulfoxide reductase A (MsrA): Direct electrochemical oxidation on carbon electrodes. *Bioelectrochemistry* **2013**, *89*, 11–18. [[CrossRef](#)] [[PubMed](#)]
37. Dourado, A.H.B.; Pastrian, F.C.; Torresi, S.I.C. The long and successful journey of electrochemically active amino acids. From fundamental adsorption studies to potential surface engineering tools. *An. Acad. Bras. Cienc.* **2018**, *90*, 607–630. [[CrossRef](#)] [[PubMed](#)]
38. Enache, T.A.; Oliveira-Brett, A.M. Alzheimer's disease amyloid beta peptides in vitro electrochemical oxidation. *Bioelectrochemistry* **2017**, *114*, 13–23. [[CrossRef](#)]
39. Sattarahmady, N.; Heli, H. An electrocatalytic transducer for L-cysteine detection based on cobalt hexacyanoferrate nanoparticles with a core-shell structure. *Anal. Biochem.* **2011**, *409*, 74–80. [[CrossRef](#)]
40. Enache, T.A.; Oliveira-Brett, A.M. Boron doped diamond and glassy carbon electrodes comparative study of the oxidation behaviour of cysteine and methionine. *Bioelectrochemistry* **2011**, *81*, 46–52. [[CrossRef](#)]
41. Prasad, B.B.; Pandey, I.; Srivastava, A.; Kumar, D.; Tiwari, M.P. Multiwalled carbon nanotubes-based pencil graphite electrode modified with an electrosynthesized molecularly imprinted nanofilm for electrochemical sensing of methionine enantiomers. *Sens. Actuators B Chem.* **2013**, *176*, 863–874. [[CrossRef](#)]
42. Paz Zanini, V.I.; Giménez, R.E.; Pérez, O.E.L.; de Mishima, B.A.L.; Borsarelli, C.D. Enhancement of amperometric response to tryptophan by proton relay effect of chitosan adsorbed on glassy carbon electrode. *Sens. Actuators B Chem.* **2015**, *209*, 391–398. [[CrossRef](#)]
43. Nguyen, N.T.; Wrona, M.Z.; Dryhurst, G. Electrochemical oxidation of tryptophan. *J. Electroanal. Chem. Interfacial Electrochem.* **1986**, *199*, 101–126. [[CrossRef](#)]
44. Ogura, K.; Kobayashi, M.; Nakayama, M.; Miho, Y. In-situ FTIR studies on the electrochemical oxidation of histidine and tyrosine. *J. Electroanal. Chem.* **1999**, *463*, 218–223. [[CrossRef](#)]
45. Paleček, E.; Bartošík, M.; Ostatná, V.; Trefulka, M. Electrocatalysis in proteins, nucleic acids and carbohydrates. *Chem. Rec.* **2012**, *12*, 27–45. [[CrossRef](#)] [[PubMed](#)]
46. Chawla, R.K.; Lewis, F.W.; Kutner, M.H.; Bate, D.M.; Roy, R.G.B.; Rudman, D. Plasma cysteine, cystine, and glutathione in cirrhosis. *Gastroenterology* **1984**, *87*, 770–776. [[CrossRef](#)]
47. Singh, M.; Jaiswal, N.; Tiwari, I.; Foster, C.W.; Banks, C.E. A reduced graphene oxide-cyclodextrin-platinum nanocomposite modified screen printed electrode for the detection of cysteine. *J. Electroanal. Chem.* **2018**, *829*, 230–240. [[CrossRef](#)]

48. Zhao, C.; Zhang, J.; Song, J. Determination of L-cysteine in amino acid mixture and human urine by flow-injection analysis with a biamperometric detector. *Anal. Biochem.* **2001**, *297*, 170–176. [[CrossRef](#)]
49. Li, Z.; Xu, H.; Wu, D.; Zhang, J.; Liu, X.; Gao, S.; Kong, Y. Electrochemical Chiral Recognition of Tryptophan Isomers Based on Nonionic Surfactant-Assisted Molecular Imprinting Sol-Gel Silica. *ACS Appl. Mater. Interfaces* **2019**, *11*, 2840–2848. [[CrossRef](#)]
50. Tai, M.; Hasanpour, F.; Habibollahi, S.; Shahidi, L. Simultaneous electrochemical sensing of cysteine, uric acid and tyrosine using a novel Au-nanoparticles/poly-Trypan Blue modified glassy carbon electrode. *J. Electroanal. Chem.* **2017**, *789*, 140–147. [[CrossRef](#)]
51. Sornambikai, S.; Kadir, M.R.A.; Kumar, A.S.; Ponpandian, N.; Viswanathan, C. Selective and low potential electrocatalytic oxidation and sensing of L-cysteine using metal impurity containing carbon black modified electrode. *Anal. Methods* **2017**, *9*, 6791–6800. [[CrossRef](#)]
52. Kannan, A.; Sevel, R. Gold nanoparticles embedded electropolymerized thin film of pyrimidine derivative on glassy carbon electrode for highly sensitive detection of L-cysteine. *Mater. Sci. Eng. C* **2017**, *78*, 513–519. [[CrossRef](#)]
53. Tai, M.; Hasanpour, F.; Salavati, H.; Banitaba, S.H.; Kazemi, F. Simultaneous determination of cysteine, uric acid and tyrosine using Au-nanoparticles/poly(E)-4-(p-tolyldiazenyl)benzene-1,2,3-triol film modified glassy carbon electrode. *Mater. Sci. Eng. C* **2016**, *59*, 120–128. [[CrossRef](#)]
54. Gu, J.; Dai, H.; Kong, Y.; Tao, Y.; Chu, H.; Tong, Z. Chiral electrochemical recognition of cysteine enantiomers with molecularly imprinted overoxidized polypyrrole-Au nanoparticles. *Synth. Met.* **2016**, *222*, 137–143. [[CrossRef](#)]
55. Wang, X.; Luo, C.; Li, L.; Duan, H. Highly selective and sensitive electrochemical sensor for L-cysteine detection based on graphene oxide/multiwalled carbon nanotube/manganese dioxide/gold nanoparticles composite. *J. Electroanal. Chem.* **2015**, *757*, 100–106. [[CrossRef](#)]
56. Abbas, M.N.; Saeed, A.A.; Singh, B.; Radowan, A.A.; Dempsey, E. A cysteine sensor based on a gold nanoparticle-iron phthalocyanine modified graphite paste electrode. *Anal. Methods* **2015**, *7*, 2529–2536. [[CrossRef](#)]
57. Wang, X.; Wen, Y.; Lu, L.; Xu, J.; Zhang, L.; Yao, Y.; He, H. A Novel L-Cysteine Electrochemical Sensor Using Sulfonated Graphene-poly(3,4-Ethylenedioxythiophene) Composite Film Decorated with Gold Nanoparticles. *Electroanalysis* **2014**, *26*, 648–655. [[CrossRef](#)]
58. Devasenathipathy, R.; Karuppiyah, C.; Chen, S.M.; Mani, V.; Vasantha, V.S.; Ramaraj, S. Highly selective determination of cysteine using a composite prepared from multiwalled carbon nanotubes and gold nanoparticles stabilized with calcium crosslinked pectin. *Microchim. Acta* **2014**, *182*, 727–735. [[CrossRef](#)]
59. Silva, F.D.A.D.S.; da Silva, M.G.A.; Lima, P.R.; Meneghetti, M.R.; Kubota, L.T.; Goulart, M.O.F. A very low potential electrochemical detection of L-cysteine based on a glassy carbon electrode modified with multi-walled carbon nanotubes/gold nanorods. *Biosens. Bioelectron.* **2013**, *50*, 202–209. [[CrossRef](#)]
60. Wang, L.H.; Huang, W.S. Electrochemical oxidation of cysteine at a film gold modified carbon fiber microelectrode its application in a flow-through voltammetric sensor. *Sensors* **2012**, *12*, 3562–3577. [[CrossRef](#)]
61. Perevezentseva, D.O.; Gorchakov, E.V. Voltammetric determination of cysteine at a graphite electrode modified with gold nanoparticles. *J. Solid State Electrochem.* **2012**, *16*, 2405–2410. [[CrossRef](#)]
62. Liu, Z.; Zhang, H.; Hou, S.; Ma, H. Highly sensitive and selective electrochemical detection of L-cysteine using nanoporous gold. *Microchim. Acta* **2012**, *177*, 427–433. [[CrossRef](#)]
63. Liu, X.; Luo, L.; Ding, Y.; Kang, Z.; Ye, D. Simultaneous determination of L-cysteine and L-tyrosine using Au-nanoparticles/poly-eriochrome black T film modified glassy carbon electrode. *Bioelectrochemistry* **2012**, *86*, 38–45. [[CrossRef](#)]
64. Ge, S.; Yan, M.; Lu, J.; Zhang, M.; Yu, F.; Yu, J.; Song, X.; Yu, S. Electrochemical biosensor based on graphene oxide-Au nanoclusters composites for L-cysteine analysis. *Biosens. Bioelectron.* **2012**, *31*, 49–54. [[CrossRef](#)] [[PubMed](#)]
65. Wang, X.; Zhang, L.; Miao, L.; Kan, M.; Kong, L.; Zhang, H. Oxidation and detection of L-cysteine using a modified Au/Nafion/glass carbon electrode. *Sci. China Chem.* **2011**, *54*, 521–525. [[CrossRef](#)]
66. Hsiao, Y.P.; Su, W.Y.; Cheng, J.R.; Cheng, S.H. Electrochemical determination of cysteine based on conducting polymers/gold nanoparticles hybrid nanocomposites. *Electrochim. Acta* **2011**, *56*, 6887–6895. [[CrossRef](#)]
67. Yusoff, N.; Rameshkumar, P.; Noor, A.M.; Huang, N.M. Amperometric determination of L-cysteine using a glassy carbon electrode modified with palladium nanoparticles grown on reduced graphene oxide in a Nafion matrix. *Microchim. Acta* **2018**, *185*, 246. [[CrossRef](#)] [[PubMed](#)]
68. Thota, R.; Ganesh, V. Simple and facile preparation of silver-polydopamine (Ag-PDA) core-shell nanoparticles for selective electrochemical detection of cysteine. *RSC Adv.* **2016**, *6*, 49578–49587. [[CrossRef](#)]
69. Li, H.; Chen, D.; Wang, H.; Li, J.; Wang, W. Sub-picomole level photoelectrochemical sensing of L-cysteine based on plasmonic silver nanoparticles modified hierarchically structured zinc oxide. *J. Electroanal. Chem.* **2015**, *759*, 21–26. [[CrossRef](#)]
70. Jin, G.P.; Chen, L.L.; Hang, G.P.; Yang, S.Z.; Wu, X.J. Stripping chronopotentiometric analysis of cysteine on nano-silver coat polyquercetin-MWCNT modified platinum electrode. *J. Solid State Electrochem.* **2010**, *14*, 1163–1169. [[CrossRef](#)]
71. Yang, S.; Zheng, Y.; Zhang, X.; Ding, S.; Li, L.; Zha, W. Molecularly imprinted electrochemical sensor based on the synergic effect of nanoporous gold and copper nanoparticles for the determination of cysteine. *J. Solid State Electrochem.* **2016**, *20*, 2037–2044. [[CrossRef](#)]
72. Zhang, L.; Ning, L.; Zhang, Z.; Li, S.; Yan, H.; Pang, H.; Ma, H. Fabrication and electrochemical determination of L-cysteine of a composite film based on V-substituted polyoxometalates and Au@2Ag core-shell nanoparticles. *Sens. Actuators B Chem.* **2015**, *221*, 28–36. [[CrossRef](#)]

73. Wu, L.; Li, J.; Zhang, H.M. One Step Fabrication of Au Nanoparticles-Ni-Al Layered Double Hydroxide Composite Film for the Determination of L-Cysteine. *Electroanalysis* **2015**, *27*, 1195–1201. [[CrossRef](#)]
74. Mo, Z.; Zhao, F.; Xiao, F.; Zeng, B. Preparation and characterization of AuPt alloy nanoparticle-multi-walled carbon nanotube-ionic liquid composite film for electrocatalytic oxidation of cysteine. *J. Solid State Electrochem.* **2010**, *14*, 1615–1620. [[CrossRef](#)]
75. Murugavelu, M.; Karthikeyan, B. Study of Ag-Pd bimetallic nanoparticles modified glassy carbon electrode for detection of L-cysteine. *Superlattices Microstruct.* **2014**, *75*, 916–926. [[CrossRef](#)]
76. Cao, F.; Dong, Q.; Li, C.; Kwak, D.; Huang, Y.; Song, D.; Lei, Y. Sensitive and Selective Electrochemical Determination of L-Cysteine Based on Cerium Oxide Nanofibers Modified Screen Printed Carbon Electrode. *Electroanalysis* **2018**, *30*, 1133–1139. [[CrossRef](#)]
77. Zhu, Y.; Xu, Z.; Yan, K.; Zhao, H.; Zhang, J. One-Step Synthesis of CuO–Cu₂O Heterojunction by Flame Spray Pyrolysis for Cathodic Photoelectrochemical Sensing of L-Cysteine. *ACS Appl. Mater. Interfaces* **2017**, *9*, 40452–40460. [[CrossRef](#)] [[PubMed](#)]
78. Yang, S.; Li, G.; Wang, G.; Deng, D.; Qu, L. A novel electrochemical sensor based on Fe₂O₃ nanoparticles/N-doped graphene for electrocatalytic oxidation of L-cysteine. *J. Solid State Electrochem.* **2015**, *19*, 3613–3620. [[CrossRef](#)]
79. Gupta, V.K.; Shamsadin-Azad, Z.; Cheraghi, S.; Agarwai, S.; Taher, M.A.; Karimi, F. Electrocatalytic determination of L-cysteine in the presence of tryptophan using carbon paste electrode modified with MgO nanoparticles and acetylferrocene. *Int. J. Electrochem. Sci.* **2018**, *13*, 4309–4318. [[CrossRef](#)]
80. Zhang, J.; Hu, J.; Wu, D.; Ma, J.; Tao, Y.; Qin, Y.; Kong, Y. Multi-templates based molecularly imprinted sodium alginate/MnO₂ for simultaneous enantioselective recognition of lysine, alanine and cysteine isomers. *Int. J. Biol. Macromol.* **2019**, *129*, 786–791. [[CrossRef](#)]
81. Yang, S.; Li, G.; Liu, L.; Wang, G.; Wang, D.; Qu, L. Preparation of nickel oxide nanoparticles on N-doped reduced graphene oxide: A two-dimensional hybrid for electrocatalytic sensing of L-cysteine. *J. Alloys Compd.* **2017**, *691*, 834–840. [[CrossRef](#)]
82. Dong, Y.; Zheng, J. A nonenzymatic L-cysteine sensor based on SnO₂-MWCNTs nanocomposites. *J. Mol. Liq.* **2014**, *196*, 280–284. [[CrossRef](#)]
83. Wang, Y.; Wang, W.; Wang, S.; Chu, W.; Wei, T.; Tao, H.; Zhang, C.; Sun, Y. Enhanced photoelectrochemical detection of L-cysteine based on the ultrathin polythiophene layer sensitized anatase TiO₂ on F-doped tin oxide substrates. *Sens. Actuators B Chem.* **2016**, *232*, 448–453. [[CrossRef](#)]
84. Sun, B.; Zhang, K.; Chen, L.; Guo, L.; Ai, S. A novel photoelectrochemical sensor based on PPIX-functionalized WO₃-rGO nanohybrid-decorated ITO electrode for detecting cysteine. *Biosens. Bioelectron.* **2013**, *44*, 48–51. [[CrossRef](#)]
85. Yang, S.; Li, G.; Wang, Y.; Wang, G.; Qu, L. Amperometric L-cysteine sensor based on a carbon paste electrode modified with Y₂O₃ nanoparticles supported on nitrogen-doped reduced graphene oxide. *Microchim. Acta* **2016**, *183*, 1351–1357. [[CrossRef](#)]
86. Yang, S.; Li, G.; Qu, C.; Wang, G.; Wang, D. Simple synthesis of ZnO nanoparticles on N-doped reduced graphene oxide for the electrocatalytic sensing of L-cysteine. *RSC Adv.* **2017**, *7*, 35004–35011. [[CrossRef](#)]
87. Szot-Karpińska, K.; Leśniewski, A.; Jönsson-Niedziółka, M.; Marken, F.; Niedziółka-Jönsson, J. Electrodes modified with bacteriophages and carbon nanofibres for cysteine detection. *Sens. Actuators B Chem.* **2019**, *287*, 78–85. [[CrossRef](#)]
88. Ziyatdinova, G.; Kozlova, E.; Budnikov, H. Selective electrochemical sensor based on the electropolymerized *p*-coumaric acid for the direct determination of L-cysteine. *Electrochim. Acta* **2018**, *270*, 369–377. [[CrossRef](#)]
89. Xu, H.; Li, C.; Song, D.; Xu, X.; Zhao, Y.; Liu, X.; Su, Z. Amperometric L-cysteine Sensor Using a Gold Electrode Modified with Thiolated Catechol. *Electroanalysis* **2017**, *29*, 2410–2416. [[CrossRef](#)]
90. Sundaram, S.; Kadir, M.R.A. A New Highly Conducting Carbon Black (CL-08) Modified Electrode Functionalized with Syringic Acid for Sensitive and Selective L-Cysteine Electroanalysis at Low Potential. *Electrochim. Acta* **2017**, *224*, 475–486. [[CrossRef](#)]
91. Safavi, A.; Ahmadi, R.; Mahyari, F.A. Simultaneous electrochemical determination of L-cysteine and L-cysteine disulfide at carbon ionic liquid electrode. *Amino Acids* **2014**, *46*, 1079–1085. [[CrossRef](#)] [[PubMed](#)]
92. Lee, P.T.; Lowinsohn, D.; Compton, R.G. The selective electrochemical detection of homocysteine in the presence of glutathione, cysteine, and ascorbic acid using carbon electrodes. *Analyst* **2014**, *139*, 3755–3762. [[CrossRef](#)]
93. Lee, P.T.; Lowinsohn, D.; Compton, R.G. The use of screen-printed electrodes in a proof of concept electrochemical estimation of homocysteine and glutathione in the presence of Cysteine using catechol. *Sensors* **2014**, *14*, 10395–10411. [[CrossRef](#)]
94. Lee, P.T.; Lowinsohn, D.; Compton, R.G. Simultaneous Detection of Homocysteine and Cysteine in the Presence of Ascorbic Acid and Glutathione Using a Nanocarbon Modified Electrode. *Electroanalysis* **2014**, *26*, 1488–1496. [[CrossRef](#)]
95. Zhou, S.; Wu, H.; Wu, Y.; Shi, H.; Feng, X.; Huang, H.; Li, J.; Song, W. Large surface area carbon material with ordered mesopores for highly selective determination of L-tyrosine in the presence of L-cysteine. *Electrochim. Acta* **2013**, *112*, 90–94. [[CrossRef](#)]
96. Liu, X.; Lv, H.; Sun, Q.; Zhong, Y.; Zhao, J.; Fu, J.; Lin, M.; Wang, J. Differential Pulse Voltammetric Determination of L-Cysteine After Cyclic Voltammetry in Presence of Catechol with Glassy Carbon Electrode. *Anal. Lett.* **2012**, *45*, 2246–2256. [[CrossRef](#)]
97. Ahmadipour, M.; Taher, M.A.; Beitollahi, H.; Hosseinzadeh, R. Electrocatalytic determination of L-cysteine using a modified carbon nanotube paste electrode: Application to the analysis of some real samples. *Chin. Chem. Lett.* **2012**, *23*, 981–984. [[CrossRef](#)]
98. Ensafi, A.A.; Dadkhah-Tehrani, S.; Karimi-Maleh, H. A voltammetric sensor for the simultaneous determination of L-cysteine and tryptophan using a *p*-aminophenol-multiwall carbon nanotube paste electrode. *Anal. Sci.* **2011**, *27*, 409–414. [[CrossRef](#)]
99. Tang, X.; Liu, Y.; Hou, H.; You, T. Electrochemical determination of L-Tryptophan, L-Tyrosine and L-Cysteine using electrospun carbon nanofibers modified electrode. *Talanta* **2010**, *80*, 2182–2186. [[CrossRef](#)] [[PubMed](#)]
100. Mazloum-Ardakania, M.; Taleata, Z.; Beitollahia, H.; Naeimib, H. Selective determination of cysteine in the presence of tryptophan by carbon paste electrode modified with quinizarine. *J. Iran. Chem. Soc.* **2010**, *7*, 251–259. [[CrossRef](#)]

101. Pakiari, A.H.; Jamshidi, Z. Nature and Strength of M–S Bonds (M = Au, Ag, and Cu) in Binary Alloy Gold Clusters. *J. Phys. Chem. A* **2010**, *114*, 9212–9221. [[CrossRef](#)]
102. Han, J.; Zhao, J.; Li, Z.; Zhang, H.; Yan, Y.; Cao, D.; Wang, G. Nanoporous carbon derived from dandelion pappus as an enhanced electrode material with low cost for amperometric detection of tryptophan. *J. Electroanal. Chem.* **2018**, *818*, 149–156. [[CrossRef](#)]
103. Ye, M.L.; Xu, B.; Zhang, W.D. Sputtering deposition of Pt nanoparticles on vertically aligned multiwalled carbon nanotubes for sensing L-cysteine. *Microchim. Acta* **2011**, *172*, 439–446. [[CrossRef](#)]
104. Liu, L.P.; Yin, Z.J.; Yang, Z.S. A L-cysteine sensor based on Pt nanoparticles/poly(*o*-aminophenol) film on glassy carbon electrode. *Bioelectrochemistry* **2010**, *79*, 84–89. [[CrossRef](#)]
105. Zhao, G.; Zhou, X.; Ran, X.; Tan, X.; Li, T.; Cao, M.; Yang, L.; Du, G. Layer-by-layer assembly of anionic-/cationic-pillar(5)arenes multilayer films as chiral interface for electrochemical recognition of tryptophan isomers. *Electrochim. Acta* **2018**, *277*, 1–8. [[CrossRef](#)]
106. Vladislavić, N.; Rončević, I.Š.; Buljac, M.; Brinić, S.; Krivić, D.; Buzuk, M. Electroanalytical determination of cysteine using the electrodes based on ternary silver-copper sulfides. *Sensors* **2018**, *18*, 3753. [[CrossRef](#)] [[PubMed](#)]
107. Farjami, F.; Mosalman, F.K.; Ebrahimpourmoghaddam, S.; Sharghi, H. Electrocatalytic Determination of Cysteine Using a Carbon Ionic Liquid Electrode Modified with Terpyridine Copper(II) Complex. *Anal. Lett.* **2016**, *49*, 1412–1423. [[CrossRef](#)]
108. Derikvand, Z.; Azadbakht, A. Copper inorganic-organic hybrid coordination compound as a novel L-cysteine electrochemical sensor: Synthesis, characterization, spectroscopy and crystal structure. *J. Chem. Sci.* **2015**, *127*, 2005–2014. [[CrossRef](#)]
109. Pei, L.Z.; Cai, Z.Y.; Pei, Y.Q.; Xie, Y.K.; Fan, C.G.; Fu, D.G. Electrochemical determination of L-cysteine using polyaniline/CuGeO₃ nanowire modified electrode. *Russ. J. Electrochem.* **2014**, *50*, 458–467. [[CrossRef](#)]
110. Majidi, M.R.; Asadpour-Zeynali, K.; Hafezi, B. Sensing L-cysteine in urine using a pencil graphite electrode modified with a copper hexacyanoferrate nanostructure. *Microchim. Acta* **2010**, *169*, 283–288. [[CrossRef](#)]
111. Dong, Y.; Pei, L.; Chu, X.; Zhang, W.; Zhang, Q. Electrochemical behavior of cysteine at a CuGeO₃ nanowires modified glassy carbon electrode. *Electrochim. Acta* **2010**, *55*, 5135–5141. [[CrossRef](#)]
112. Duan, D.; Yang, H.; Ding, Y.; Li, L.; Ma, G. A three-dimensional conductive molecularly imprinted electrochemical sensor based on MOF derived porous carbon/carbon nanotubes composites and prussian blue nanocubes mediated amplification for chiral analysis of cysteine enantiomers. *Electrochim. Acta* **2019**, *302*, 137–144. [[CrossRef](#)]
113. Zhou, H.; Ran, G.; Masson, J.F.; Wang, C.; Zhao, Y.; Song, Q. Rational Design of Magnetic Micronanoelectrodes for Recognition and Ultrasensitive Quantification of Cysteine Enantiomers. *Anal. Chem.* **2018**, *90*, 3374–3381. [[CrossRef](#)]
114. Bonacin, J.A.; Santos, P.L.D.; Katic, V.; Foster, C.W.; Banks, C.E. Use of Screen-Printed Electrodes Modified by Prussian Blue and Analogues in Sensing of Cysteine. *Electroanalysis* **2018**, *30*, 170–179. [[CrossRef](#)]
115. Amiri, M.; Salavati-Niasari, M.; Akbari, A. A magnetic CoFe₂O₄/SiO₂ nanocomposite fabricated by the sol-gel method for electrocatalytic oxidation and determination of L-cysteine. *Microchim. Acta* **2017**, *184*, 825–833. [[CrossRef](#)]
116. Wang, Y.; Wang, W.; Li, G.; Liu, Q.; Wei, T.; Li, B.; Jiang, C.; Sun, Y. Electrochemical detection of L-cysteine using a glassy carbon electrode modified with a two-dimensional composite prepared from platinum and Fe₃O₄ nanoparticles on reduced graphene oxide. *Microchim. Acta* **2016**, *183*, 3221–3228. [[CrossRef](#)]
117. Wang, L.; Tricard, S.; Yue, P.; Zhao, J.; Fang, J.; Shen, W. Polypyrrole and graphene quantum dots @ Prussian Blue hybrid film on graphite felt electrodes: Application for amperometric determination of L-cysteine. *Biosens. Bioelectron.* **2016**, *77*, 1112–1118. [[CrossRef](#)]
118. Devasenathipathy, R.; Mani, V.; Chen, S.M.; Kohilarani, K.; Ramaraj, S. Determination of L-cysteine at iron tetrasulfonated phthalocyanine decorated multiwalled carbon nanotubes film modified electrode. *Int. J. Electrochem. Sci.* **2015**, *10*, 682–690.
119. Corrêa, C.C.; Jannuzzi, S.A.V.; Santhiago, M.; Timm, R.A.; Formiga, A.L.B.; Kubota, L.T. Modified electrode using multi-walled carbon nanotubes and a metallopolymer for amperometric detection of L-cysteine. *Electrochim. Acta* **2013**, *113*, 332–339. [[CrossRef](#)]
120. Shaidarova, L.G.; Ziganshina, S.A.; Gedmina, A.V.; Chelnokova, I.A.; Budnikov, G.K. Electrochemical behavior and voltammetric determination of cysteine and cystine at carbon-paste electrodes modified with metal phthalocyanines. *J. Anal. Chem.* **2011**, *66*, 633–641. [[CrossRef](#)]
121. Liu, S.; Dai, G. Preparation and electrochemical behaviour of silver pentacyanonitrosylferrate film modified glassy carbon electrode and its electrocatalytic oxidation to L-cysteine. *J. Chin. Chem. Soc.* **2011**, *58*, 617–622. [[CrossRef](#)]
122. Raoof, J.B.; Ojani, R.; Mohammadpour, Z. Homogeneous electrocatalytic oxidation and voltammetric determination of L-cysteine by 1,1'-Ferrocenedicarboxylic acid at glassy carbon electrode. *Anal. Bioanal. Electrochem.* **2010**, *2*, 24–35.
123. Benvidi, A.; Ansariipour, M.M.; Rajabzadeh, N.; Zare, H.R.; Mirjalili, B.B.F. Developing a nanostructure electrochemical sensor for simultaneous determination of cysteine and tryptophan. *Anal. Methods* **2015**, *7*, 3920–3928. [[CrossRef](#)]
124. Matsunaga, T.; Kondo, T.; Shitanda, I.; Hoshi, Y.; Itagaki, M.; Tojo, T.; Yuasa, M. Sensitive electrochemical detection of L-Cysteine at a screen-printed diamond electrode. *Carbon* **2021**, *173*, 395–402. [[CrossRef](#)]
125. Yang, S.; Li, G.; Xia, N.; Wang, Y.; Liu, P.; Qu, L. Fabrication of hierarchical 3D prickly ball-like Co–La oxides/reduced graphene oxide composite for electrochemical sensing of L-cysteine. *J. Alloys Compd.* **2021**, *853*, 157077. [[CrossRef](#)]
126. Yang, S.; Li, G.; Xia, N.; Liu, P.; Wang, Y.; Qu, L. High performance electrochemical L-cysteine sensor based on hierarchical 3D straw-bundle-like Mn-La oxides/reduced graphene oxide composite. *J. Electroanal. Chem.* **2020**, *877*, 114654. [[CrossRef](#)]

127. Balasubramanian, P.; He, S.-B.; Deng, H.-H.; Peng, H.-P.; Chen, W. Defects engineered 2D ultrathin cobalt hydroxide nanosheets as highly efficient electrocatalyst for non-enzymatic electrochemical sensing of glucose and L-cysteine. *Sens. Actuators B Chem.* **2020**, *320*, 128374. [[CrossRef](#)]
128. Zhai, X.; Li, S.; Chen, X.; Hua, Y.; Wang, H. Coating silver metal-organic frameworks onto nitrogen-doped porous carbons for the electrochemical sensing of cysteine. *Microchim. Acta* **2020**, *187*, 493. [[CrossRef](#)]
129. Jerome, R.; Keerthivasan, P.V.; Murugan, N.; Devi, N.R.; Sundramoorthy, A.K. Preparation of Stable CuO/Boron Nitride Nanocomposite Modified Electrode for Selective Electrochemical Detection of L-Cysteine. *ChemistrySelect* **2020**, *5*, 9111–9118. [[CrossRef](#)]
130. Fallahi, M.; Norouzi, B. Synthesis of cobalt oxide nanoparticles using *Cirsium vulgare* leaves extract and evaluation of electrocatalytic effects on oxidation of L-cysteine. *Ionics* **2020**, *26*, 1951–1961. [[CrossRef](#)]
131. Mazloum-Ardakani, M.; Alizadeh, Z. A Certain Electrochemical Nanosensor Based on Functionalized Multi-Walled Carbon Nanotube for Determination of Cysteine in the Presence of Paracetamol. *J. Nanostruct.* **2020**, *10*, 258–267.
132. Vladislavić, N.; Rončević, I.Š.; Buzuk, M.; Buljac, M.; Drventić, I. Electrochemical/chemical synthesis of hydroxyapatite on glassy carbon electrode for electroanalytical determination of cysteine. *J. Solid State Electrochem.* **2020**, *25*, 841. [[CrossRef](#)]
133. Li, J.; Zhang, L. 3D pothole-rich hierarchical carbon framework-encapsulated Ni nanoparticles for highly selective nonenzymatic cysteine detection. *Electrochim. Acta* **2019**, *328*, 135126. [[CrossRef](#)]
134. De Souza Magossi, M.; Fernandes, D.S.; do Carmo, D.R. Synthesis of a novel hybrid nanocomposite based on copper pentacyanonitrosylferrate and octa(aminopropyl)silsesquioxane and its behavior on L-cysteine electrooxidation. *Solid State Sci.* **2019**, *95*, 105931. [[CrossRef](#)]
135. Kumar, D.R.; Baynosa, M.L.; Shim, J.-J. Cu²⁺-1,10-phenanthroline-5,6-dione@electrochemically reduced graphene oxide modified electrode for the electrocatalytic determination of L-cysteine. *Sens. Actuators B Chem.* **2019**, *293*, 107–114. [[CrossRef](#)]
136. Maheshwari, H.; Vilà, N.; Herzog, G.; Walcarius, A. Selective Detection of Cysteine at a Mesoporous Silica Film Electrode Functionalized with Ferrocene in the Presence of Glutathione. *ChemElectroChem* **2020**, *7*, 2095–2101. [[CrossRef](#)]
137. Manibalan, G.; Murugadoss, G.; Thangamuthu, R.; Kumar, M.R.; Kumar, R.M.; Jayavel, R. CeO₂-based heterostructure nanocomposite for electrochemical determination of L-cysteine biomolecule. *Inorg. Chem. Commun.* **2020**, *113*, 107793. [[CrossRef](#)]
138. Le, H.T.; Tran, D.T.; Doan, T.L.L.; Kim, N.H.; Lee, J.H. Hierarchical Cu@Cu₂O nanowires arrays-coated gold nanodots as a highly sensitive self-supported electrocatalyst for L-cysteine oxidation. *Biosens. Bioelectron.* **2019**, *139*, 111327. [[CrossRef](#)]
139. Rasheed, P.A.; Pandey, R.P.; Jabbar, K.A.; Ponraj, J.; Mahmoud, K.A. Sensitive electrochemical detection of L-cysteine based on a highly stable Pd@Ti₃C₂T_x (MXene) nanocomposite modified glassy carbon electrode. *Anal. Methods* **2019**, *11*, 3851–3856. [[CrossRef](#)]
140. Manibalan, G.; Murugadoss, G.; Thangamuthu, R.; Kumar, M.R.; Kumar, R.M. Facile synthesis of CeO₂-SnO₂ nanocomposite for electrochemical determination of L-cysteine. *J. Alloys Compd.* **2019**, *792*, 1150–1161. [[CrossRef](#)]
141. Atacan, K. CuFe₂O₄/reduced graphene oxide nanocomposite decorated with gold nanoparticles as a new electrochemical sensor material for L-cysteine detection. *J. Alloys Compd.* **2019**, *791*, 391–401. [[CrossRef](#)]
142. Heidari, M.; Ghaffarinejad, A. Electrochemical sensor for L-cysteine by using a cobalt(II)/aluminum(III) layered double hydroxide as a nanocatalyst. *Microchim. Acta* **2019**, *186*, 365. [[CrossRef](#)]
143. Yuan, B.; Wang, H.; Cai, J.; Peng, Y.; Niu, Y.; Chen, H.; Bai, L.; Zhang, S.; Jin, J.; Liu, L.; et al. A novel oxidation-reduction method for highly selective detection of cysteine over reduced glutathione based on synergistic effect of fully fluorinated cobalt phthalocyanine and ordered mesoporous carbon. *Sens. Actuators B Chem.* **2019**, *288*, 180–187. [[CrossRef](#)]
144. Beitollahi, H.; Ganjali, M.R.; Norouzi, P.; Movlaee, K.; Hosseinzadeh, R.; Tajik, S. A novel electrochemical sensor based on graphene nanosheets and ethyl 2-(4-ferrocenyl-[1,2,3]triazol-1-yl) acetate for electrocatalytic oxidation of cysteine and tyrosine. *Meas. J. Int. Meas. Confed.* **2020**, *152*, 107302. [[CrossRef](#)]
145. Hussain, M.; Khaliq, N.; Nisar, A.; Khan, M.; Karim, S.; Khan, A.A.; Yi, X.; Maqbool, M.; Ali, G. TiO₂ nanotube array-modified electrodes for L-cysteine biosensing: Experimental and density-functional theory study. *Nanotechnology* **2020**, *31*, 505501. [[CrossRef](#)]
146. Norouzi, B.; Gorji, A. Preparation of cobalt-poly (naphthylamine)/sodium dodecylsulfate-modified carbon paste electrode as a sensitive sensor for L-cysteine. *Ionics* **2019**, *25*, 797–807. [[CrossRef](#)]
147. Kurniawan, A.; Kurniawan, F.; Gunawan, F.; Chou, S.H.; Wang, M.J. Disposable electrochemical sensor based on copper-electrodeposited screen-printed gold electrode and its application in sensing L-Cysteine. *Electrochim. Acta* **2019**, *293*, 318–327. [[CrossRef](#)]
148. Keshavananda Prabhu, C.P.; Manjunatha, N.; Shambhulinga, A.; Imadadulla, M.; Shivaprasad, K.H.; Amshumali, M.K.; Lokesh, K.S. Synthesis and characterization of novel imine substituted phthalocyanine for sensing of L-cysteine. *J. Electroanal. Chem.* **2019**, *834*, 130–137. [[CrossRef](#)]
149. Zhang, Y.; Ma, Y.; Wei, T.; Lin, F.F.; Qiu, F.L.; Pei, L.Z. Polyaniline/zinc bismuthate nanocomposites for the enhanced electrochemical performance of the determination of L-Cysteine. *Meas. J. Int. Meas. Confed.* **2018**, *128*, 55–62. [[CrossRef](#)]
150. Tajyani, S.; Babaei, A. A new sensing platform based on magnetic Fe₃O₄@NiO core/shell nanoparticles modified carbon paste electrode for simultaneous voltammetric determination of Quercetin and Tryptophan. *J. Electroanal. Chem.* **2018**, *808*, 50–58. [[CrossRef](#)]

151. Premlatha, S.; Selvarani, K.; Bapu, G.N.K.R. Facile Electrodeposition of Hierarchical Co-Gd₂O₃ Nanocomposites for Highly Selective and Sensitive Electrochemical Sensing of L-Cysteine. *ChemistrySelect* **2018**, *3*, 2665–2674. [[CrossRef](#)]
152. Pei, L.Z.; Wei, T.; Lin, N.; Zhang, H.; Fan, C.G. Bismuth Tellurate Nanospheres and Electrochemical Behaviors of L-Cysteine at the Nanospheres Modified Electrode. *Russ. J. Electrochem.* **2018**, *54*, 84–91. [[CrossRef](#)]
153. Bananezhad, A.; Karimi-Maleh, H.; Ganjali, M.R.; Norouzi, P. MnO₂-TiO₂ Nanocomposite and 2-(3,4-Dihydroxyphenethyl) Isoindoline-1,3-Dione as an Electrochemical Platform for the Concurrent Determination of Cysteine, Tryptophan and Uric Acid. *Electroanalysis* **2018**, *30*, 1759–1765. [[CrossRef](#)]
154. Wen, Y.; Pei, L.Z.; Wei, T. Growth of Li doped bismuth oxide nanorods and its electrochemical performance for the determination of L-cysteine. *Mater. Res.* **2017**, *20*, 592–600. [[CrossRef](#)]
155. Lin, F.F.; Wei, T.; Pei, L.Z.; Lin, N. Sensitive electrochemical determination of L-cysteine using bismuth nickelate nanorods modified electrode. *J. Bionanosci.* **2017**, *11*, 177–182. [[CrossRef](#)]
156. Hooshmand, S.; Es'haghi, Z. Simultaneous quantification of arginine, alanine, methionine and cysteine amino acids in supplements using a novel bioelectro-nanosensor based on CdSe quantum dot/modified carbon nanotube hollow fiber pencil graphite electrode via Taguchi method. *J. Pharm. Biomed. Anal.* **2017**, *146*, 226–235. [[CrossRef](#)] [[PubMed](#)]
157. Sakthivel, M.; Sivakumar, M.; Chen, S.M.; Lun-Cheng, W. Thulium (III) hexacyanoferrate star fruit-like structure modified electrode for L-cysteine electrochemical sensor. *Int. J. Electrochem. Sci.* **2016**, *11*, 8016–8026. [[CrossRef](#)]
158. Pei, L.Z.; Wei, T.; Lin, N.; Cai, Z.Y.; Fan, C.G.; Yang, Z. Synthesis of Zinc bismuthate nanorods and electrochemical performance for sensitive determination of L-Cysteine. *J. Electrochem. Soc.* **2016**, *163*, H1–H8. [[CrossRef](#)]
159. Pazalja, M.; Kahrović, E.; Zahirović, A.; Turkušić, E. Electrochemical sensor for determination of L-cysteine based on carbon electrodes modified with Ru(III) Schiff base complex, carbon nanotubes and nafion. *Int. J. Electrochem. Sci.* **2016**, *11*, 10939–10952. [[CrossRef](#)]
160. Hernández-Ibáñez, N.; Sanjuán, I.; Montiel, M.Á.; Foster, C.W.; Banks, C.E.; Iniesta, J. L-Cysteine determination in embryo cell culture media using Co(II)-phthalocyanine modified disposable screen-printed electrodes. *J. Electroanal. Chem.* **2016**, *780*, 303–310. [[CrossRef](#)]
161. Hashemi, H.S.; Nezamzadeh-Ejehieh, A.; Karimi-Shamsabadi, M. A novel cysteine sensor based on modification of carbon paste electrode by Fe(II)-exchanged zeolite X nanoparticles. *Mater. Sci. Eng. C* **2016**, *58*, 286–293. [[CrossRef](#)]
162. Geng, D.; Li, M.; Bo, X.; Guo, L. Molybdenum nitride/nitrogen-doped multi-walled carbon nanotubes hybrid nanocomposites as novel electrochemical sensor for detection L-cysteine. *Sens. Actuators B Chem.* **2016**, *237*, 581–590. [[CrossRef](#)]
163. Da Silveira, T.S.; Fernandes, D.S.; Magossi, M.S.; Barbosa, P.P.; Souza, T.R.; Magossi, M.S.; Do Carmo, D.R. A novel composite obtained through of chemical interaction of zirconium (IV) phosphated with silver hexacyanoferrate (III) for voltammetric detection of L-cysteine. *Int. J. Electrochem. Sci.* **2016**, *11*, 7527–7539. [[CrossRef](#)]
164. Areias, M.C.C.; Shimizu, K.; Compton, R.G. Cysteine determination: Via adsorptive stripping voltammetry using a bare glassy carbon electrode. *Analyst* **2016**, *141*, 5563–5570. [[CrossRef](#)] [[PubMed](#)]
165. Safavi, A.; Abbaspour, A.; Ajamian, M. Determination of Cysteine at Bismuth Nanostructure—Carbon Ionic Liquid Electrode by Square Wave Voltammetry. *Electroanalysis* **2015**, *27*, 2335–2340. [[CrossRef](#)]
166. Lee, P.T.; Thomson, J.E.; Karina, A.; Salter, C.; Johnston, C.; Davies, S.G.; Compton, R.G. Selective electrochemical determination of cysteine with a cyclotricatechylene modified carbon electrode. *Analyst* **2015**, *140*, 236–242. [[CrossRef](#)] [[PubMed](#)]
167. Khalilzadeh, M.A.; Karimi-Maleh, H.; Gupta, V.K. A Nanostructure Based Electrochemical Sensor for Square Wave Voltammetric Determination of L-Cysteine in the Presence of High Concentration of Folic Acid. *Electroanalysis* **2015**, *27*, 1766–1773. [[CrossRef](#)]
168. Vladislavic', N.; Brinic', S.; Grubac, Z.; Buzuk, M. Study of bi film formation on different carbon based electrodes for possible applicability in electroanalytical determination of cysteine. *Int. J. Electrochem. Sci.* **2014**, *9*, 6020–6032.
169. Aswini, K.K.; Mohan, A.M.V.; Biju, V.M. Molecularly imprinted polymer based electrochemical detection of L-cysteine at carbon paste electrode. *Mater. Sci. Eng. C* **2014**, *37*, 321–326. [[CrossRef](#)]
170. Majd, S.M.; Teymourian, H.; Salimi, A. Fabrication of an electrochemical L-cysteine sensor based on graphene nanosheets decorated manganese oxide nanocomposite modified glassy carbon electrode. *Electroanalysis* **2013**, *25*, 2201–2210. [[CrossRef](#)]
171. Liu, S.; Luo, T.; Li, L. Sensitive L-cysteine amperometric sensor based on a glassy carbon electrode modified by MnO₂ nanoparticles. *Instrum. Sci. Technol.* **2013**, *41*, 382–393. [[CrossRef](#)]
172. Wang, Y.; Peng, W.; Liu, L.; Gao, F.; Li, M. The electrochemical determination of L-cysteine at a Ce-doped Mg-Al layered double hydroxide modified glassy carbon electrode. *Electrochim. Acta* **2012**, *70*, 193–198. [[CrossRef](#)]
173. Nezamzadeh-Ejehieh, A.; Hashemi, H.S. Voltammetric determination of cysteine using carbon paste electrode modified with Co(II)-Y zeolite. *Talanta* **2012**, *88*, 201–208. [[CrossRef](#)]
174. Cumba, L.R.; Bicalho, U.O.; Carmo, D.R. Preparation and voltammetric studies of titanium (IV) Phosphate modified with silver hexacyanoferrate to a voltammetric determination of L-cysteine. *Int. J. Electrochem. Sci.* **2012**, *7*, 4465–4478.
175. Xiao, C.; Chen, J.; Liu, B.; Chu, X.; Wu, L.; Yao, S. Sensitive and selective electrochemical sensing of L-cysteine based on a caterpillar-like manganese dioxide-carbon nanocomposite. *Phys. Chem. Chem. Phys.* **2011**, *13*, 1568–1574. [[CrossRef](#)] [[PubMed](#)]
176. Qu, L.; Yang, S.; Li, G.; Yang, R.; Li, J.; Yu, L. Preparation of yttrium hexacyanoferrate/carbon nanotube/Nafion nanocomposite film-modified electrode: Application to the electrocatalytic oxidation of L-cysteine. *Electrochim. Acta* **2011**, *56*, 2934–2940. [[CrossRef](#)]

177. Long, Y.T.; Kong, C.; Li, D.W.; Li, Y.; Chowdhury, S.; Tian, H. Ultrasensitive determination of cysteine based on the photocurrent of nafion-functionalized CdS-MV quantum dots on an ITO electrode. *Small* **2011**, *7*, 1624–1628. [[CrossRef](#)]
178. Kannan, P.; John, S.A. Ultrasensitive detection of L-cysteine using gold-5-amino-2-mercapto-1,3,4-thiadiazole core-shell nanoparticles film modified electrode. *Biosens. Bioelectron.* **2011**, *30*, 276–281. [[CrossRef](#)] [[PubMed](#)]
179. Lai, Y.T.; Ganguly, A.; Chen, L.C.; Chen, K.H. Direct voltammetric sensing of L-Cysteine at pristine GaN nanowires electrode. *Biosens. Bioelectron.* **2010**, *26*, 1688–1691. [[CrossRef](#)]
180. Stabler, S.P.; Marcell, P.D.; Podell, E.R.; Allen, R.H. Quantitation of total homocysteine, total cysteine, and methionine in normal serum and urine using capillary gas chromatography-mass spectrometry. *Anal. Biochem.* **1987**, *162*, 185–196. [[CrossRef](#)]
181. Odewunmi, N.A.; Kawde, A.N.; Ibrahim, M. In-situ single-step electrochemical AgO modified graphite pencil electrode for trace determination of DL-methionine in human serum sample. *Sens. Actuators B Chem.* **2019**, *281*, 765–773. [[CrossRef](#)]
182. Tavakkoli, N.; Soltani, N.; Khorshidi, E. Preparation of Ru-Pt bimetallic monolayer on nanoporous gold film electrode and its application as an ultrasensitive sensor for determination of methionine. *RSC Adv.* **2017**, *7*, 21827–21836. [[CrossRef](#)]
183. Murugavelu, M.; Karthikeyan, B. Synthesis, characterization of Ag-Au core-shell bimetal nanoparticles and its application for electrocatalytic oxidation/sensing of L-methionine. *Mater. Sci. Eng. C* **2017**, *70*, 656–664. [[CrossRef](#)]
184. Perevezentseva, D.O.; Skirdin, K.V.; Gorchakov, E.V.; Bimatov, V.I. Electrochemical activity of methionine at graphite electrode modified with gold nanoparticles. *Key Eng. Mater.* **2016**, *685*, 563–568. [[CrossRef](#)]
185. Li, Y.; Mei, S.; Liu, S.; Hun, X. A photoelectrochemical sensing strategy based on single-layer MoS₂ modified electrode for methionine detection. *J. Pharm. Biomed. Anal.* **2019**, *165*, 94–100. [[CrossRef](#)] [[PubMed](#)]
186. Molaakbari, E.; Mostafavi, A.; Beitollahi, H. Simultaneous electrochemical determination of dopamine, melatonin, methionine and caffeine. *Sens. Actuators B Chem.* **2015**, *208*, 195–203. [[CrossRef](#)]
187. Sasikumar, R.; Chen, T.W.; Chen, S.M.; Rwei, S.P.; Yu, M.C. Facile synthesis of Mn₂O₃ for highly active catalytic oxidation and reduction of organic substances and electrochemical determination of L-Methionine. *Int. J. Electrochem. Sci.* **2018**, *13*, 4561–4574. [[CrossRef](#)]
188. Pourbahman, F.; Sattarahmady, N.; Heli, H. Electrodeposition of Nickel Hydroxide Nanoparticles on Glassy Carbon Electrode-Applied to Electroanalysis of L-Methionine. *Sens. Lett.* **2016**, *14*, 65–71. [[CrossRef](#)]
189. Chekin, F.; Bagheri, S.; Hamid, S.B.A. Synthesis of Pt doped TiO₂ nanoparticles: Characterization and application for electrocatalytic oxidation of L-methionine. *Sens. Actuators B Chem.* **2013**, *177*, 898–903. [[CrossRef](#)]
190. Jeevagan, A.J.; John, S.A. Electrochemical determination of L-methionine using the electropolymerized film of non-peripheral amine substituted Cu(II) phthalocyanine on glassy carbon electrode. *Bioelectrochemistry* **2012**, *85*, 50–55. [[CrossRef](#)] [[PubMed](#)]
191. Tabeshnia, M.; Rashvandavei, M.; Amini, R.; Pashae, F. Electrocatalytic oxidation of some amino acids on a cobalt hydroxide nanoparticles modified glassy carbon electrode. *J. Electroanal. Chem.* **2010**, *647*, 181–186. [[CrossRef](#)]
192. Zor, E.; Saglam, M.E.; Alpaydin, S.; Bingol, H. A reduced graphene oxide/ α -cyclodextrin hybrid for the detection of methionine: Electrochemical, fluorometric and computational studies. *Anal. Methods* **2014**, *6*, 6522–6530. [[CrossRef](#)]
193. Zhang, D.; Xu, C.; Li, S.; Zhang, R.; Yan, H.; Miao, H.; Fan, Y.; Yuan, B. Electrochemically controlling oxygen functional groups in graphene oxide for the optimization in the electro-catalytic oxidation of dihydroxybenzene isomers and L-methionine. *J. Electroanal. Chem.* **2014**, *717*, 219–224. [[CrossRef](#)]
194. Gómez-Mingot, M.; Iniesta, J.; Montiel, V.; Kadara, R.O.; Banks, C.E. Direct oxidation of methionine at screen printed graphite macroelectrodes: Towards rapid sensing platforms. *Sens. Actuators B Chem.* **2011**, *155*, 831–836. [[CrossRef](#)]
195. Ziyatdinova, G.; Grigor'Eva, L.; Morozov, M.; Gilmutdinov, A.; Budnikov, H. Electrochemical oxidation of sulfur-containing amino acids on an electrode modified with multi-walled carbon nanotubes. *Microchim. Acta* **2009**, *165*, 353–359. [[CrossRef](#)]
196. Kalinke, C.; Neumsteir, N.V.; de Oliveira, P.R.; Janegitz, B.C.; Bonacin, J.A. Sensing of L-methionine in biological samples through fully 3D-printed electrodes. *Anal. Chim. Acta* **2021**, *1142*, 135–142. [[CrossRef](#)]
197. Tajik, S.; Taher, M.A.; Beitollahi, H.; Hosseinzadeh, R.; Ranjbar, M. Preparation, Characterization and Electrochemical Application of ZnS/ZnAl₂S₄ Nanocomposite for Voltammetric Determination of Methionine and Tryptophan Using Modified Carbon Paste Electrode. *Electroanalysis* **2016**, *28*, 656–662. [[CrossRef](#)]
198. Beitollahi, H.; Mohadesi, A.; Ghorbani, F.; Maleh, H.K.; Baghayeri, M.; Hosseinzadeh, R. Electrocatalytic measurement of methionine concentration with a carbon nanotube paste electrode modified with benzoylferrocene. *Chin. J. Catal.* **2013**, *34*, 1333–1338. [[CrossRef](#)]
199. Revin, S.B.; John, S.A. Selective and Sensitive Electrochemical Sensor for L-Methionine at Physiological pH Using Functionalized Triazole Polymer Film Modified Electrode. *Electroanalysis* **2012**, *24*, 1277–1283. [[CrossRef](#)]
200. Tan, W.T.; Goh, J.K. Electrochemical oxidation of methionine mediated by a fullerene-C 60 modified gold electrode. *Electroanalysis* **2008**, *20*, 2447–2453. [[CrossRef](#)]
201. Idili, A.; Gerson, J.; Parolo, C.; Kippin, T.; Plaxco, K.W. An electrochemical aptamer-based sensor for the rapid and convenient measurement of L-tryptophan. *Anal. Bioanal. Chem.* **2019**, *411*, 4629. [[CrossRef](#)] [[PubMed](#)]
202. Smith, D.F. Effects of age on serum tryptophan and urine indican in adults given a tryptophan load test. *Eur. J. Drug Metab. Pharmacokinet.* **1982**, *7*, 55–58. [[CrossRef](#)]
203. Ghoreishi, S.M.; Behpour, M.; Ghoreishi, F.S.; Mousavi, S. Voltammetric determination of tryptophan in the presence of uric acid and dopamine using carbon paste electrode modified with multi-walled carbon nanotubes. *Arab. J. Chem.* **2017**, *10*, S1546–S1552. [[CrossRef](#)]

204. Roushani, M.; Sarabaegi, M. Novel electrochemical sensor based on carbon nanodots/chitosan nanocomposite for the detection of tryptophan. *J. Iran. Chem. Soc.* **2015**, *12*, 1875–1882. [[CrossRef](#)]
205. Wang, L.; Yang, R.; Li, J.; Qu, L.; Harrington, P.B. A highly selective and sensitive electrochemical sensor for tryptophan based on the excellent surface adsorption and electrochemical properties of PSS functionalized graphene. *Talanta* **2019**, *196*, 309–316. [[CrossRef](#)]
206. Sakthivel, R.; Mutharani, B.; Chen, S.M.; Kubendhiran, S.; Chen, T.W.; Al-Hemaid, F.M.A.; Ali, M.A.; Elshikh, M.S. A simple and rapid electrochemical determination of L-tryptophan based on functionalized carbon black/poly-L-histidine nanocomposite. *J. Electrochem. Soc.* **2018**, *165*, B422–B430. [[CrossRef](#)]
207. Xiao, Q.; Lu, S.; Huang, C.; Su, W.; Zhou, S.; Sheng, J.; Huang, S. An electrochemical chiral sensor based on amino-functionalized graphene quantum dots/ β -cyclodextrin modified glassy carbon electrode for enantioselective detection of tryptophan isomers. *J. Iran. Chem. Soc.* **2017**, *14*, 1957–1970. [[CrossRef](#)]
208. Yu, L.Y.; Liu, Q.; Wu, X.W.; Jiang, X.Y.; Yu, J.G.; Chen, X.Q. Chiral electrochemical recognition of tryptophan enantiomers at a multi-walled carbon nanotube-chitosan composite modified glassy carbon electrode. *RSC Adv.* **2015**, *5*, 98020–98025. [[CrossRef](#)]
209. Zou, J.; Huang, L.; Jiang, X.; Jiao, F.; Yu, J. Enhanced chiral electrochemical recognition of tryptophan enantiomers using a novel triple-layered GO/BSA/CS modified glassy carbon electrode. *Nanosci. Nanotechnol. Lett.* **2017**, *9*, 1700–1707. [[CrossRef](#)]
210. Ou, J.; Tao, Y.; Xue, J.; Kong, Y.; Dai, J.; Deng, L. Electrochemical enantiorecognition of tryptophan enantiomers based on graphene quantum dots-chitosan composite film. *Electrochem. Commun.* **2015**, *57*, 5–9. [[CrossRef](#)]
211. Ba, X.; Luo, L.; Ding, Y.; Liu, X. Determination of L-tryptophan in the presence of ascorbic acid and dopamine using poly(sulfosalicylic acid) modified glassy carbon electrode. *Sens. Actuators B Chem.* **2013**, *187*, 27–32. [[CrossRef](#)]
212. Kumar, J.V.; Karthik, R.; Chen, S.M.; Marikkani, S.; Elangovan, A.; Muthuraj, V. Green synthesis of a novel flower-like cerium vanadate microstructure for electrochemical detection of tryptophan in food and biological samples. *J. Colloid Interface Sci.* **2017**, *496*, 78–86. [[CrossRef](#)]
213. Yang, X.; Kirsch, J.; Fergus, J.; Simonian, A. Modeling analysis of electrode fouling during electrolysis of phenolic compounds. *Electrochim. Acta* **2013**, *94*, 259–268. [[CrossRef](#)]
214. Singh, V.V.; Nigam, A.K.; Batra, A.; Boopathi, M.; Singh, B.; Vijayaraghavan, R. Applications of Ionic Liquids in Electrochemical Sensors and Biosensors. *Int. J. Electrochem.* **2012**, *2012*, 165683. [[CrossRef](#)]
215. Safavi, A.; Momeni, S. Electrocatalytic oxidation of tryptophan at gold nanoparticle-modified carbon ionic liquid electrode. *Electroanalysis* **2010**, *22*, 2848–2855. [[CrossRef](#)]
216. Thomas, T.; Mascarenhas, R.J.; D'Souza, O.J.; Martis, P.; Dalhalla, J.; Swamy, B.E.K. Multi-walled carbon nanotube modified carbon paste electrode as a sensor for the amperometric detection of L-tryptophan in biological samples. *J. Colloid Interface Sci.* **2013**, *402*, 223–229. [[CrossRef](#)]
217. Fiorucci, A.R.; Cervini, P.; Filho, O.F.; Cavaleiro, É.T.G. Tryptophan determination at carbon fiber ultramicroelectrodes by fast-scan cyclic voltammetry. *J. Braz. Chem. Soc.* **2013**, *24*, 1228–1236. [[CrossRef](#)]
218. Rejithamol, R.; Krishnan, R.G.; Beena, S. Disposable pencil graphite electrode decorated with a thin film of electro-polymerized 2, 3, 4, 6, 7, 8, 9, 10-octahydropyrimido [1, 2-a] azepine for simultaneous voltammetric analysis of dopamine, serotonin and tryptophan. *Mater. Chem. Phys.* **2021**, *258*, 123857. [[CrossRef](#)]
219. Deng, P.; Nie, X.; Wu, Y.; Tian, Y.; Li, J.; He, Q. A cost-saving preparation of nickel nanoparticles/nitrogen-carbon nanohybrid as effective advanced electrode materials for highly sensitive tryptophan sensor. *Microchem. J.* **2021**, *160*, 105744. [[CrossRef](#)]
220. Zagitova, L.R.; Maistrenko, V.N.; Yarkaeva, Y.A.; Zagitov, V.V.; Zilberg, R.A.; Kovyazin, P.V.; Parfenova, L.V. Novel chiral voltammetric sensor for tryptophan enantiomers based on 3-neomenthylindene as recognition element. *J. Electroanal. Chem.* **2021**, *880*, 114939. [[CrossRef](#)]
221. Nie, X.; Zhang, R.; Tang, Z.; Wang, H.; Deng, P.; Tang, Y. Sensitive and selective determination of tryptophan using a glassy carbon electrode modified with nano-CeO₂/reduced graphene oxide composite. *Microchem. J.* **2020**, *159*, 105367. [[CrossRef](#)]
222. Zhang, J.-W.; Zhang, X. Electrode material fabricated by loading cerium oxide nanoparticles on reduced graphene oxide and its application in electrochemical sensor for tryptophan. *J. Alloys Compd.* **2020**, *842*, 155934. [[CrossRef](#)]
223. Mousavi, S.-F.; Alimoradi, M.; Shirmardi, A.; Zare-Shahabadi, V. Preparation, characterization and electrochemical application of an Ag/zeolite nanocomposite: Application to sub-micromolar quantitation of tryptophan. *J. Porous Mater.* **2020**, *27*, 1505–1514. [[CrossRef](#)]
224. Yıldız, C.; Bayraktepe, D.E.; Yazan, Z. Electrochemical low-level detection of L-tryptophan in human urine samples: Use of pencil graphite leads as electrodes for a fast and cost-effective voltammetric method. *Chem. Mon.* **2020**, *151*, 871–879. [[CrossRef](#)]
225. Khoshnevisan, K.; Torabi, F.; Baharifar, H.; Sajjadi-Jazi, S.M.; Afjeh, M.S.; Faridbod, F.; Larijani, B.; Khorramizadeh, M.R. Determination of the biomarker L-tryptophan level in diabetic and normal human serum based on an electrochemical sensing method using reduced graphene oxide/gold nanoparticles/18-crown-6. *Anal. Bioanal. Chem.* **2020**, *412*, 3615–3627. [[CrossRef](#)] [[PubMed](#)]
226. Zhang, R.; Jamal, R.; Ge, Y.; Zhang, W.; Yu, Z.; Yan, Y.; Liu, Y.; Abdiryim, T. Functionalized PProDOT@nitrogen-doped carbon hollow spheres composites for electrochemical sensing of tryptophan. *Carbon* **2020**, *161*, 842–855. [[CrossRef](#)]
227. Nazarpour, S.; Hajian, R.; Sabzvari, M.H. A novel nanocomposite electrochemical sensor based on green synthesis of reduced graphene oxide/gold nanoparticles modified screen printed electrode for determination of tryptophan using response surface methodology approach. *Microchem. J.* **2020**, *154*, 104634. [[CrossRef](#)]

228. GunaVathana, S.D.; Thivya, P.; Wilson, J.; Peter, A.C. Sensitive voltammetric sensor based on silver dendrites decorated polythiophene nanocomposite: Selective determination of L-Tryptophan. *J. Mol. Struct.* **2020**, *1205*, 127649. [[CrossRef](#)]
229. Wu, Y.; Deng, P.; Tian, Y.; Ding, Z.; Li, G.; Liu, J.; Zuberi, Z.; He, Q. Rapid recognition and determination of tryptophan by carbon nanotubes and molecularly imprinted polymer-modified glassy carbon electrode. *Bioelectrochemistry* **2020**, *131*, 107393. [[CrossRef](#)] [[PubMed](#)]
230. He, Q.; Liu, J.; Feng, J.; Wu, Y.; Tian, Y.; Li, G.; Chen, D. Sensitive Voltammetric Sensor for Tryptophan Detection by Using Polyvinylpyrrolidone Functionalized Graphene/GCE. *Nanomaterials* **2020**, *10*, 125. [[CrossRef](#)]
231. Sangili, A.; Vinothkumar, V.; Chen, S.-M.; Veerakumar, P.; Chang, C.-W.; Muthuselvam, I.P.; Lin, K.-C. Highly Selective Voltammetric Sensor for L-Tryptophan Using Composite-Modified Electrode Composed of CuSn(OH)₆ Microsphere Decorated on Reduced Graphene Oxide. *J. Phys. Chem. C* **2020**, *124*, 25821–25834. [[CrossRef](#)]
232. Pandey, P.C.; Shukla, S.; Pandey, G.; Narayan, R.J. Organotrialkoxysilane-mediated synthesis of functional noble metal nanoparticles and their bimetallic for electrochemical recognition of L-tryptophan. *MRS Adv.* **2020**, *5*, 2429–2444. [[CrossRef](#)]
233. Gao, J.; Li, H.; Li, M.; Wang, G.; Long, Y.; Li, P.; Li, C.; Yang, B. Polydopamine/graphene/MnO₂ composite-based electrochemical sensor for in situ determination of free tryptophan in plants. *Anal. Chim. Acta* **2020**, *1145*, 103. [[CrossRef](#)]
234. Xia, Y.; Zhao, F.; Zeng, B. A molecularly imprinted copolymer based electrochemical sensor for the highly sensitive detection of L-Tryptophan. *Talanta* **2020**, *206*, 120245. [[CrossRef](#)]
235. Zhang, Y.; Waterhouse, G.I.N.; Xiang, Z.-p.; Che, J.; Chen, C.; Sun, W. A highly sensitive electrochemical sensor containing nitrogen-doped ordered mesoporous carbon (NOMC) for voltammetric determination of L-tryptophan. *Food Chem.* **2020**, *326*, 126976. [[CrossRef](#)]
236. Erbilen, N.; Zor, E.; Saf, A.O.; Akgemci, E.G.; Bingol, H. An electrochemical chiral sensor based on electrochemically modified electrode for the enantioselective discrimination of D-/L-tryptophan. *J. Solid State Electrochem.* **2019**, *23*, 2695–2705. [[CrossRef](#)]
237. Govindasamy, M.; Wang, S.-F.; Pan, W.C.; Subramanian, B.; Ramalingam, R.J.; Al-lohedan, H. Facile sonochemical synthesis of perovskite-type SrTiO₃ nanocubes with reduced graphene oxide nanocatalyst for an enhanced electrochemical detection of α -amino acid (tryptophan). *Ultrason. Sonochem.* **2019**, *56*, 193–199. [[CrossRef](#)]
238. Prongmanee, W.; Alam, I.; Asanithi, P. Hydroxyapatite/Graphene oxide composite for electrochemical detection of L-Tryptophan. *J. Taiwan Inst. Chem. Eng.* **2019**, *102*, 415–423. [[CrossRef](#)]
239. Karabozhikova, V.; Tsakova, V.; Lete, C.; Marin, M.; Lupu, S. Poly(3,4-ethylenedioxythiophene)-modified electrodes for tryptophan voltammetric sensing. *J. Electroanal. Chem.* **2019**, *848*, 113309. [[CrossRef](#)]
240. Niu, X.; Yang, X.; Mo, Z.; Liu, N.; Guo, R.; Pan, Z.; Liu, Z. Electrochemical chiral sensing of tryptophan enantiomers by using 3D nitrogen-doped reduced graphene oxide and self-assembled polysaccharides. *Microchim. Acta* **2019**, *186*, 557. [[CrossRef](#)] [[PubMed](#)]
241. Kokulnathan, T.; Chen, T.-W.; Chen, S.-M.; Kumar, J.V.; Sakthinathan, S.; Nagarajan, E.R. Hydrothermal synthesis of silver molybdate/reduced graphene oxide hybrid composite: An efficient electrode material for the electrochemical detection of tryptophan in food and biological samples. *Compos. Part B Eng.* **2019**, *169*, 249–257. [[CrossRef](#)]
242. Tian, Y.; Deng, P.; Wu, Y.; Ding, Z.; Li, G.; Liu, J.; He, Q. A Simple and Efficient Molecularly Imprinted Electrochemical Sensor for the Selective Determination of Tryptophan. *Biomolecules* **2019**, *9*, 294. [[CrossRef](#)] [[PubMed](#)]
243. Yang, X.; Niu, X.; Mo, Z.; Guo, R.; Liu, N.; Zhao, P.; Liu, Z. Perylene-functionalized graphene sheets modified with chitosan for voltammetric discrimination of tryptophan enantiomers. *Microchim. Acta* **2019**, *186*, 333. [[CrossRef](#)]
244. Zhou, S.; Deng, Z.; Wu, Z.; Xie, M.; Tian, Y.; Wu, Y.; Liu, J.; Li, G.; He, Q. Ta₂O₅/rGO Nanocomposite Modified Electrodes for Detection of Tryptophan through Electrochemical Route. *Nanomaterials* **2019**, *9*, 811. [[CrossRef](#)]
245. Qian, J.; Yi, Y.; Zhang, D.; Zhu, G. Electrochemical recognition of tryptophan enantiomers using a multi-walled carbon nanotube@polydopamine composite loaded with copper(II). *Microchim. Acta* **2019**, *186*, 358. [[CrossRef](#)]
246. Duan, S.; Wang, W.; Yu, C.; Liu, M.; Yu, L. Development of Electrochemical Sensor for Detection of L-Tryptophan Based on Exfoliated Graphene/PEDOT:PSS. *Nano* **2019**, *14*, 1950058. [[CrossRef](#)]
247. He, Q.; Tian, Y.; Wu, Y.; Liu, J.; Li, G.; Deng, P.; Chen, D. Electrochemical Sensor for Rapid and Sensitive Detection of Tryptophan by a Cu₂O Nanoparticles-Coated Reduced Graphene Oxide Nanocomposite. *Biomolecules* **2019**, *9*, 176. [[CrossRef](#)]
248. Rebekah, A.; Kokulnathan, T.; Wang, T.-J.; Viswanathan, C.; Ponpandian, N. MnCo₂O₄-rGO Hybrid Magnetic Nanocomposite Modified Glassy Carbon Electrode for Sensitive Detection of L-Tryptophan. *J. Electrochem. Soc.* **2019**, *166*, B845–B852. [[CrossRef](#)]
249. Liu, J.; Dong, S.; He, Q.; Yang, S.; Xie, M.; Deng, P.; Xia, Y.; Li, G. Facile Preparation of Fe₃O₄/C Nanocomposite and Its Application for Cost-Effective and Sensitive Detection of Tryptophan. *Biomolecules* **2019**, *9*, 245. [[CrossRef](#)]
250. Mattioli, I.A.; Baccarin, M.; Cervini, P.; Cavalheiro, É.T.G. Electrochemical investigation of a graphite-polyurethane composite electrode modified with electrodeposited gold nanoparticles in the voltammetric determination of tryptophan. *J. Electroanal. Chem.* **2019**, *835*, 212–219. [[CrossRef](#)]
251. Taleb, M.; Ivanov, R.; Bereznev, S.; Kazemi, S.H.; Hussainova, I. Alumina/graphene/Cu hybrids as highly selective sensor for simultaneous determination of epinephrine, acetaminophen and tryptophan in human urine. *J. Electroanal. Chem.* **2018**, *823*, 184–192. [[CrossRef](#)]
252. Sun, D.; Li, H.; Li, M.; Li, C.; Dai, H.; Sun, D.; Yang, B. Electrodeposition synthesis of a NiO/CNT/PEDOT composite for simultaneous detection of dopamine, serotonin, and tryptophan. *Sens. Actuators B Chem.* **2018**, *259*, 433–442. [[CrossRef](#)]

253. Song, J.; Yang, C.; Ma, J.; Han, Q.; Ran, P.; Fu, Y. Voltammetric chiral discrimination of tryptophan using a multilayer nanocomposite with implemented amino-modified β -cyclodextrin as recognition element. *Microchim. Acta* **2018**, *185*, 230. [[CrossRef](#)]
254. Shamsipur, M.; Taherpour, A.; Sharghi, H.; Pashabadi, A. Transduction of interaction between trace tryptophan and surface-confined chromium salen using impedance spectroscopy. A sensing device that works based on highly selective inhibition of mediator's Faradaic process. *Anal. Chim. Acta* **2018**, *1030*, 70–76. [[CrossRef](#)]
255. Saini, A.K.; Saraf, M.; Kumari, P.; Mobin, S.M. A highly selective and sensitive chemosensor for L-tryptophan by employing a Schiff based Cu(II) complex. *New J. Chem.* **2018**, *42*, 3509–3518. [[CrossRef](#)]
256. Rezaee, E.; Honarasa, F. Determination of Tryptophan by Using of Activated Multi-Walled Carbon Nanotube Ionic Liquid Electrode. *Russ. J. Electrochem.* **2018**, *54*, 1073–1080. [[CrossRef](#)]
257. Porifreva, A.V.; Gorbachuk, V.V.; Evtugyn, V.G.; Stoikov, I.I.; Evtugyn, G.A. Glassy Carbon Electrode Modified with Silver Nanodendrites Implemented in Polylactide-Thiacalix[4]arene Copolymer for the Electrochemical Determination of Tryptophan. *Electroanalysis* **2018**, *30*, 641–649. [[CrossRef](#)]
258. Naganathan, D.; Thangamani, P.; Selvam, T.; Narayanasamy, T. Ce doped ZnO/f-MWCNT moss ball like nanocomposite: A strategy for high responsive current detection of L-tryptophan. *Microchim. Acta* **2018**, *185*, 96. [[CrossRef](#)]
259. Mukdasai, S.; Poosittsak, S.; Ngeontae, W.; Srijaranai, S. A highly sensitive electrochemical determination of L-tryptophan in the presence of ascorbic acid and uric acid using in situ addition of tetrabutylammonium bromide on the β -cyclodextrin incorporated multi-walled carbon nanotubes modified electrode. *Sens. Actuators B Chem.* **2018**, *272*, 518–525. [[CrossRef](#)]
260. Mohammadi, S.Z.; Beitollahi, H.; Hassanzadeh, M. Voltammetric determination of tryptophan using a carbon paste electrode modified with magnesium core shell nanocomposite and ionic liquids. *Anal. Bioanal. Chem. Res.* **2018**, *5*, 55–65.
261. Li, J.; Jiang, J.; Xu, Z.; Liu, M.; Tang, S.; Yang, C.; Qian, D. Facile synthesis of Pd–Cu@Cu₂O/N-RGO hybrid and its application for electrochemical detection of tryptophan. *Electrochim. Acta* **2018**, *260*, 526–535. [[CrossRef](#)]
262. Kubendhiran, S.; Karikalan, N.; Chen, S.M.; Sundaresan, P.; Karthik, R. Synergistic activity of single crystalline bismuth sulfide and sulfur doped graphene towards the electrocatalysis of tryptophan. *J. Catal.* **2018**, *367*, 252–263. [[CrossRef](#)]
263. Khan, M.Z.H.; Liu, X.; Tang, Y.; Zhu, J.; Hu, W.; Liu, X. A glassy carbon electrode modified with a composite consisting of gold nanoparticle, reduced graphene oxide and poly(L-arginine) for simultaneous voltammetric determination of dopamine, serotonin and L-tryptophan. *Microchim. Acta* **2018**, *185*, 439. [[CrossRef](#)]
264. Karim-Nezhad, G.; Sarkary, A.; Khorablou, Z.; Dorraji, P.S. Electrochemical analysis of tryptophan using a nanostructuring electrode with multi-walled carbon nanotubes and cetyltrimethylammonium bromide nanocomposite. *J. Nanostruct.* **2018**, *8*, 266–275.
265. Karimi, S.; Heydari, M. Voltammetric mixture analysis of tyrosine and tryptophan using carbon paste electrode modified by newly synthesized mesoporous silica nanoparticles and clustering of variable-partial least square: Efficient strategy for template extraction in mesoporous silica nanoparticle synthesis. *Sens. Actuators B Chem.* **2018**, *257*, 1134–1142.
266. Hasanzadeh, M.; Karimzadeh, A.; Shadjou, N. Magnetic graphene quantum dots as a functional nanomaterial towards voltammetric detection of L-tryptophan at physiological pH. *J. Nanostruct.* **2018**, *8*, 21–30.
267. Ghanbari, K.; Bonyadi, S. An electrochemical sensor based on reduced graphene oxide decorated with polypyrrole nanofibers and zinc oxide-copper oxide p-n junction heterostructures for the simultaneous voltammetric determination of ascorbic acid, dopamine, paracetamol, and tryptophan. *New J. Chem.* **2018**, *42*, 8512–8523.
268. Bahmanzadeh, S.; Noroozifar, M. Fabrication of modified carbon paste electrodes with Ni-doped Lewatit FO₃₆ nano ion exchange resin for simultaneous determination of epinephrine, paracetamol and tryptophan. *J. Electroanal. Chem.* **2018**, *809*, 153–162. [[CrossRef](#)]
269. Zhao, D.; Lu, Y.; Ding, Y.; Fu, R. An amperometric L-tryptophan sensor platform based on electrospun tricobalt tetroxide nanoparticles decorated carbon nanofibers. *Sens. Actuators B Chem.* **2017**, *241*, 601–606. [[CrossRef](#)]
270. Zeinali, H.; Bagheri, H.; Monsef-Khoshhesab, Z.; Khoshsafari, H.; Hajian, A. Nanomolar simultaneous determination of tryptophan and melatonin by a new ionic liquid carbon paste electrode modified with SnO₂-Co₃O₄@rGO nanocomposite. *Mater. Sci. Eng. C* **2017**, *71*, 386–394. [[CrossRef](#)] [[PubMed](#)]
271. Wang, C.; Xiong, Z.; Sun, P.; Wang, R.; Zhao, X.; Wang, Q. Facile longitudinal unzipped multiwalled carbon nanotubes incorporated overoxidized poly(*p*-aminophenol) modified electrode for sensitive simultaneous determination of dopamine, uric acid and tryptophan. *J. Electroanal. Chem.* **2017**, *801*, 395–402. [[CrossRef](#)]
272. Tiğ, G.A. Development of electrochemical sensor for detection of ascorbic acid, dopamine, uric acid and L-tryptophan based on Ag nanoparticles and poly(L-arginine)-graphene oxide composite. *J. Electroanal. Chem.* **2017**, *807*, 19–28. [[CrossRef](#)]
273. Shabani-Nooshabadi, M.; Roostaei, M.; Karimi-Maleh, H. Incorporation of graphene oxide–NiO nanocomposite and *n*-hexyl-3-methylimidazolium hexafluoro phosphate into carbon paste electrode: Application as an electrochemical sensor for simultaneous determination of benserazide, levodopa and tryptophan. *J. Iran. Chem. Soc.* **2017**, *14*, 955–961. [[CrossRef](#)]
274. Nunes da Silva, D.; Tarley, C.R.T.; Pereira, A.C. Development of a Sensor Based on Modified Carbon Paste with Com Iron(III) Protoporphyrin Immobilized on SiNbZn Silica Matrix for L-tryptophan Determination. *Electroanalysis* **2017**, *29*, 2793–2802. [[CrossRef](#)]
275. Narouei, F.H.; Tammandani, H.K.; Ghalandarzehi, Y.; Sabbaghi, N.; Noroozifar, M. An electrochemical sensor based on conductive polymers/graphite paste electrode for simultaneous determination of dopamine, uric acid and tryptophan in biological samples. *Int. J. Electrochem. Sci.* **2017**, *12*, 7739–7753. [[CrossRef](#)]

276. Liu, X.; Zhang, J.; Di, J.; Long, Y.; Li, W.; Tu, Y. Graphene-like carbon nitride nanosheet as a novel sensing platform for electrochemical determination of tryptophan. *J. Colloid Interface Sci.* **2017**, *505*, 964–972. [[CrossRef](#)] [[PubMed](#)]
277. Haldorai, Y.; Yeon, S.H.; Huh, Y.S.; Han, Y.K. Electrochemical determination of tryptophan using a glassy carbon electrode modified with flower-like structured nanocomposite consisting of reduced graphene oxide and SnO₂. *Sens. Actuators B Chem.* **2017**, *239*, 1221–1230. [[CrossRef](#)]
278. Chen, J.; He, P.; Bai, H.; He, S.; Zhang, T.; Zhang, X.; Dong, F. Poly(β -cyclodextrin)/carbon quantum dots modified glassy carbon electrode: Preparation, characterization and simultaneous electrochemical determination of dopamine, uric acid and tryptophan. *Sens. Actuators B Chem.* **2017**, *252*, 9–16. [[CrossRef](#)]
279. Habibi, B.; Ayazi, Z.; Dadkhah, M. Multi-walled carbon nanotubes/ionic liquid nanocomposite modified carbon/ceramic electrode: Electrochemistry and measurement of tryptophan in the presence of uric acid. *Anal. Bioanal. Chem. Res.* **2017**, *4*, 155–169.
280. Ghoreishi, S.M.; Malekian, M. Curve resolution on overlapped voltammograms for simultaneous determination of tryptophan and tyrosine at carbon paste electrode modified with ZnFe₂O₄ nanoparticles. *J. Electroanal. Chem.* **2017**, *805*, 1–10. [[CrossRef](#)]
281. Alizadeh, T.; Amjadi, S. A tryptophan assay based on the glassy carbon electrode modified with a nano-sized tryptophan-imprinted polymer and multi-walled carbon nanotubes. *New J. Chem.* **2017**, *41*, 4493–4502. [[CrossRef](#)]
282. Yokuş, Ö.A.; Kardaş, F.; Akyildirim, O.; Eren, T.; Atar, N.; Yola, M.L. Sensitive voltammetric sensor based on polyoxometalate/reduced graphene oxide nanomaterial: Application to the simultaneous determination of L-tyrosine and L-tryptophan. *Sens. Actuators B Chem.* **2016**, *233*, 47–54. [[CrossRef](#)]
283. Yang, Y.J.; Yu, X. Cetyltrimethylammonium bromide assisted self-assembly of phosphotungstic acid on graphene oxide nanosheets for selective determination of tryptophan. *J. Solid State Electrochem.* **2016**, *20*, 1697–1704. [[CrossRef](#)]
284. Xu, J.; Wang, Q.; Xuan, C.; Xia, Q.; Lin, X.; Fu, Y. Chiral Recognition of Tryptophan Enantiomers Based on β -Cyclodextrin-platinum Nanoparticles/Graphene Nanohybrids Modified Electrode. *Electroanalysis* **2016**, *28*, 868–873. [[CrossRef](#)]
285. Xiao, Q.; Lu, S.; Huang, C.; Su, W.; Huang, S. Novel N-doped carbon dots/ β -cyclodextrin nanocomposites for enantioselective recognition of tryptophan enantiomers. *Sensors* **2016**, *16*, 1874. [[CrossRef](#)] [[PubMed](#)]
286. Wang, Y.; Ouyang, X.; Ding, Y.; Liu, B.; Xu, D.; Liao, L. An electrochemical sensor for determination of tryptophan in the presence of DA based on poly(L-methionine)/graphene modified electrode. *RSC Adv.* **2016**, *6*, 10662–10669. [[CrossRef](#)]
287. Wang, C.; Li, T.; Liu, Z.; Guo, Y.; Li, C.; Dong, C.; Shuang, S. An ultra-sensitive sensor based on β -cyclodextrin modified magnetic graphene oxide for detection of tryptophan. *J. Electroanal. Chem.* **2016**, *781*, 363–370. [[CrossRef](#)]
288. Sheng, Q.; Liu, R.; Zhang, H.; Zheng, J. A L-tryptophan sensor based on tellurium nanorods modified glassy carbon electrode. *J. Iran. Chem. Soc.* **2016**, *13*, 1189–1195. [[CrossRef](#)]
289. Liu, B.; Ouyang, X.; Ding, Y.; Luo, L.; Xu, D.; Ning, Y. Electrochemical preparation of nickel and copper oxides-decorated graphene composite for simultaneous determination of dopamine, acetaminophen and tryptophan. *Talanta* **2016**, *146*, 114–121. [[CrossRef](#)] [[PubMed](#)]
290. Raj, R.M.; Goyal, R.N. A facile method to anchor reduced graphene oxide polymer nanocomposite on the glassy carbon surface and its application in the voltammetric estimation of tryptophan in presence of 5-hydroxytryptamine. *Sens. Actuators B Chem.* **2016**, *233*, 445–453.
291. Tashkhourian, J.; Daneshi, M.; Nami-Ana, S.F. Simultaneous determination of tyrosine and tryptophan by mesoporous silica nanoparticles modified carbon paste electrode using H-point standard addition method. *Anal. Chim. Acta* **2016**, *902*, 89–96. [[CrossRef](#)]
292. Shabani-Nooshabadi, M.; Roostaei, M. Coupling of NiO nanoparticles and room temperature ionic liquid for fabrication of highly sensitive voltammetric sensor in tryptophan analysis. *Anal. Bioanal. Electrochem.* **2016**, *8*, 578–588.
293. Peng, Z.; Jiang, Z.; Huang, X.; Li, Y. A novel electrochemical sensor of tryptophan based on silver nanoparticles/metal-organic framework composite modified glassy carbon electrode. *RSC Adv.* **2016**, *6*, 13742–13748. [[CrossRef](#)]
294. Khaleghi, F.; Irai, A.E.; Gupta, V.K.; Agarwal, S.; Bijad, M.; Abbasghorbani, M. Highly sensitive nanostructure voltammetric sensor employing Pt/CNTs and 1-butyl-3-methylimidazolium hexafluoro phosphate for determination of tryptophan in food and pharmaceutical samples. *J. Mol. Liq.* **2016**, *223*, 431–435. [[CrossRef](#)]
295. Jarošová, R.; Rutherford, J.; Swain, G.M. Evaluation of a nitrogen-incorporated tetrahedral amorphous carbon thin film for the detection of tryptophan and tyrosine using flow injection analysis with amperometric detection. *Analyst* **2016**, *141*, 6031–6041. [[CrossRef](#)] [[PubMed](#)]
296. Fu, Y.; Su, W.; Wang, T.; Hu, J. Electrochemical sensor of tryptophan based on an Ag/CP electrode prepared by the filtered cathodic vacuum arc technique. *J. Electrochem. Soc.* **2016**, *163*, B107–B112. [[CrossRef](#)]
297. Yang, F.; Xie, Q.; Zhang, H.; Yu, S.; Zhang, X.; Shen, Y. Simultaneous determination of ascorbic acid, uric acid, tryptophan and adenine using carbon-supported NiCoO₂ nanoparticles. *Sens. Actuators B Chem.* **2015**, *210*, 232–240. [[CrossRef](#)]
298. Wang, C.; Zou, X.; Zhao, X.; Wang, Q.; Tan, J.; Yuan, R. Cu-nanoparticles incorporated overoxidized-poly(3-amino-5-mercapto-1,2,4-triazole) film modified electrode for the simultaneous determination of ascorbic acid, dopamine, uric acid and tryptophan. *J. Electroanal. Chem.* **2015**, *741*, 36–41. [[CrossRef](#)]
299. Taei, M.; Shavakhi, M.; Hadadzadeh, H.; Movahedi, M.; Rahimi, M.; Habibollahi, S. Simultaneous determination of epinephrine, acetaminophen, and tryptophan using Fe₂O₃(0.5)/SnO₂(0.5) nanocomposite sensor. *J. Appl. Electrochem.* **2015**, *45*, 185–195. [[CrossRef](#)]

300. Tadayon, F.; Sepehri, Z. A new electrochemical sensor based on a nitrogen-doped graphene/CuCo₂O₄ nanocomposite for simultaneous determination of dopamine, melatonin and tryptophan. *RSC Adv.* **2015**, *5*, 65560–65568. [[CrossRef](#)]
301. Kim, S.; Sun, S.; Li, Y.; He, X. One-pot synthesis of graphene oxide coated with sol-gel for electrochemical determination of tryptophan. *Anal. Methods* **2015**, *7*, 6352–6359. [[CrossRef](#)]
302. Baytak, A.K.; Aslanoglu, M. Voltammetric quantification of tryptophan using a MWCNT modified GCE decorated with electrochemically produced nanoparticles of nickel. *Sens. Actuators B Chem.* **2015**, *220*, 1161–1168. [[CrossRef](#)]
303. Zhu, S.; Zhang, J.; Zhao, X.E.; Wang, H.; Xu, G.; You, J. Electrochemical behavior and voltammetric determination of L-tryptophan and L-tyrosine using a glassy carbon electrode modified with single-walled carbon nanohorns. *Microchim. Acta* **2014**, *181*, 445–451. [[CrossRef](#)]
304. Xia, X.; Zheng, Z.; Zhang, Y.; Zhao, X.; Wang, C. Synthesis of Ag-MoS₂/chitosan nanocomposite and its application for catalytic oxidation of tryptophan. *Sens. Actuators B Chem.* **2014**, *192*, 42–50. [[CrossRef](#)]
305. Zhao, F.; Li, X.; Xu, W.; Zhang, W.; Ying, X. An Electrochemical Sensor for L-Tryptophan Using a Molecularly Imprinted Polymer Film Produced by Copolymerization of *o*-Phenylenediamine and Hydroquinone. *Anal. Lett.* **2014**, *47*, 1712–1725. [[CrossRef](#)]
306. Rajalakshmi, K.; John, S.A. Sensitive and selective determination of L-tryptophan at physiological pH using functionalized multiwalled carbon nanotubes-nanostructured conducting polymer composite modified electrode. *J. Electroanal. Chem.* **2014**, *734*, 31–37. [[CrossRef](#)]
307. Pang, T.T.; Cai, Z.F.; Liu, H.L.; Du, L.M.; Guo, M.D.; Fu, Y.L. Determination of Tryptophan using a *p*-Sulfonated Calix [4,6,8]arene Modified Gold Electrode. *Anal. Lett.* **2014**, *47*, 1808–1820. [[CrossRef](#)]
308. Divya, P.; Sudarvizhi, A.; Pandian, K. Single step synthesis of gold nanoparticles decorated graphene oxide using aniline as reducing agent and study its application on electrocatalytic detection of tryptophan. *Adv. Mater. Res.* **2014**, *938*, 182–191. [[CrossRef](#)]
309. Deng, P.; Xu, Z.; Feng, Y. Acetylene black paste electrode modified with graphene as the voltammetric sensor for selective determination of tryptophan in the presence of high concentrations of tyrosine. *Mater. Sci. Eng. C* **2014**, *35*, 54–60. [[CrossRef](#)]
310. Boonchiangma, S.; Srijaranai, S.; Tuntulani, T.; Ngeontae, W. A highly selective electrochemical sensor for L-tryptophan based on a screen-printed carbon electrode modified with poly-*p*-phenylenediamine and CdS quantum dots. *J. Appl. Polym. Sci.* **2014**, *131*, 40356. [[CrossRef](#)]
311. Wu, F.H.; Chen, L.; Chu, X.F.; Wei, X.W. Synthesis of ruthenium xanthate complex and its electrocatalytic activity for tryptophan oxidation. *Chem. Res. Chin. Univ.* **2013**, *29*, 574–578. [[CrossRef](#)]
312. Majidi, M.R.; Salimi, A.; Alipour, E. Development of voltammetric sensor for determination of tryptophan using MWCNTs-modified sol-gel electrode. *J. Chin. Chem. Soc.* **2013**, *60*, 1473–1478. [[CrossRef](#)]
313. Liu, H.; Chen, Y.; Liu, Y.; Yang, Z. A sensitive sensor for determination of L-tryptophan based on gold nanoparticles/poly(alizarin red S)-modified glassy carbon electrode. *J. Solid State Electrochem.* **2013**, *17*, 2623–2631. [[CrossRef](#)]
314. D'Souza, O.J.; Mascarenhas, R.J.; Thomas, T.; Namboothiri, I.N.N.; Rajamathi, M.; Martis, P.; Dalhalla, J. Electrochemical determination of L-Tryptophan based on a multiwall carbon nanotube/Mg-Al layered double hydroxide modified carbon paste electrode as a sensor. *J. Electroanal. Chem.* **2013**, *704*, 220–226. [[CrossRef](#)]
315. Deng, K.-Q.; Zhou, J.-H.; Li, X.-F. Direct electrochemical reduction of graphene oxide and its application to determination of L-tryptophan and L-tyrosine. *Colloids Surf. B Biointerfaces* **2013**, *101*, 183–188. [[CrossRef](#)]
316. Zeng, L.; Wang, H.; Bo, X.; Guo, L. Electrochemical sensor for amino acids based on gold nanoparticles/macroporous carbon composites modified glassy carbon electrode. *J. Electroanal. Chem.* **2012**, *687*, 117–122. [[CrossRef](#)]
317. Ye, D.; Luo, L.; Ding, Y.; Liu, B.; Liu, X. Fabrication of Co₃O₄ nanoparticles-decorated graphene composite for determination of L-tryptophan. *Analyst* **2012**, *137*, 2840–2845. [[CrossRef](#)] [[PubMed](#)]
318. Xu, M.; Ma, M.; Ma, Y. Electrochemical determination of tryptophan based on silicon dioxide nanoparticles modified carbon paste electrode. *Russ. J. Electrochem.* **2012**, *48*, 489–494. [[CrossRef](#)]
319. Xu, C.-X.; Huang, K.-J.; Fan, Y.; Wu, Z.-W.; Li, J.; Gan, T. Simultaneous electrochemical determination of dopamine and tryptophan using a TiO₂-graphene/poly(4-aminobenzenesulfonic acid) composite film based platform. *Mater. Sci. Eng. C* **2012**, *32*, 969–974. [[CrossRef](#)]
320. Wang, H.; Zhou, Y.; Guo, Y.; Liu, W.; Dong, C.; Wu, Y.; Li, S.; Shuang, S. β-Cyclodextrin/Fe₃O₄ hybrid magnetic nano-composite modified glassy carbon electrode for tryptophan sensing. *Sens. Actuators B Chem.* **2012**, *163*, 171–178. [[CrossRef](#)]
321. Wan, M.; Li, W.; Long, Y.; Tu, Y. Electrochemical determination of tryptophan based on Si-doped nano-TiO₂ modified glassy carbon electrode. *Anal. Methods* **2012**, *4*, 2860–2865. [[CrossRef](#)]
322. Özcan, A.; Şahin, Y. A novel approach for the selective determination of tryptophan in blood serum in the presence of tyrosine based on the electrochemical reduction of oxidation product of tryptophan formed in situ on graphite electrode. *Biosens. Bioelectron.* **2012**, *31*, 26–31. [[CrossRef](#)]
323. Li, W.; Li, C.; Kuang, Y.; Deng, P.; Zhang, S.; Xu, J. A carbon paste electrode modified with a cobalt(II) coordination polymer for the direct voltammetric determination of tryptophan. *Microchim. Acta* **2012**, *176*, 455–461. [[CrossRef](#)]
324. Xu, J.; Yuan, Y.; Li, W.; Deng, P.; Deng, J. Carbon paste electrode modified with a binuclear manganese complex as a sensitive voltammetric sensor for tryptophan. *Microchim. Acta* **2011**, *174*, 239–245. [[CrossRef](#)]
325. Shahrokhian, S.; Bayat, M. Pyrolytic graphite electrode modified with a thin film of a graphite/diamond nano-mixture for highly sensitive voltammetric determination of tryptophan and 5-hydroxytryptophan. *Microchim. Acta* **2011**, *174*, 361–366. [[CrossRef](#)]

326. Prabhu, P.; Babu, R.S.; Narayanan, S.S. Electrocatalytic oxidation of L-tryptophan using copper hexacyanoferrate film modified gold nanoparticle graphite-wax electrode. *Colloids Surf. B Biointerfaces* **2011**, *87*, 103–108. [[CrossRef](#)]
327. Kia, M.; Islamnezhad, A.; Shariati, S.; Biparva, P. Preparation of voltammetric biosensor for tryptophan using multi-walled carbon nanotubes. *Korean J. Chem. Eng.* **2011**, *28*, 2064–2068. [[CrossRef](#)]
328. Güney, S.; Yildiz, G. Determination of tryptophan using electrode modified with poly(9-aminoacridine) functionalized multi-walled carbon nanotubes. *Electrochim. Acta* **2011**, *57*, 290–296. [[CrossRef](#)]
329. Gholivand, M.B.; Pashabadi, A.; Azadbakht, A.; Menati, S. A nano-structured Ni(II)-ACDA modified gold nanoparticle self-assembled electrode for electrocatalytic oxidation and determination of tryptophan. *Electrochim. Acta* **2011**, *56*, 4022–4030. [[CrossRef](#)]
330. Fan, Y.; Liu, J.H.; Lu, H.T.; Zhang, Q. Electrochemistry and voltammetric determination of L-tryptophan and L-tyrosine using a glassy carbon electrode modified with a Nafion/TiO₂-graphene composite film. *Microchim. Acta* **2011**, *173*, 241–247. [[CrossRef](#)]
331. Szunerits, S.; Coffinier, Y.; Galopin, E.; Brenner, J.; Boukherroub, R. Preparation of boron-doped diamond nanowires and their application for sensitive electrochemical detection of tryptophan. *Electrochem. Commun.* **2010**, *12*, 438–441. [[CrossRef](#)]
332. Srivastava, A.K.; Gaichore, R.R. Macrocyclic compounds based chemically modified electrodes for voltammetric determination of L-tryptophan using electrocatalytic oxidation. *Anal. Lett.* **2010**, *43*, 1933–1950. [[CrossRef](#)]
333. Jiang, Q.; Sun, W.; Jiao, K. Electrochemical behavior and determination of L-tryptophan on carbon ionic liquid electrode. *J. Anal. Chem.* **2010**, *65*, 648–651. [[CrossRef](#)]
334. Huang, K.J.; Xu, C.X.; Sun, J.Y.; Xie, W.Z.; Peng, L. Electrochemical oxidation of tryptophan and its analysis in pharmaceutical formulations at a poly(methyl red) film-modified electrode. *Anal. Lett.* **2010**, *43*, 176–185. [[CrossRef](#)]
335. Guo, Y.; Guo, S.; Fang, Y.; Dong, S. Gold nanoparticle/carbon nanotube hybrids as an enhanced material for sensitive amperometric determination of tryptophan. *Electrochim. Acta* **2010**, *55*, 3927–3931. [[CrossRef](#)]
336. Shumyantseva, V.; Bulko, T.; Kuzikov, A.; Masamrekh, R.; Archakov, A. Analysis of L-tyrosine based on electrocatalytic oxidative reactions via screen-printed electrodes modified with multi-walled carbon nanotubes and nanosized titanium oxide (TiO₂). *Amino Acids* **2018**, *50*, 823–829. [[CrossRef](#)]
337. Maes, M.; Verkerk, R.; Vandoolaeghe, E.; van Hunsel, F.; Neels, H.; Wauters, A.; Demedts, P.; Scharpé, S. Serotonin-immune interactions in major depression: Lower serum tryptophan as a marker of an immune-inflammatory response. *Eur. Arch. Psychiatry Clin. Neurosci.* **1997**, *247*, 154–161. [[CrossRef](#)] [[PubMed](#)]
338. Geisler, S.; Mayersbach, P.; Becker, K.; Schennach, H.; Fuchs, D.; Gostner, J.M. Serum tryptophan, kynurenine, phenylalanine, tyrosine and neopterin concentrations in 100 healthy blood donors. *Pteridines* **2015**, *26*, 31. [[CrossRef](#)]
339. Canadian Agency for Drugs and Technologies in Health. *Clinical Review Report: Nitisinone (Nitisinone Tablets): (Cycle Pharmaceuticals Ltd.): Indication: For the Treatment of Patients with Hereditary Tyrosinemia Type 1 in Combination with Dietary Restriction of Tyrosine and Phenylalanine [Internet]; Appendix 4, Validity of Outcome Measures; Canadian Agency for Drugs and Technologies in Health: Ottawa, ON, Canada, 2018.*
340. Tallan, H.H.; Bella, S.T.; Stein, W.H.; Moore, S. Tyrosine-O-sulfate as a constituent of normal human urine. *J. Biol. Chem.* **1955**, *217*, 703–708. [[CrossRef](#)]
341. Holme, E.; Lindstedt, S. Nontransplant treatment of tyrosinemia. *Clin. Liver Dis.* **2000**, *4*, 805–814. [[CrossRef](#)]
342. Baig, N.; Kawde, A.N. A novel, fast and cost effective graphene-modified graphite pencil electrode for trace quantification of L-tyrosine. *Anal. Methods* **2015**, *7*, 9535–9541. [[CrossRef](#)]
343. D'Souza, O.J.; Mascarenhas, R.J.; Satpati, A.K.; Aiman, L.V.; Mekhalif, Z. Electrocatalytic oxidation of L-tyrosine at carboxylic acid functionalized multi-walled carbon nanotubes modified carbon paste electrode. *Ionics* **2016**, *22*, 405–414. [[CrossRef](#)]
344. Yu, X.; Mai, Z.; Xiao, Y.; Zou, X. Electrochemical behavior and determination of L-tyrosine at single-walled carbon nanotubes modified glassy carbon electrode. *Electroanalysis* **2008**, *20*, 1246–1251. [[CrossRef](#)]
345. Shadjou, N.; Hasanzadeh, M.; Talebi, F. Graphene Quantum Dots Incorporated into β -cyclodextrin: A Novel Polymeric Nanocomposite for Non-Enzymatic Sensing of L-Tyrosine at Physiological pH. *J. Anal. Chem.* **2018**, *73*, 602–612. [[CrossRef](#)]
346. Wang, Q.; Vasilescu, A.; Subramanian, P.; Vezeanu, A.; Andrei, V.; Coffinier, Y.; Li, M.; Boukherroub, R.; Szunerits, S. Simultaneous electrochemical detection of tryptophan and tyrosine using boron-doped diamond and diamond nanowire electrodes. *Electrochem. Commun.* **2013**, *35*, 84–87. [[CrossRef](#)]
347. Habibi, E.; Heidari, H. Renewable Surface Carbon-Composite Electrode Bulk Modified with GQD-RuCl₃ Nano-Composite for High Sensitive Detection of L-Tyrosine. *Electroanalysis* **2016**, *28*, 2559–2564. [[CrossRef](#)]
348. Zhu, Q.; Liu, C.; Zhou, L.; Wu, L.; Bian, K.; Zeng, J.; Wang, J.; Feng, Z.; Yin, Y.; Cao, Z. Highly sensitive determination of L-tyrosine in pig serum based on ultrathin CuS nanosheets composite electrode. *Biosens. Bioelectron.* **2019**, *140*, 111356. [[CrossRef](#)]
349. Gu, W.; Wang, M.; Mao, X.; Wang, Y.; Li, L.; Xia, W. A facile sensitive L-tyrosine electrochemical sensor based on a coupled CuO/Cu₂O nanoparticles and multi-walled carbon nanotubes nanocomposite film. *Anal. Methods* **2015**, *7*, 1313–1320. [[CrossRef](#)]
350. D'Souza, O.J.; Mascarenhas, R.J.; Satpati, A.K.; Namboothiri, I.N.N.; Detriche, S.; Mekhalif, Z.; Delhalle, J. A multi-walled carbon nanotube/poly-2,6-dichlorophenolindophenol film modified carbon paste electrode for the amperometric determination of L-tyrosine. *RSC Adv.* **2015**, *5*, 91472–91481. [[CrossRef](#)]
351. Quintana, C.; Suárez, S.; Hernández, L. Nanostructures on gold electrodes for the development of an L-tyrosine electrochemical sensor based on host-guest supramolecular interactions. *Sens. Actuators B Chem.* **2010**, *149*, 129–135. [[CrossRef](#)]

352. Ma, Q.; Ai, S.; Yin, H.; Chen, Q.; Tang, T. Towards the conception of an amperometric sensor of L-tyrosine based on Hemin/PAMAM/MWCNT modified glassy carbon electrode. *Electrochim. Acta* **2010**, *55*, 6687–6694. [[CrossRef](#)]
353. Chekin, F.; Bagheri, S. Tyrosine sensing on phthalic anhydride functionalized chitosan and carbon nanotube film coated glassy carbon electrode. *Russ. J. Electrochem.* **2016**, *52*, 174–180. [[CrossRef](#)]
354. Zou, J.; Mao, D.; Wee, A.T.S.; Jiang, J. Micro/nano-structured ultrathin g-C₃N₄/Ag nanoparticle hybrids as efficient electrochemical biosensors for L-tyrosine. *Appl. Surf. Sci.* **2019**, *467*, 608–618. [[CrossRef](#)]
355. Zhao, G.; Qi, Y.; Tian, Y. Simultaneous and direct determination of tryptophan and tyrosine at boron-doped diamond electrode. *Electroanalysis* **2006**, *18*, 830–834. [[CrossRef](#)]
356. Zribi, R.; Maalej, R.; Gillibert, R.; Donato, M.G.; Gucciardi, P.G.; Leonardi, S.G.; Neri, G. Simultaneous and selective determination of dopamine and tyrosine in the presence of uric acid with 2D-MoS₂ nanosheets modified screen-printed carbon electrodes. *FlatChem* **2020**, *24*, 100187. [[CrossRef](#)]
357. Zhao, J.; Cong, L.; Ding, Z.; Zhu, X.; Zhang, Y.; Li, S.; Liu, J.; Chen, X.; Hou, H.; Fan, Z.; et al. Enantioselective electrochemical sensor of tyrosine isomers based on macroporous carbon embedded with sulfato-β-Cyclodextrin. *Microchem. J.* **2020**, *159*, 105469. [[CrossRef](#)]
358. Wu, X.-Q.; Feng, P.-Q.; Guo, Z.; Wei, X. Water-Stage 1D Double-Chain Cu Metal–Organic Framework-Based Electrochemical Biosensor for Detecting L-Tyrosine. *Langmuir* **2020**, *36*, 14123–14129. [[CrossRef](#)]
359. Zou, J.; Lan, X.-W.; Zhao, G.-Q.; Huang, Z.-N.; Liu, Y.-P.; Yu, J.-G. Immobilization of 6-O-α-maltosyl-β-cyclodextrin on the surface of black phosphorus nanosheets for selective chiral recognition of tyrosine enantiomers. *Microchim. Acta* **2020**, *187*, 636. [[CrossRef](#)] [[PubMed](#)]
360. Alam, M.M.; Uddin, M.T.; Asiri, A.M.; Rahman, M.M.; Islam, M.A. Detection of L-Tyrosine by electrochemical method based on binary mixed CdO/SnO₂ nanoparticles. *Measurement* **2020**, *163*, 107990. [[CrossRef](#)]
361. Zou, H.-Y.; Lu, X.-Y.; Kong, F.-Y.; Wang, Z.-X.; Li, H.-Y.; Fang, H.-L.; Wang, W. A voltammetric sensor based on reduced graphene oxide-hemin-Ag nanocomposites for sensitive determination of tyrosine. *RSC Adv.* **2020**, *10*, 28026–28031. [[CrossRef](#)]
362. Cioates Negut, C.; Stefanov, C.; van Staden, J.F. Graphite Based Microsensors Developed for the Electrochemical Determination of L-Tyrosine from Pharmaceutical Samples. *Electroanalysis* **2020**, *32*, 1488–1497. [[CrossRef](#)]
363. Chen, B.; Zhang, Y.; Lin, L.; Chen, H.; Zhao, M. Au nanoparticles @metal organic framework/polythionine loaded with molecularly imprinted polymer sensor: Preparation, characterization, and electrochemical detection of tyrosine. *J. Electroanal. Chem.* **2020**, *863*, 114052. [[CrossRef](#)]
364. Khoobi, A.; Shahdost-fard, F.; Arbabi, M.; Akbari, M.; Mirzaei, H.; Nejati, M.; Lotfinia, M.; Sobhani-Nasab, A.; Banafshe, H.R. Sonochemical synthesis of ErVO₄/MnWO₄ heterostructures: Application as a novel nanostructured surface for electrochemical determination of tyrosine in biological samples. *Polyhedron* **2020**, *177*, 114302. [[CrossRef](#)]
365. Zribi, R.; Maalej, R.; Messina, E.; Gillibert, R.; Donato, M.G.; Maragò, O.M.; Gucciardi, P.G.; Leonardi, S.G.; Neri, G. Exfoliated 2D-MoS₂ nanosheets on carbon and gold screen printed electrodes for enzyme-free electrochemical sensing of tyrosine. *Sens. Actuators B Chem.* **2020**, *303*, 127229. [[CrossRef](#)]
366. Karthika, A.; Rosaline, D.R.; Inbanathan, S.S.R.; Suganthi, A.; Rajarajan, M. Fabrication of Cupric oxide decorated β-cyclodextrin nanocomposite solubilized Nafion as a high performance electrochemical sensor for L-tyrosine detection. *J. Phys. Chem. Solids* **2020**, *136*, 109145. [[CrossRef](#)]
367. Feng, J.; Deng, P.; Xiao, J.; Li, J.; Tian, Y.; Wu, Y.; Liu, J.; Li, G.; He, Q. New voltammetric method for determination of tyrosine in foodstuffs using an oxygen-functionalized multi-walled carbon nanotubes modified acetylene black paste electrode. *J. Food Compos. Anal.* **2021**, *96*, 103708. [[CrossRef](#)]
368. Parsa, A.; Akbarzadeh-Torbati, N.; Beitollahi, H. Rapid and sensitive electrochemical monitoring of tyrosine using NiO nanoparticles modified graphite screen printed electrode. *Int. J. Electrochem. Sci.* **2019**, *14*, 1556–1565. [[CrossRef](#)]
369. Hassanvand, Z.; Jalali, F. Simultaneous determination of L-DOPA, L-tyrosine and uric acid by cysteic acid—Modified glassy carbon electrode. *Mater. Sci. Eng. C* **2019**, *98*, 496–502. [[CrossRef](#)]
370. Arani, N.H.; Ghoreishi, S.M.; Khoobi, A. Increasing the electrochemical system performance using a magnetic nanostructured sensor for simultaneous determination of L-tyrosine and epinephrine. *Anal. Methods* **2019**, *11*, 1159–1167. [[CrossRef](#)]
371. Zheng, W.; Zhao, M.; Liu, W.; Yu, S.; Niu, L.; Li, G.; Li, H.; Liu, W. Electrochemical sensor based on molecularly imprinted polymer/reduced graphene oxide composite for simultaneous determination of uric acid and tyrosine. *J. Electroanal. Chem.* **2018**, *813*, 75–82. [[CrossRef](#)]
372. Heidari, H.; Habibi, E. Lead-doped carbon ceramic electrode as a renewable surface composite electrode for the preparation of lead dioxide film and detection of L-tyrosine. *J. Iran. Chem. Soc.* **2018**, *15*, 885–892. [[CrossRef](#)]
373. García-Carmona, L.; Moreno-Guzmán, M.; Sierra, T.; González, M.C.; Escarpa, A. Filtered carbon nanotubes-based electrodes for rapid sensing and monitoring of L-tyrosine in plasma and whole blood samples. *Sens. Actuators B Chem.* **2018**, *259*, 762–767. [[CrossRef](#)]
374. Ermiş, N.; Tinkiliç, N. Preparation of molecularly imprinted polypyrrole modified gold electrode for determination of tyrosine in biological samples. *Int. J. Electrochem. Sci.* **2018**, *13*, 2286–2298. [[CrossRef](#)]
375. Wang, Y.; Bian, L.; Tan, D.; Chen, S.; Gan, Y. Sonochemical synthesis of “sea-island” structure silver/polyaniline nanocomposites for the detection of L-tyrosine. *J. Thermoplast. Compos. Mater.* **2017**, *30*, 1033–1044. [[CrossRef](#)]

376. Shi, X.; Wang, Y.; Peng, C.; Zhang, Z.; Chen, J.; Zhou, X.; Jiang, H. Enantio-recognition of Tyrosine Based on a Novel Magnetic Electrochemical Chiral Sensor. *Electrochim. Acta* **2017**, *241*, 386–394. [[CrossRef](#)]
377. Tian, F.; Li, H.; Li, M.; Li, C.; Lei, Y.; Yang, B. A tantalum electrode coated with graphene nanowalls for simultaneous voltammetric determination of dopamine, uric acid, L-tyrosine, and hydrochlorothiazide. *Microchim. Acta* **2017**, *184*, 1611–1619. [[CrossRef](#)]
378. Karimi-Maleh, H.; Ganjali, M.R.; Norouzi, P.; Bananezhad, A. Amplified nanostructure electrochemical sensor for simultaneous determination of captopril, acetaminophen, tyrosine and hydrochlorothiazide. *Mater. Sci. Eng. C* **2017**, *73*, 472–477. [[CrossRef](#)] [[PubMed](#)]
379. Karami, Z.; Sheikhshoaei, I. rGO/ZnO nanocomposite modified carbon paste electrode as sensor for tyrosine analysis. *Anal. Bioanal. Electrochem.* **2017**, *9*, 834–840.
380. Narayanan, K.R.; Sadanandhan, N.K.; Devaki, S.J. Silver Patterned Supramolecular Liquid Crystalline Gels as Electrochemical Sensor of Tyrosine. *ChemistrySelect* **2017**, *2*, 320–328. [[CrossRef](#)]
381. Huang, Y.; Chen, M.; Li, X.; Zhang, C. Voltammetric Separation and Determination of Glutathione and L-tyrosine with Chlorogenic Acid as an Electrocatalytic Mediator. *Electroanalysis* **2017**, *29*, 1141–1146. [[CrossRef](#)]
382. Foroughi, M.M.; Tajik, S. SiO₂@Fe₃O₄ nanocomposite decorated graphene modified carbon ionic liquid electrode as an electrochemical sensor for the determination of tyrosine. *Anal. Bioanal. Electrochem.* **2017**, *9*, 495–505.
383. Dong, S.; Bi, Q.; Qiao, C.; Sun, Y.; Zhang, X.; Lu, X.; Zhao, L. Electrochemical sensor for discrimination tyrosine enantiomers using graphene quantum dots and β-cyclodextrins composites. *Talanta* **2017**, *173*, 94–100. [[CrossRef](#)]
384. Shrestha, S.; Mascarenhas, R.J.; D'Souza, O.J.; Satpati, A.K.; Mekhalif, Z.; Dhason, A.; Martis, P. Amperometric sensor based on multi-walled carbon nanotube and poly (Bromocresol purple) modified carbon paste electrode for the sensitive determination of L-tyrosine in food and biological samples. *J. Electroanal. Chem.* **2016**, *778*, 32–40. [[CrossRef](#)]
385. Yola, M.L.; Eren, T.; Atar, N. A sensitive molecular imprinted electrochemical sensor based on gold nanoparticles decorated graphene oxide: Application to selective determination of tyrosine in milk. *Sens. Actuators B Chem.* **2015**, *210*, 149–157. [[CrossRef](#)]
386. Rahman, M.M.; Lopa, N.S.; Kim, K.; Lee, J.J. Selective detection of L-tyrosine in the presence of ascorbic acid, dopamine, and uric acid at poly(thionine)-modified glassy carbon electrode. *J. Electroanal. Chem.* **2015**, *754*, 87–93. [[CrossRef](#)]
387. Razavian, A.S.; Ghoreishi, S.M.; Esmaeili, A.S.; Behpour, M.; Monzon, L.M.A.; Coey, J.M.D. Simultaneous sensing of L-tyrosine and epinephrine using a glassy carbon electrode modified with nafion and CeO₂ nanoparticles. *Microchim. Acta* **2014**, *181*, 1947–1955. [[CrossRef](#)]
388. Kanchana, P.; Lavanya, N.; Sekar, C. Development of amperometric L-tyrosine sensor based on Fe-doped hydroxyapatite nanoparticles. *Mater. Sci. Eng. C* **2014**, *35*, 85–91. [[CrossRef](#)]
389. Cipri, A.; Del Valle, M. Pd nanoparticles/multiwalled carbon nanotubes electrode system for voltammetric sensing of tyrosine. *J. Nanosci. Nanotechnol.* **2014**, *14*, 6692–6698. [[CrossRef](#)]
390. Liu, Y.; Yang, Z.; Zhong, Y.; Yu, J. Construction of europium hexacyanoferrate film and its electrocatalytic activity to tyrosine determination. *Appl. Surf. Sci.* **2010**, *256*, 3148–3154. [[CrossRef](#)]
391. Moro, J.; Tomé, D.; Schmidely, P.; Demersay, T.C.; Azzout-Marniche, D. Histidine: A systematic review on metabolism and physiological effects in human and different animal species. *Nutrients* **2020**, *12*, 1414. [[CrossRef](#)]
392. Teloh, J.K.; Dohle, D.-S.; Petersen, M.; Verhaegh, R.; Waack, I.N.; Roehrborn, F.; Jakob, H.; de Groot, H. Histidine and other amino acids in blood and urine after administration of Bretschneider solution (HTK) for cardioplegic arrest in patients: Effects on N-metabolism. *Amino Acids* **2016**, *48*, 1423–1432. [[CrossRef](#)]
393. Alevridis, A.; Tsiasioti, A.; Zacharis, C.K.; Tzanavaras, P.D. Fluorimetric Method for the Determination of Histidine in Random Human Urine Based on Zone Fluidics. *Molecules* **2020**, *25*, 1665. [[CrossRef](#)]
394. Su, J.; Li, Y.; Gu, W.; Liu, X. Spiropyran-modified upconversion nanocomposite as a fluorescent sensor for diagnosis of histidinemia. *RSC Adv.* **2020**, *10*, 26664–26670. [[CrossRef](#)]
395. Guo Nan, C.; Ping, W.X.; Ping, D.J.; Qing, C.H. A study on electrochemistry of histidine and its metabolites based on the diazo coupling reaction. *Talanta* **1999**, *49*, 319–330. [[CrossRef](#)]
396. Hua, Y.; Li, S.; Cai, Y.; Liu, H.; Wan, Y.; Yin, M.; Wang, F.; Wang, H. A sensitive and selective electroanalysis strategy for histidine using the wetttable well electrodes modified with graphene quantum dot-scaffolded melamine and copper nanocomposites. *Nanoscale* **2019**, *11*, 2126–2130. [[CrossRef](#)] [[PubMed](#)]
397. Hua, Y.; Lv, X.; Cai, Y.; Liu, H.; Li, S.; Wan, Y.; Wang, H. Highly selective and reproducible electroanalysis for histidine in blood with turn-on responses at a potential approaching zero using tetrahedral copper metal organic frameworks. *Chem. Commun.* **2019**, *55*, 1271–1274. [[CrossRef](#)]
398. Hua, Y.; Cai, Y.; Liu, H.; Wan, Y.; Ding, X.; Li, S.; Wang, H. A highly selective “turn-on” electroanalysis strategy with reduced copper metal-organic frameworks for sensing histamine and histidine. *Nanoscale* **2019**, *11*, 17401–17406. [[CrossRef](#)] [[PubMed](#)]
399. Prasad, B.B.; Kumar, D.; Madhuri, R.; Tiwari, M.P. Metal ion mediated imprinting for electrochemical enantioselective sensing of L-histidine at trace level. *Biosens. Bioelectron.* **2011**, *28*, 117–126. [[CrossRef](#)]
400. Zhang, Z.; Hu, Y.; Zhang, H.; Luo, L.; Yao, S. Layer-by-layer assembly sensitive electrochemical sensor for selectively probing L-histidine based on molecular imprinting sol-gel at functionalized indium tin oxide electrode. *Biosens. Bioelectron.* **2010**, *26*, 696–702. [[CrossRef](#)]
401. Stefan-Van Staden, R.I. Enantioanalysis of D-histidine based on its interaction with [5,6]fullerene-C70 and diethyl (1,2-methanofullerene-C 70)-71,71-dicarboxylate. *New J. Chem.* **2010**, *34*, 1141–1147. [[CrossRef](#)]

402. Stefan-van Staden, R.I.; Holo, L. Enantioanalysis of L-histidine using enantioselective, potentiometric membrane electrodes based on maltodextrins. *Anal. Lett.* **2011**, *44*, 968–975. [[CrossRef](#)]
403. Chen, Z.; Nai, J.; Ma, H.; Li, Z. Nickel hydroxide nanocrystals-modified glassy carbon electrodes for sensitive L-histidine detection. *Electrochim. Acta* **2014**, *116*, 258–262. [[CrossRef](#)]
404. Nai, J.; Chen, Z.; Li, H.; Li, F.; Bai, Y.; Li, L.; Guo, L. Structure-dependent electrocatalysis of Ni(OH)₂ hourglass-like nanostructures towards L-histidine. *Chem. Eur. J.* **2013**, *19*, 501–508. [[CrossRef](#)]
405. Mers, S.V.S.; Muthurasu, A.; Ganesh, V. Polydopamine Decorated Co₃O₄/Reduced Graphene Oxide Composite for Efficient and Selective Sensing of Histidine: Restructuring α -Cobalt Hydroxide to Highly Crystalline Co₃O₄ Sheets. *J. Electrochem. Soc.* **2018**, *165*, B753–B761. [[CrossRef](#)]
406. Chen, L.-C.; Chang, C.-C.; Chang, H.-C. Electrochemical oxidation of histidine at an anodic oxidized boron-doped diamond electrode in neutral solution. *Electrochim. Acta* **2008**, *53*, 2883–2889. [[CrossRef](#)]
407. Sutradhar, S.; Jacob, G.V.; Patnaik, A. Structure and dynamics of a DL-homocysteine functionalized fullerene-C60-gold nanocomposite: A femtomolar L-histidine sensor. *J. Mater. Chem. B* **2017**, *5*, 5835–5844. [[CrossRef](#)]
408. Pei, L.Z.; Wei, T.; Lin, N.; Cai, Z.Y. Electrochemical sensing of histidine based on the copper germanate nanowires modified electrode. *J. Bionanosci.* **2015**, *9*, 161–165. [[CrossRef](#)]
409. Suprun, E.V.; Radko, S.P.; Kozin, S.A.; Mitkevich, V.A.; Makarov, A.A. Electrochemical detection of Zn(II)-induced amyloid- β aggregation: Insights into aggregation mechanisms. *J. Electroanal. Chem.* **2018**, *830*, 34–42. [[CrossRef](#)]
410. Chiorcea-Paquim, A.M.; Enache, T.A.; Oliveira-Brett, A.M. Electrochemistry of alzheimer disease amyloid beta peptides. *Curr. Med. Chem.* **2018**, *25*, 4066–4083. [[CrossRef](#)]
411. Suprun, E.V.; Radko, S.P.; Farafonova, T.E.; Kozin, S.A.; Makarov, A.A.; Archakov, A.I.; Shumyantseva, V.V. Electrochemical detection of protein post-translational modifications: Phosphorylation and nitration of amyloid-beta (1–16). *Electrochim. Acta* **2017**, *258*, 1182–1190. [[CrossRef](#)]
412. Suprun, E.V.; Khmeleva, S.A.; Radko, S.P.; Kozin, S.A.; Archakov, A.I.; Shumyantseva, V.V. Direct electrochemical oxidation of amyloid- β peptides via tyrosine, histidine, and methionine residues. *Electrochem. Commun.* **2016**, *65*, 53–56. [[CrossRef](#)]
413. Niu, X.; Yang, X.; Mo, Z.; Guo, R.; Liu, N.; Zhao, P.; Liu, Z.; Ouyang, M. Voltammetric enantiomeric differentiation of tryptophan by using multiwalled carbon nanotubes functionalized with ferrocene and β -cyclodextrin. *Electrochim. Acta* **2019**, *297*, 650–659. [[CrossRef](#)]
414. Fedorowski, J.; LaCourse, W.R. A review of pulsed electrochemical detection following liquid chromatography and capillary electrophoresis. *Anal. Chim. Acta* **2015**, *861*, 1–11. [[CrossRef](#)]
415. Jöhl, M.E.; Williams, D.G.; Johnson, D.C. Activated pulsed amperometric detection of cysteine at platinum electrodes in acidic media. *Electroanalysis* **1997**, *9*, 1397–1402. [[CrossRef](#)]
416. Cataldi, T.R.I.; Nardiello, D. A pulsed potential waveform displaying enhanced detection capabilities towards sulfur-containing compounds at a gold working electrode. *J. Chromatogr. A* **2005**, *1066*, 133–142. [[CrossRef](#)] [[PubMed](#)]
417. Cheng, J.; Jandik, P.; Avdalovic, N. Use of disposable gold working electrodes for cation chromatography-integrated pulsed amperometric detection of sulfur-containing amino acids. *J. Chromatogr. A* **2003**, *997*, 73–78. [[CrossRef](#)]
418. Hanssen, B.L.; Siraj, S.; Wong, D.K.Y. Recent strategies to minimise fouling in electrochemical detection systems. *Rev. Anal. Chem.* **2016**, *35*, 1–28. [[CrossRef](#)]